Road profile statistics relevant for vehicle fatigue

Bogsjö, Klas

2007

Road Profile Statistics Relevant for Vehicle Fatigue

Klas Bogsjö

Lund University

Faculty of Engineering
Centre for Mathematical Sciences
Mathematical Statistics

Mathematical Statistics
Centre for Mathematical Sciences
Lund University
Box 118
SE-221 00 Lund
Sweden

http://www.maths.lth.se/

Doctoral Theses in Mathematical Sciences 2007:6
ISSN 1404-0034

ISBN 978-91-628-7291-5
LUTFMS-1032-2007

Printed in Sweden by KFS AB, Lund 2007

Contents

Acknowledgements

First I like to acknowledge the financial support from Scania and The Programme Council for Vehicle Research within the Swedish Agency for Innovation Systems (PFF/VINNOVA).

I am very pleased with the help from my two excellent supervisors, Anders Forsén at Scania and Igor Rychlik at Chalmers University of Technology, formerly at Lund Institute of Technology.

Anders has been very devoted to this project from the start. He provided help with everything from implementation of vehicle models in MATLAB to general improvement of paper content. His comments are always insightful and accurate!

Igor has supervised many PhD-student the last years, in their acknowledgements, all of them prise Igor for his encouragement and guidance. So being number 9, I can confirm that he really is a great supervisor, and I can only congratulate his coming students. I especially like his creativeness, always full of new ideas!

Anders and Igor have attacked the encountered problems from different point of views, Anders with the application and Igor with the mathematics in mind. This has given me help from two sides, and in the end, resulting in a better thesis. Besides being great supervisors, they are two very likable fellows!

I am very grateful to my co-supervisor Georg Lindgren. His enthusiastic teaching when I studied "Stochastic processes" in 2001, catched my attention for mathematical statistics. In 2002 I got the opportunity to do my Master Thesis with Georg as the supervisor. So I am very thankful for his encouragement previous to, and during, this project. Georg was also very helpful in reading manuscripts and suggesting final changes before submission.

My boss at Scania, Björn Rickfält supported me throughout the project, which has made it a lot easier, and I appreciate that he allowed me to focus entirely on this work. Bengt Fura, Christer Olsson and Gunnar Strandell were a part of the steering committee of this PhD-project. The steering committee meetings gave me instant input on the latest ideas, which was especially important in the early stages of the project.

Mona Forsler, Aurelia Vogel, James Hakim and Joakim Lübeck have provided much help with practical things during these 5 years. Thank you! I am also grateful to: Lars Ängquist for the help with grammatical and layout issues, and finding misprints in the text, Finn Lindgren for help with LaTeX-related problems and the librarians at Scania, Göran Henriksson and Iréne Wahlqvist. Also, all the nice colleagues and friends at Mathematical Statistics and at Scania, has made the work very enjoyable.

During these 5 years I sometimes (as it appears) had other things on my mind. As a result, me and my wife Lisa now have two wonderful children Alfred and Alma. Lisa, these last years would have been so dull without your love,

support and liveliness. Finally, my thanks go to my parents Jan and Elvi, my siblings Kristin and André and all friends, out there in the real world.

Och, *naturligtvis*, tack Anders Svensson för återkomsten till IF Elfsborg.

Lund, October 2007

Klas Bogsjö

Summary

Road profiles are studied from a vehicle fatigue point of view. A wide range of roads have been measured: from smooth motorways to very rough gravel roads. It is observed that the road profiles consist of irregular sections, which makes the stationary Gaussian model unsuitable (Paper A). In Paper B, a method for automatic identification of such irregularities is presented. It is verified that the irregular sections cause the major part of the fatigue damage induced in vehicles. Based on this result, a new single track model is proposed, which includes randomly shaped and located irregularities. In Paper C, an evaluation method of single track models is proposed. This evaluation method is extended to models of parallel tracks in Paper D. A new 'parallel tracks' model is proposed and evaluated accordingly. In Paper E, the coherence between the parallel road tracks is studied. A simple one-parametric model is proposed for the coherence. In Paper F a new theoretical method to compute the expected vehicle fatigue damage caused by road irregularities is presented.

Appended papers

This thesis is based on the following six papers:

A. Klas Bogsjö and Anders Forsén (2004), Fatigue relevant road surface statistics. *Supplement to Vehicle System Dynamics*, Vol 41, pp. 724–733.

B. Klas Bogsjö (2006), Development of analysis tools and stochastic models of road profiles regarding their influence on heavy vehicle fatigue. *Supplement to Vehicle System Dynamics*, Vol 44, pp. 780–790.

C. Klas Bogsjö (2006), Accuracy of stochastic road models. Submitted for publication.

D. Klas Bogsjö (2007), Evaluation of stochastic models of parallel road tracks. *Probabilistic Engineering Mechanics*, (In press). doi:10.1016/j.probengmech.2007.08.002

E. Klas Bogsjö (2007), Coherence of road roughness in left and right wheelpath. Accepted for publication in *Supplement to Vehicle System Dynamics*.

F. Klas Bogsjö and Igor Rychlik (2007), Vehicle fatigue damage caused by road irregularities. Submitted for publication.

1 Background

Travelling vehicles are exposed to dynamic loads caused by unevenness in the road. These loads induce fatigue damage in the vehicle, which may cause structural failures.

Manufacturers verify vehicle durability on test tracks, in test rigs, or, increasingly, by computer simulations. Erroneous design targets may lead to unnecessarily heavy or too fragile vehicles. To avoid inaccurate testing it is necessary to collect vehicle fatigue relevant information from actual roads.

Road roughness is studied in order to answer key questions: Do the tests represent real-life vehicle usage? How many times should a vehicle travel over the test track to verify the durability? How should input signals to test rigs be generated?

This thesis is focused on the description of road roughness. In particular, measurements of left and right wheel-paths are statistically analysed. In Papers A–C and F left and right profiles are analysed separately, whereas in Papers D–E the profiles are jointly analysed. The thesis is restricted to 'vertical' loads; lateral and longitudinal loads are not treated.

1.1 Road measurements

In this thesis 20 measured roads are analysed. The profile of the left and right wheel-path is measured by laser/inertial profilometers. The equipment used to measure roads 4–20 is described in [1]. Here, laser number 3 and 15, as numbered in [1], represent the left and right wheel-path, respectively. The total distance of the measured roads is 520 km and the sample distance is 5 cm (10 cm for road 3). The roads are measured with a slightly changing sample distance (varying around 5 cm). The sampled profiles are linearly interpolated with a fixed sample distance at exactly 5 cm, in order to facilitate the statistical analysis and vehicle simulation. Vehicle simulations verify that this linear interpolation scheme has no significant effect on the assessed fatigue damage.

The roads are of varying quality, ranging from smooth motorways to rough gravel roads. Prior to analysis the measured profiles are high-pass filtered to remove measurement drift and very long-wave disturbances (hills and slopes). Figure 1 shows a measurement of three kilometres of a rough Swedish main road.

Remark: Initially, not all measurements were available for analysis. In Paper A roads 1–3 are analysed, in Papers B–C roads 1–14 are analysed and in Papers D–F roads 1–20 are analysed.

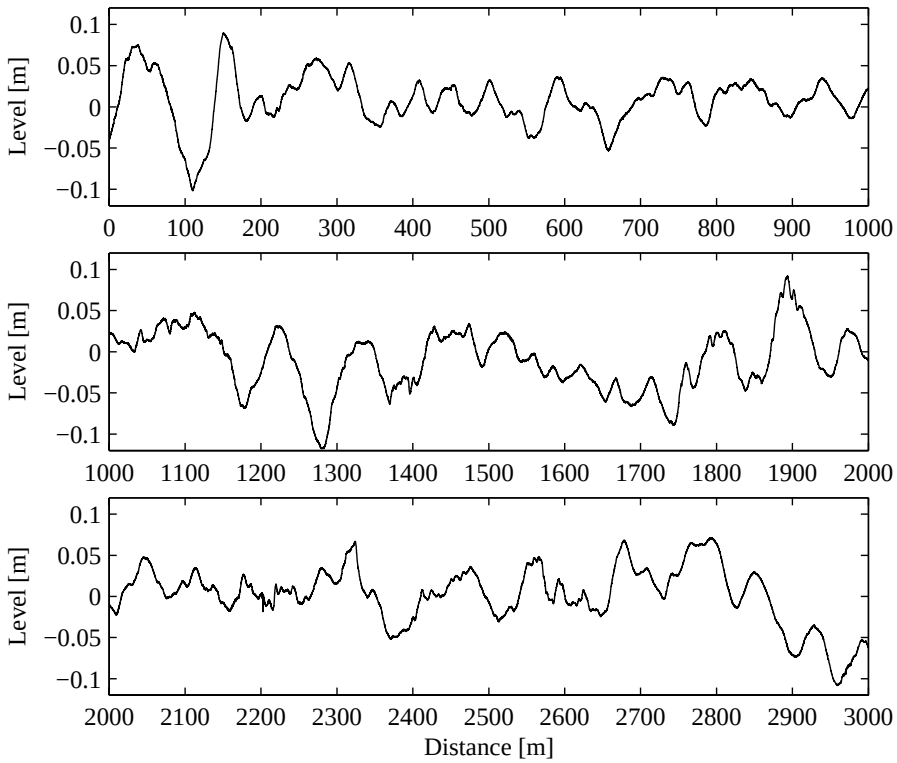

Figure 1: A rough main road in northern Sweden (left wheel-path of road 7)

1.2 The need for a stochastic model

Measured profiles display a random behaviour. For example, from a one kilometre long road profile we cannot compute the shape of the following kilometre. Thus, it is natural to model the profiles as stochastic processes. Moreover, stochastic modelling provides a tool for data compression. The measured profiles (5–45 km long, sample distance 5 cm) have 10^5–10^6 sample points. A stochastic model can characterise these large data sets, using only a few model parameters.

The statistical parameters should, ideally, define the important road characteristics, i.e. two roads with similar parameter values should induce a similar amount of fatigue damage to a vehicle. The parameters could then be used to compare different geographical regions or road types, and define normal/severe conditions for operating vehicles. Also, an accurate stochastic model enables extrapolation to events which have not been measured. Thus, from a limited

number of road measurements, it will be possible to predict the properties of unobserved extreme irregularities.

This thesis is focused on road statistics, not vehicle modelling or fatigue assessment. The main goal is to define a stochastic road model. A secondary goal is to develop an evaluation tool for comparing stochastic road models with respect to accuracy. The vehicle modelling and fatigue assessment are used primarily for road model validation. Observe that the purpose is *not* to accurately assess the fatigue damage of a specific vehicle component when the vehicle travels over a given road stretch. Firstly, that would demand a complex vehicle model. And, secondly, it would necessitate a more precise description of the component's fatigue properties, possibly taking into account mean stress effects, the order of appearance of large load cycles, the fatigue limit, crack closure features, etc.

The task of extracting vehicle fatigue relevant information from a measured profile is complicated by the fact that different vehicles and their components react differently to the same road. Moreover, the vehicles may, of course, travel at different velocities. Hence, analysis of a road profile must extract general information, relevant for a wide range of vehicles travelling at different velocities.

2 Methodology

The proposed methodology to find an appropriate stochastic road-profile model, is divided into six steps (also presented in Figure 2):

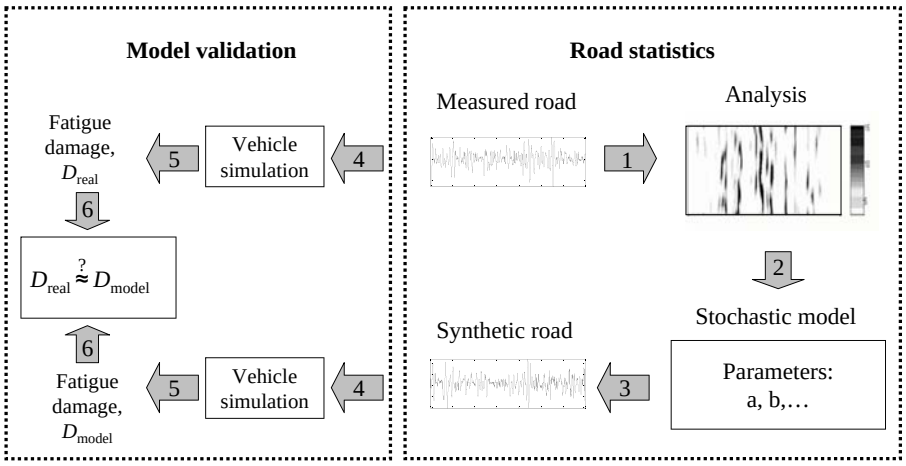

Figure 2: Overview

1. A measured road is statistically analysed.
2. A stochastic model is defined based on the analysis.
3. Synthetic (computer simulated) roads are generated according to the model assumptions.
4. A vehicle is simulated travelling at constant speed over the measured and synthetic roads.
5. The vehicle fatigue damage-values D_{real} and D_{model} indicated by the measured and the synthetic roads are computed.
6. The accuracy of the road model is assessed by comparison of indicated fatigue damage-values.

The steps 1–2, where a measurement is characterised by a few parameters, are given the main attention in this thesis. The steps 3–6 are performed primarily to validate the stochastic model and its parameter values. Several velocities are used in step 4 to avoid velocity-dependent road modelling. Similarly, in step 5, a range of fatigue properties is utilised to minimise the risk of vehicle-dependent road modelling.

3 A brief literature survey

3.1 Analysis and modelling of single profiles

Historically, analysis of road profiles has been performed in the frequency domain, using 'Power Spectral Density' (PSD) analysis. Several studies (e.g. [2]–[8]) have shown that the shape of the analysed PSD is independent of road type. Andrén [9] compiles 11 different parametric PSD approximations suggested in the road statistics literature. One of these PSD parameterisations is standardised in ISO 8608, 'Mechanical vibration — Road surface profiles — Reporting of measured data' [10].

In mathematical statistics, the outcome of a PSD analysis of a stationary process is treated as an estimate of a true spectrum. Further, it is convenient (and common) to assume Gaussianity in conjunction with PSD analysis, since a Gaussian process is uniquely defined by its spectrum.

However, in actual roads there usually exist irregular sections, with properties significantly deviating from the properties of surrounding sections. Such deviant parts, *irregularities*, appear too seldom in Gaussian models. Thus, recently, several papers are devoted to this deviance from Gaussianity: Bruscella et al [11] compute the mean-square of the second derivative of the road level along the road, in order to locate deviant parts. Steinwolf et al [12] and Öijer and Edlund [13] utilise wavelets to locate deviant parts. Wei and Fwa [14] use a wavelet transform to define a new roughness index. Frinkle et al [15] decompose the road profile into constitutive positive (bumps) and negative (holes) events.

Chaika and Gorsich [16] describe a statistical test suitable to check road profile stationarity.

Numerous stochastic models of road profiles can be found in the literature. Stationary Gaussian models with given frequency domain characteristics are by far the most common (e.g. [2]–[4], [17]–[21]). Another stationary Gaussian model is the ARMA-model [22]. Other propositions are a Markov chain model [23] and a transformed Gaussian model [24].

A widely used roughness statistic is the 'International Roughness Index' (IRI), which quantifies the roughness of a measured profile. The computation of the IRI is based on computer simulation of a quarter-vehicle travelling at 80 km/h on the profile. The IRI is defined as the accumulated suspension motion of the quarter-vehicle divided by the travelled distance. Thus, this measure is vehicle and velocity dependent. However, here, it is not suitable to use the IRI since more specific road information is needed, e.g. severity of irregularities, occurrence rate of irregularities, etc. For an introduction to IRI, see [25] and [26].

3.2 Joint analysis and modelling of parallel profiles

The covariation between left and right wheel-path has not been as extensively studied as the variation within one track. Historically, analysis of parallel road tracks has also been performed in the frequency domain, i.e. by estimation of spectra, coherence and phase function. However, there has been a shortage of large data sets of simultaneously measured parallel tracks. For example, the study in 1978 by Bormann [27] included analysis of three roads. The total length of these measurements was 800 meters.

A series of papers [2], [17], and [18], describe the homogeneous, isotropic Gaussian model. Homogeneity and isotropy imply that all profiles following a straight-line on the road surface have the same statistical properties, irrespectively of direction and position of the line. The accuracy of the isotropic model is further studied in [19] and [28]–[30].

Some different Gaussian parallel tracks models are proposed in the literature: the Parkhilovskii model [31], the isotropic model [2], the anisotropic Heath model [29] and the Ammon model [4], which were published in 1968, 1973, 1989 and 1991, respectively. For a comparison of the Parkhilovskii and the isotropic model, see [32]. Gaussian models are still widely used, for recent publications, see [30] and [33]–[36].

4 A short introduction to vehicle fatigue

4.1 Vehicle models

Fatigue damage is assessed by studying a quarter-vehicle model travelling at constant velocity on single profiles (Papers A–C & F) and a half-vehicle model travelling at constant velocity on parallel profiles (Papers D–E). The models are shown in Figure 3. These very simple models cannot be expected to predict loads on a physical vehicle exactly, but they will high-light the most important road characteristics as far as fatigue damage accumulation is concerned; they might be viewed as 'fatigue-load filters'. The models comprise masses, linear springs and linear dampers; the only non-linearity is their ability to loose road contact. The parameters are set to mimic heavy vehicle dynamics. Vehicle fatigue is assessed by analysis of the forces acting on the sprung mass.

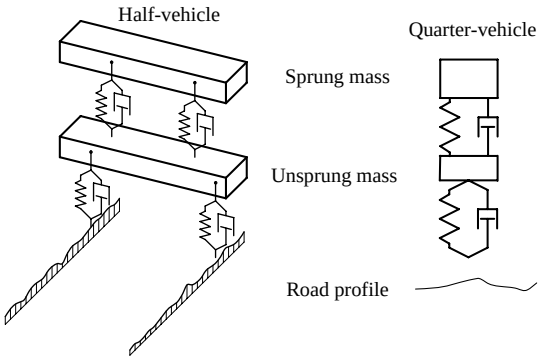

Figure 3: The half- and quarter-vehicle models

4.2 Vehicle fatigue

A common laboratory experiment is to subject test specimens to a sinusoidal load with amplitude U, and count the number of cycles N to breakdown. Commonly, the simple parametric model $N(U) = k^{-1}U^{-\beta}$ (Basquin's relation, [37]) is fitted to experimental data from (almost) identical specimens. Usually, for vehicle components, the fatigue exponent β takes values between 3 and 8. Hence, increasing the amplitude rapidly decreases the number of cycles to failure. However, loads caused by road roughness fluctuate randomly. To assess the fatigue damage, it is necessary to extract cycles from the load sequence.

The load sequence acting on the sprung mass is rainflow-counted, to extract the load cycles U_j. The rainflow counting method was introduced by Endo in 1968 [38]. A simplified equivalent definition was given by Rychlik [39]. This

definition (stated below) enables uncomplicated cycle extraction, as illustrated in Figure 4.

Definition (*Rainflow cycle*) From each local maximum M_j one shall try to reach above the same level, in the backward (left) and forward (right) directions, with an as small downward excursion as possible. The minima m_j^- and m_j^+ on each side are identified. That minimum which represents the smallest deviation from the maximum M_j is defined as the corresponding rainflow minimum. The j:th rainflow cycle is defined as $(m_j^{\texttt{RFC}},M_j)$.

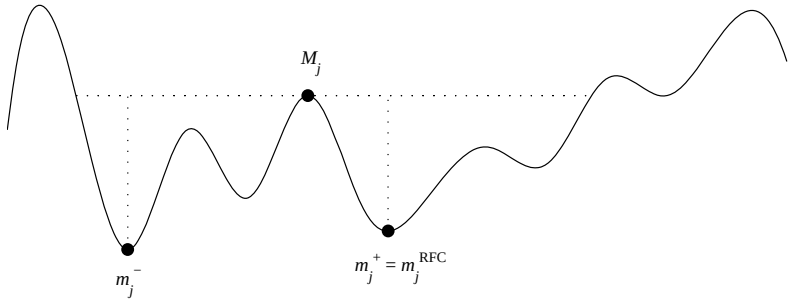

Figure 4: Definition of the rainflow cycle as given by Rychlik.

Palmgren-Miner's linear accumulation hypothesis ([40], [41]) is used to estimate fatigue damage. Thus, the damage caused by the j:th cycle equals $1/N(U_j)$, where $U_j = M_j - m_j^{\texttt{RFC}}$. The total fatigue damage caused by the rainflow-counted load sequence is

$$D = k \sum_j U_j^\beta.$$

Computations of fatigue damage from a given load sequence is performed using WAFO, which is a MATLAB toolbox developed by Mathematical statistics, Lund University [42].

5 Overview of appended papers

The main part of this thesis is presented in the appended papers.

5.1 Paper A

This paper is a preliminary study: five simple road models are evaluated. The purpose is to investigate if there are any straight forward simple models, which give satisfactory results. The PRS-model coincides with the suggestion in the

standard ISO 8608. More precisely, the road is characterised by the two spectral parameters $G_d(0.1)$ and w, which are estimated according to the standard.

The empirical marginal distribution of the measured profiles deviates from the Gaussian distribution. Therefore a transformed Gaussian model is also studied. Unfortunately, the outcome shows that the Gaussian models and the transformed Gaussian model are unsatisfactory. Adding squared shaped potholes to a Gaussian process improves the results slightly, but further studies of transient events are needed (see Paper B).

5.2 Paper B

In this paper a method is presented for automatic identification of rough road sections, irregularities. These irregularities are shown to cause the major part of the vehicle fatigue damage. Based on this result, a stochastic model is proposed, which includes irregularities. The model is further evaluated in Paper C.

Irregularities are identified using a normalised spectrogram. Figure 5 shows such a normalised spectrogram of the three kilometres of road 7 shown in Figure 1. High values of the normalised spectrogram are indicated by the black areas. Two identified irregularities, one long-wave (LW) and one short-wave (SW) are shown in Figure 6.

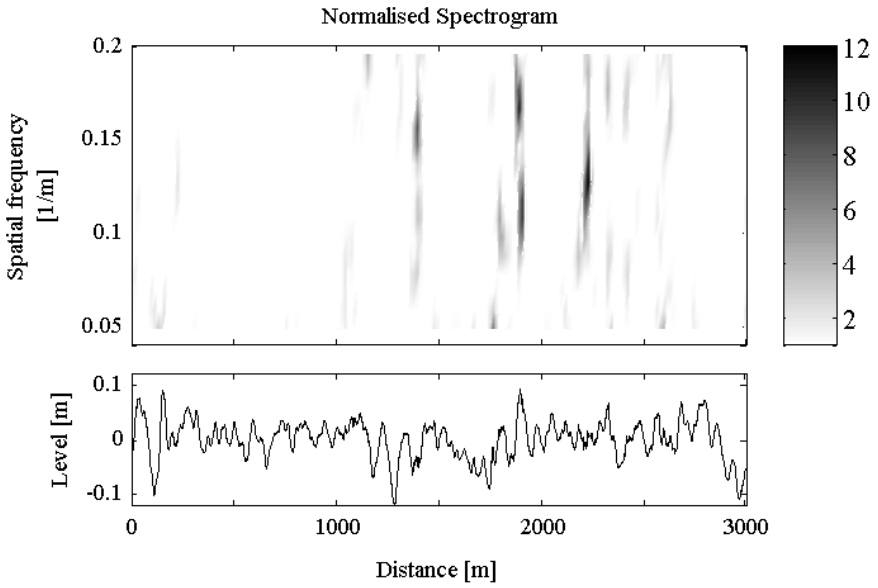

Figure 5: A normalised spectrogram of a measured profile.

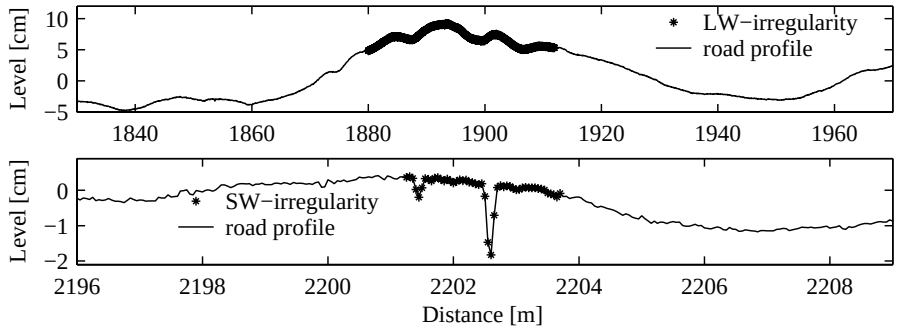

Figure 6: Automatically identified irregularities.

The damage caused by the irregularities is compared to the total damage caused by the whole road, for different velocities and different values of β. The results verify the importance of the irregularities. The outcome at $v = 60$ km/h and $\beta = 5$ is presented in Figure 7. As seen, the irregularities cover only 4–9 % of the total distance, but they cause the major part of the damage, 59–96 %.

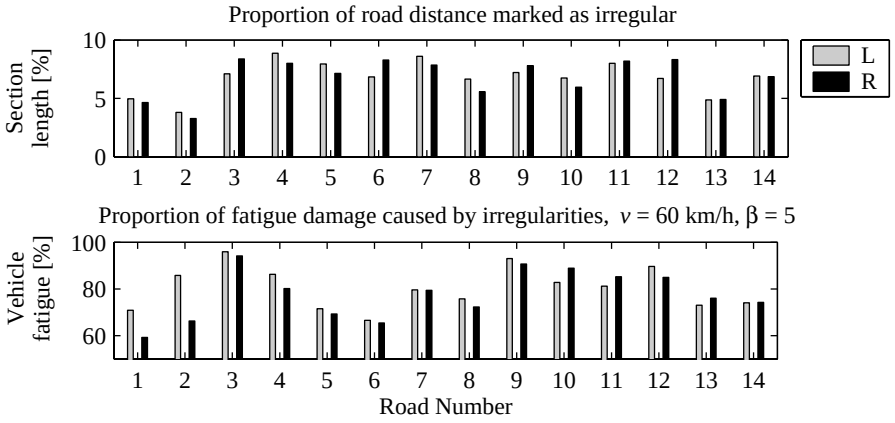

Figure 7: The irregularities' impact on vehicle fatigue.

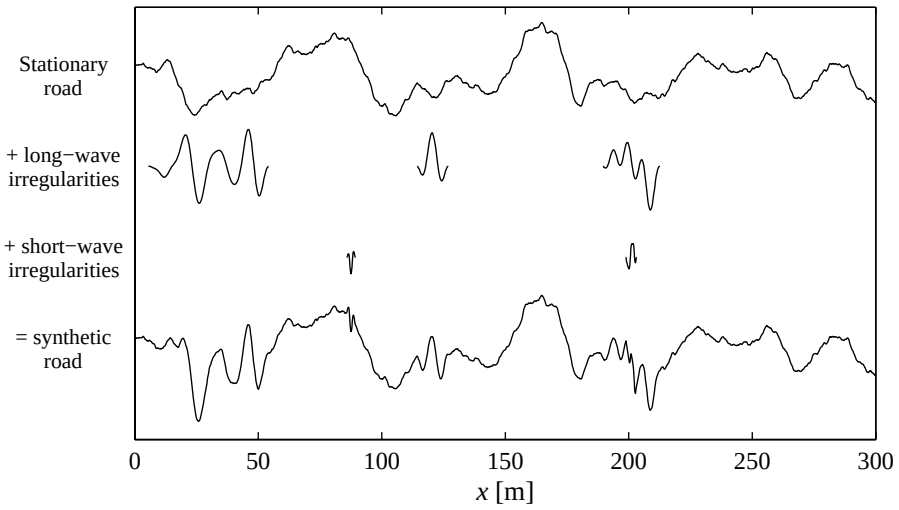

Figure 8: A synthetic road profile, realized from the RS-model.

The proposed Roughness Summation (RS) model, superimposes 'irregularities' of random shape, location and length onto a stationary Gaussian process. The irregularities are of two types: long-wave and short-wave, which occur independently of each other. The superimposed long-wave and short-wave irregularities are modelled as non-stationary Gaussian processes. An example of a realized road is shown in Figure 8.

5.3 Paper C

Several stochastic models of single road profiles are proposed in the literature; some examples were given above in the literature survey (Section 3). However, there is no generally accepted method to evaluate the vehicle fatigue relevance of road models. Thus, an objective method to compare accuracy of these models is needed. This paper describes such a method.

A lack-of-fit measure is defined which quantifies discrepancy between a model and a measurement. A target region of [-4, 4] is set for the lack-of-fit. Values outside this interval indicate unsatisfactory model performance. An example is shown where a Gaussian model, a transformed Gaussian model and the model proposed in Paper B (the RS-model) are compared. The result is shown in Figure 9. The benefit of introducing irregularities in a road model is demonstrated: The RS-model satisfies the target in 11 out of 14 roads, whereas the two other models only satisfy the target in 1 out of 14 roads.

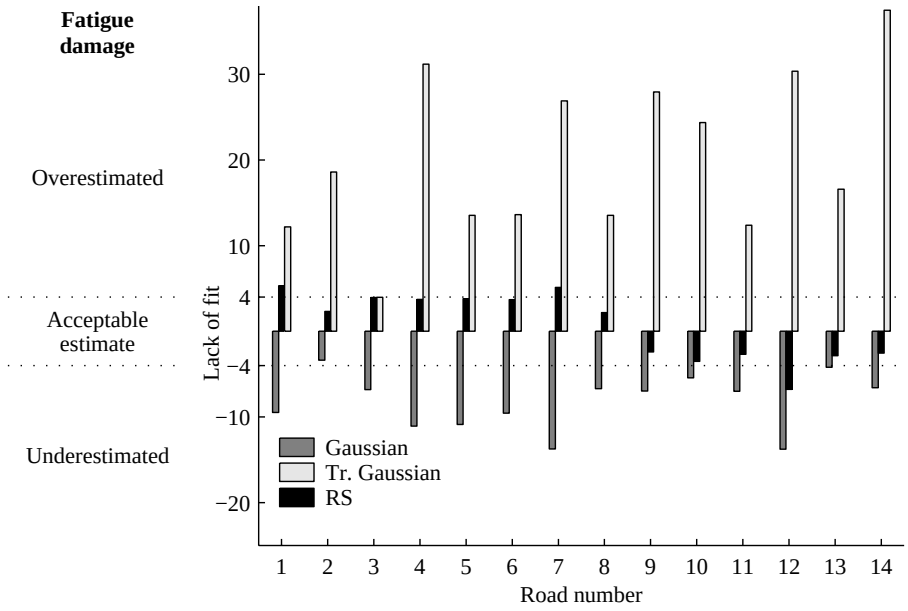

Figure 9: Results from Paper C, lack of fit for three models.

5.4 Paper D

Here, the evaluation method in Paper C is extended to models of parallel tracks. Two models are evaluated accordingly, referred to as Models A and B. Model A is the isotropic Gaussian model [2], and Model B is a new model, an extension of the single track model in Paper C. Figure 10 shows a 300 meter long realization from Model B. The model comprises three two-dimensional components, a Gaussian process, long-wave irregularities and short-wave irregularities. The two black lines of each component correspond to left and right wheel-path. Similar to Paper C, a lack-of-fit measure is defined which quantifies discrepancy between a model and a measurement. If the absolute value of the lack-of-fit measure $|\delta_{\max}|$ belong to the interval $[0, 5]$, $(5, 7]$ or $[7, \infty)$ then the model accuracy is deemed satisfactory, doubtful or unsatisfactory, respectively.

The evaluation results unambiguously show that Model B surpasses Model A. Model A is inaccurate: It has 0 satisfactory, 2 doubtful and 18 unsatisfactory values of $\delta_{\max}$. Model B performs better: It has 7 satisfactory, 9 doubtful and 4 unsatisfactory values of $\delta_{\max}$.

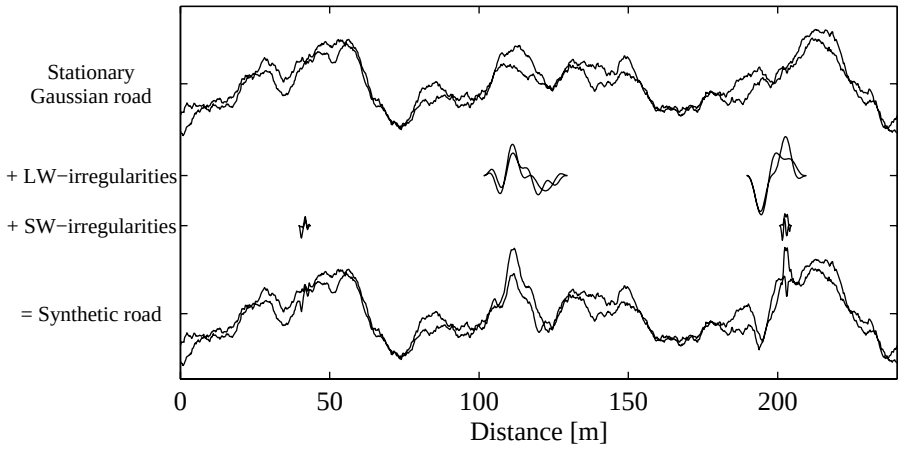

Figure 10: A realization from Model B in Paper D.

5.5 Paper E

This paper is devoted to the coherence between left and right wheel-path, when the paths are 2 meters apart. Two basic results are presented, concerning classification and the isotropic assumption.

It is difficult to distinguish between road types by coherence analysis of parallel road tracks. Figure 11 presents a typical analysis result of three very different roads, a smooth motorway, a semi-smooth main road and a very rough gravel road. The left plot shows estimated spectra from left and right tracks and the right plot shows estimated coherence between left and right tracks. The spectra are clearly separated, whereas the coherence functions are very similar. Thus, a motorway can have the same empirical coherence function as a very rough gravel road.

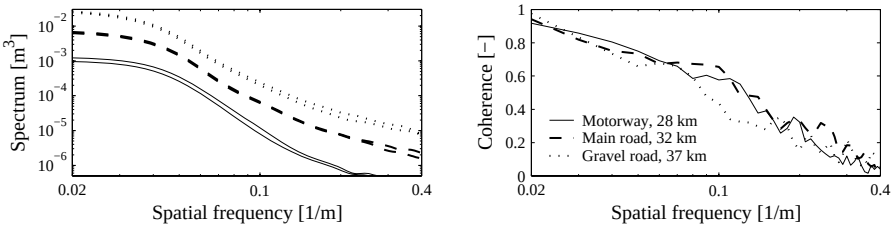

Figure 11: Spectrum and coherence functions

Often (e.g. [2], [10], [18], [33], [35]) roads are assumed to be isotropic surfaces. However, the results in this paper clearly show that the isotropic model is not accurate enough: it underestimates roll disturbance. Instead of the isotropic model, a more accurate parametric coherence model is proposed.

In the paper from 1973 by Dodds and Robson a figure is shown where the empirical coherence functions from a motorway and a minor road are very different (Figure 6, page 181 in [2]). Also, Ammon concludes in his study from 1991 that that the isotropic model overestimates the roll disturbance (page 35 in [4]). These two results are not in line with the results in this study. A reason may be that the modern measurement equipment used nowadays make it easier to collect longer measurement. As mentioned earlier, in this study 520 km have been analysed. The analysed measurement length in [2] and [4] are not given, but are both most likely shorter than 520 km. If so, the increased measurement length can perhaps explain the different results.

5.6 Paper F

A new method to compute the expected vehicle fatigue damage caused by road irregularities is presented. Figure 12 shows the expected vehicle damage-intensity due to road irregularities of same statistical properties but different length. The stationary level, marked by the dashed line, is the damage-intensity that an infinitely long irregularity would induce. With parameter values set as in the example in Figure 12, the expected damage of 30 irregularities of length 20 m is similar to the expected damage of one irregularity of length 60 m. This kind of length effects are important to consider when designing test sequences.

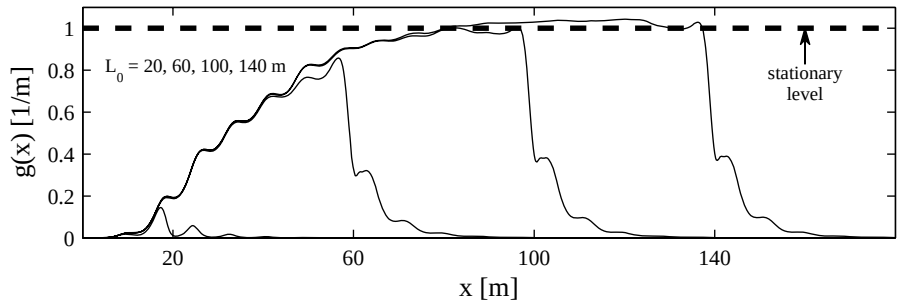

Figure 12: Damage-intensity for different irregularity lengths. (Normalised so that the stationary level is one.)

6 Conclusions

- It is quite difficult to create a synthetic road profile that causes the same amount of vehicle fatigue damage as a measured profile.
- Stationary Gaussian models are not accurate models of road profiles.
- Stochastic models need to include irregularities.
- The normalised spectrogram (Paper B) is a suitable tool for identification of road irregularities.
- Irregularities are conveniently modelled as non-stationary Gaussian processes.
- A motorway can have the same empirical coherence function as a very rough gravel road.
- The proposed simple parametric model in Paper E gives better coherence approximations than the isotropic model.
- The lack-of-fit measures in Papers C and D facilitates objective comparison of road-profile models.
- The suggested road-profile model perform significantly better than traditional road-profile models from the literature.

References

[1] Ahlin K, Granlund J and Lindström F (2004), Comparing road profiles with vehicle perceived roughness, *Int. J. Vehicle Design*, Vol. 36, Nos. 2/3, pp. 270–286.

[2] Dodds CJ and Robson JD (1973), The description of road surface roughness, *J. Sound and vibration*, Vol. 31, pp. 175–183.

[3] Dodds CJ (1974), The laboratory simulation of vehicle service stress, *J. Engineering for industry*, ASME transactions, pp. 391–398.

[4] Ammon D (1991), Problems in road surface modelling. *Vehicle System Dynamics*, Vol. 20, pp. 28–41.

[5] Kropáč O and Múčka P (2004), Non-standard longitudinal profiles of roads and indicators for their characterisation, *Int. J. Vehicle Design*, Vol. 36, Nos. 2/3, pp. 149-172.

[6] Rouillard V, Sek MA and Perry T (1996), Analysis and simulation of road profiles, *J. Transportation Engineering*, Vol. 122, No. 3, pp. 241–245.

[7] Šprinc J, Kropáč O, Šprinc M (2002), Characterization of Longitudinal Road Unevenness in the Light of the International PIARC – EVEN Experiment 1998, *Vehicle System Dynamics*, Vol. 37, No. 4, pp. 263–281.

[8] Heath AN (1988), *The mechanics of dynamic pavement loading by heavy vehicles*, PhD thesis, Department of Mechanical and Manufacturing Engineering, University of Melbourne, Australia.

[9] Andrén P (2006), Power spectral density approximations of longitudinal road profiles, *Int. J. Vehicle Design*, Vol. 40, No. 1/2/3, pp. 2–14.

[10] ISO 8608 (1995), *Mechanical Vibration — Road Surface Profiles — Reporting of Measured Data*, International Organization for Standardization, Geneva.

[11] Bruscella B, Rouillard V and Sek MA (2000), Classification of road profiles, *J. Transportation Engineering*, Vol. 126, No. 1, pp. 41–45.

[12] Steinwolf A, Giacomin JA and Staszewski WJ (2002), On the need for bump event correction in vibration test profiles representing road excitations in automobiles, *J. Automobile Engineering*, Proc. of the institution of mechanical engineers, Part D, Vol. 216, pp. 279–295.

[13] Öijer F and Edlund S (2004), Identification of Transient Road Obstacle Distributions and Their Impact on Vehicle Durability and Driver Comfort, *Supplement to Vehicle System Dynamics*, Vol. 41, pp. 744–753.

[14] Wei L and Fwa TF (2004), Characterizing road roughness by wavelet transform, Pavement Rehabilitation, strength and deformation characteristics and surface properties. *Transportation Research Record*, Vol. 1869, pp. 152–158.

[15] Frinkle M, Weir R and Ferris JB (2004), A graphical representation of road profile characteristics, *SAE technical paper series*, 2004-01-0769.

[16] Chaika M and Gorsich D (2004), Some statistical tests in the study of terrain modelling, *Int. J. Vehicle Design*, Vol. 36, Nos. 2/3, pp. 132–148.

[17] Kamash KMA and Robson JD (1977), Implications of isotropy in random surfaces, *J. Sound and Vibration*, Vol. 54, No. 1, pp. 131–145.

[18] Kamash KMA and Robson JD (1978), The application of isotropy in road surface modelling, *J. Sound and Vibration*, Vol. 57, No. 1, pp. 89–100.

[19] Cebon D and Newland DE (1983), The artificial generation of road surface topography by the inverse FFT method, *Proc. 8th IAVSD Symposium on the dynamics of vehicles on roads and on railway tracks*, Cambridge, MA, pp. 29–42.

[20] Sun L and Deng X (1998), Predicting Vertical Dynamic Loads Caused by Vehicle-Pavement Interaction. *J. Transp. Engineering*, Vol. 124, Issue 5, pp. 470-478

[21] Gonzalez OM, Jauregui JC, Lozano A and Herrera G (2007), Effect of road profile on heavy vehicles with air suspension, *Int. J. Heavy Vehicle Systems*, Vol. 14, No. 1, pp. 98-110.

[22] Zhu JJ and Zhu W (1996), Stochastic modeling of pavement roughness, *28th Southeastern Symposium on System Theory*, pp. 28–32.

[23] Ferris JB (2004), Characterising road profiles as Markov chains, *Int. J. Vehicle Design*, Vol. 36, Nos. 2/3, pp. 103–115.

[24] Steinwolf A and Connon WH (2005), Limitations on the use of Fourier transform approach to describe test course profiles, *Sound and Vibration, the noise and vibration control magazine*, Vol. 39, No. 2, Acoustical Publications Inc, pp. 12–17.

[25] Sayers MW (1995), On the Calculation of International Roughness Index from Longitudinal Road Profile, *Transportation Research Record 1501*, pp. 1–12.

[26] Sayers MW and Karamihas SM (1997), The Little Book of Profiling, University of Michigan Transportation Research Institute. *http://www.umtri.umich.edu/content/LittleBook98R.pdf*

[27] Bormann V (1978), Messungen von Fahrbahn-Unebenheiten paralleler Fahrspuhren und Anwendung der Ergebnisse, *Vehicle System Dynamics*, Vol. 7, pp. 65–81.

[28] Heath AN (1987), Application of the isotropic road roughness assumption. *J. Sound and Vibration*, Vol. 115, No. 1, pp. 131–144.

[29] Heath AN (1989), Modelling and simulation of road roughness. *Proc. 11th IAVSD symposium. The Dynamics of vehicles on roads and on tracks*, pp. 275–284.

[30] Lu Sun and Jie Su (2001), Modeling random fields of road surface irregularities, *Int. J. Road Materials and Pavement Design*, Vol. 2, No. 1, pp. 49–70.

[31] Parkhilovskii IG (1968), Investigation of probability characteristics of surfaces of distributed types of roads. *Avtom. Prom.* Vol. 8, pp. 18-22 (In Russian).

[32] Robson JD (1978), The Role of the Parkhilovskii Model in Road Description, *Vehicle System Dynamics*, Vol. 7, pp. 153-162.

[33] Sun L, Kenis W and Wang W (2006), Stochastic spatial excitation induced by a distributed contact on homogenous Gaussian random fields. *J. Engineering Mechanics* Vol. 132, No. 7, pp. 714–722.

[34] Song Jian and Jin Ruichen (1999), Generation of virtual road surfaces and simulation of nonlinear vibration of vehicles. *Proc. IEEE International vehicle electronics conference* (IVEC'99), Vol. 1, Changchun, China, pp. 355–359.

[35] Szöke D and Kuti I (2004), A new development in the numerical description of road profile realisations. *Int. J. Vehicle Design*, Vol. 34, No. 2, pp. 183–190.

[36] Zhang Younglin, Zhang Jiafan (2006), Numerical simulation of stochastic road process using white noise filtration, *Mechanical Systems and Signal Processing*, Vol. 20, No. 2, pp. 363–372.

[37] Basquin OH (1910), The exponential law of endurance tests. *American Society for Testing and Materials*. Vol. 10, Part II, pp. 625–630.

[38] Matsuishi M and Endo T (1968), Fatigue of metals subjected to varying stress, Paper presented to Japan Soc. Mech. Eng. Jukvoka, Japan.

[39] Rychlik I (1987), A new definition of the rainflow cycle counting method, *Int. J. Fatigue*, Vol. 9, pp. 119–121.

[40] Palmgren A (1924), Die Lebensdauer von Kugellagern. *Zeitschrift des Vereins Deutscher Ingenieure*, Vol. 68, pp. 339–341.

[41] Miner MA (1945), Cumulative damage in fatigue. *J. Applied Mechanics*, Vol. 12, pp. 159–164.

[42] WAFO, A MATLAB Toolbox for analysis of random waves and loads. *http://www.maths.lth.se/matstat/wafo/*, Lund University, 2005.

A

Paper A

Fatigue relevant road surface statistics

KLAS BOGSJÖ AND ANDERS FORSÉN

Summary

Road roughness is a major source of vehicle fatigue. To improve the understanding of vehicle durability, statistical methods are applied to characterise measured road profiles. Different statistical road models are used to generate corresponding synthetic road profiles. Vehicle fatigue is assessed utilising a simple quarter-vehicle model in combination with the Palmgren-Miner damage hypothesis, Basquin's relation and Rainflow counting. Several road realizations (Monte-Carlo simulation) provide an estimate of the expected fatigue damage. The results suggest that actual roads cause more damage than synthetic Gaussian roads, possibly due to occasional road transients (bumps and holes), causing large loads on the vehicle. Thus, a road model being the sum of Gaussian 'noise' and transient events is suggested.

1 Introduction

Road roughness is a major source of vehicle fatigue. Statistical analysis provides compact description of measured roads and offers the possibility to generate synthetic 'statistically equivalent' roads.

The overall target is to find a statistical, parametric road profile description, with as few parameters as possible, which can be used to generate synthetic road profiles for test and simulation purposes. Expected vehicle fatigue should differ less than, say, 10 %, between actual and synthetic roads characterised by the same parametric description (a very ambitious target).

The study consists of statistical analysis of measured road profiles, Monte-Carlo simulation of road profiles and assessments of fatigue damage induced in vehicles.

The measured road profile data used in this study is highpass filtered prior to analysis, to remove long-wave disturbances (hills), which are irrelevant to road-induced vehicle fatigue, and to remove spurious results caused by profile measurement system 'drift'.

2 Road profile characterisation

Reporting of road profile measurements is standardised by ISO [1]. Wavelengths between 0.1 and 100 m are considered relevant to road-induced vibrations.

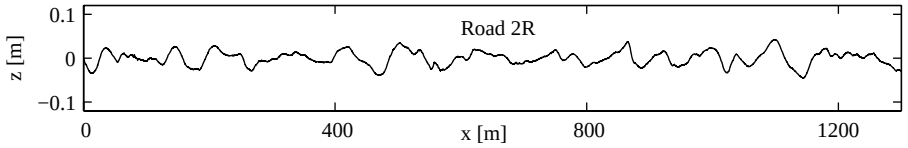

Figure 1: Road profile sample

Data from three road measurements are utilised. Profiles from left and right wheel-path are designated 'Road 1L', 'Road 2R' etc. Profiles are characterised by probability distribution and spectrum ("smoothed spectrum" according to ISO 8608).

2.1 Distribution of road elevation

2.1.1 Upcrossing intensity

The upcrossing intensity is proportional to the probability density function if the derivative at all locations x, is independent of the value of the process (i.e. the profile height) at the same location x. This is the case for stationary Gaussian processes [2].

2.1.2 Empirical road level distributions

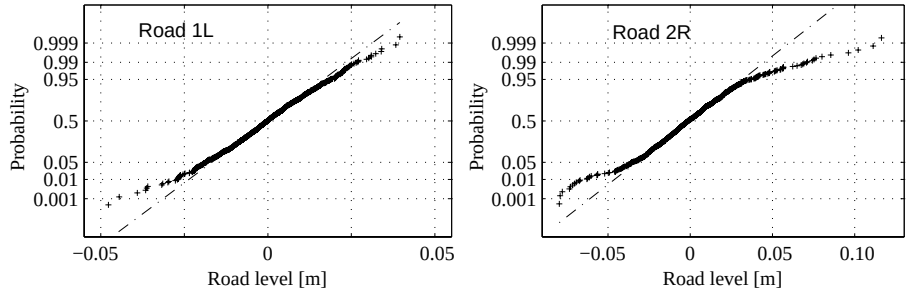

Figure 2: Distribution of measured road data compared to the Gaussian (Normal) distribution.

Figure 2 shows that the height distribution of Road 1L and Road 2R is very close to Gaussian for values above the smallest 2 % and below the highest 2 %. However, the highest and lowest values differ clearly from the Gaussian distribution, especially for Road 2 (and Road 3).

2.1.3 Non-Gaussian distribution

Gaussian distributions are convenient in statistical analysis, but real roads are not Gaussian, as shown in Figure 2. One way to handle this problem is to transform the actual distribution to a Gaussian, perform the statistical analysis on the transformed data, and finally apply an inverse transformation. With this method, it is possible to design a synthetic road with statistical properties similar to the measured road's.

The transformation is estimated by applying a smoothing process to the actual (measured) road profile's distribution, an example is shown in Figure 3.

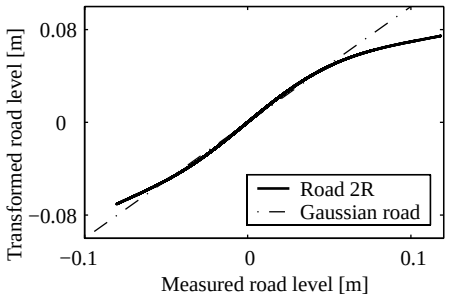

Figure 3: Smoothed transformation

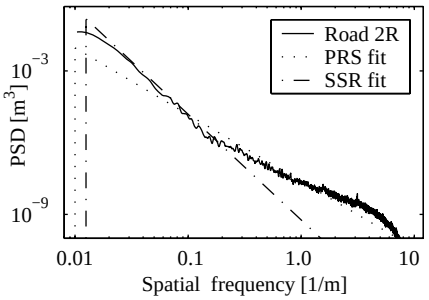

Figure 4: Estimated and fitted spectra

2.2 Spectral analysis

Four different ways to parameterise the measured road's spectra are investigated.

2.2.1 PRS: Gaussian distribution, broad-band spectrum fit

ISO 8608 [1] suggests a straight line fit in log-log scale (Figure 4) to the power spectrum generated from the measured road profile. The resulting parametric road spectrum (PRS) is described by:

$$R_{\mathrm{PRS}}(n) = \begin{cases} A(\frac{n}{n_0})^{-w}, & 0.01 < n < 10, \\ 0, & \text{otherwise}, \end{cases} \tag{1}$$

where n_0 is 0.1 m^{-1} and A indicates degree of road unevenness. Parameter values are determined by least-square fit over the spatial frequency range 0.011 – 2.83 m^{-1}. For the three measured roads utilised in this study A varies around 10^{-5} and w around 2–3.

2.2.2 SSR: Gaussian distribution, resonance-band spectrum fit

An important range to fit correctly to the road spectrum is the frequency range containing the lowest resonance frequency of the vehicle, i.e. 1–2 Hz. When the vehicle travels at constant velocity v m/s, the corresponding spatial frequency range becomes:

$$1/v < n \leq 2/v. \tag{2}$$

The shifted spatial frequency range (SSR) spectrum is defined by least square fit in this range,

$$R_{\mathrm{SSR}}(n) = \begin{cases} A(\frac{n}{n_0})^{-w}, & n_{\mathrm{start}} < n < 10, \\ 0, & \text{otherwise}, \end{cases} \tag{3}$$

followed by adjustment of the lower frequency limit to preserve the measured profile's variance σ^2, cf Figure 4.

$$n_{\mathrm{start}}(n) = \max \begin{cases} \left(10^{1-w} - \frac{1-w}{An_0^w}\sigma^2\right)^{\frac{1}{1-w}}, \\ 0.01 \end{cases} \tag{4}$$

2.2.3 DSE: Gaussian distribution, direct spectrum estimate

In order to be able to produce synthetic roads with similar power spectrum as real roads, the power spectrum of the actual road is smoothed and utilised for generation of synthetic road profiles. This method to generate synthetic roads with a power spectrum given by a Direct Spectrum Estimation is labelled DSE.

2.2.4 TrDSE: Transformed Gaussian distribution, direct spectrum estimate

The procedure outlined in Section 2.1.3 is applied, an empirical transformation function is estimated from the measured road profile and utilised to produce a transformed road profile. This profile is then analysed and its spectral parameters are calculated with the DSE method described above. The road is described by:

1. A transformation function (Figure 3).
2. The direct spectrum estimate of the transformed road (Figure 4).

2.3 Sampling and signal length

The highest spatial frequency of interest in the present study is 10 m^{-1}. (The tires are assumed to smooth disturbances shorter than 0.1 m, i.e. spatial frequencies higher than 10 m^{-1}.) Theoretically, the sample rate has to be at least twice the highest frequency in the signal to avoid aliasing. Thus, with appropriate filtering prior to digitalisation, a sampling frequency of 20 m^{-1} should be adequate, but proper description of transient's shape may well require higher sample rates.

Roads 1 and 2 are measured with a sample distance of 0.05 m, just about adequate for random (non-transient) road profiles. Unfortunately the sample distance in road 3 measurement is twice the theoretical minimum, 0.1 m.

To get a smooth and detailed response spectrum, even if the vehicle has narrow (undamped) resonance peaks and travels at high velocity, a fine spatial frequency resolution, maybe $4 \cdot 10^{-4}$ m^{-1}, is desirable. This sets the signal length requirement to (at least) 2.5 km. This is fulfilled by the studied roads, the measured distance on roads 1 and 2 being 5 and 5.8 km, while the measurement on road 3 covers 25 km.

Longer measurements reduce statistical uncertainty and scatter; longer measurements also increase the probability that several rare events (large transients) are included, thus enabling statistical analysis of the extreme events. An old MIRA investigation [3] concludes that in order to get stable statistics of road induced loads in vehicles, the measured distance should be at least 100 miles (160 km). However, this is not fulfilled by the three studied road samples, which are 5–25 km long.

3 Synthetic road realization

A stationary zero-mean Gaussian process is uniquely defined by its spectrum. Thus, when the spectrum is known, any number of statistically equivalent realizations may be created. (The realization method is briefly described in the appendix).

The six measured and analysed road profiles provide parameter values to five different stochastic models of each road profile:

- PRS: Gaussian with parameters from a 'broad-band' evaluation of the real road.
- SSR: Gaussian with parameters from a Shifted Spatial Range evaluation.
- DSE: Gaussian with a direct spectrum estimation of the real road.
- TrDSE: Non-Gaussian, being the inverse transformed realization of a Gaussian process with a direct spectrum estimate of the transformed

road's spectrum.

- SSRq: Non-Gaussian road, q artificial holes per km added to the SSR model.

The software MATLAB is utilised to create 80 realizations of each road and model, in total $80 \cdot 6 \cdot 5 = 2400$ synthetic road profiles. An actual, measured road profile is compared to corresponding realizations of synthetic roads in Figure 5.

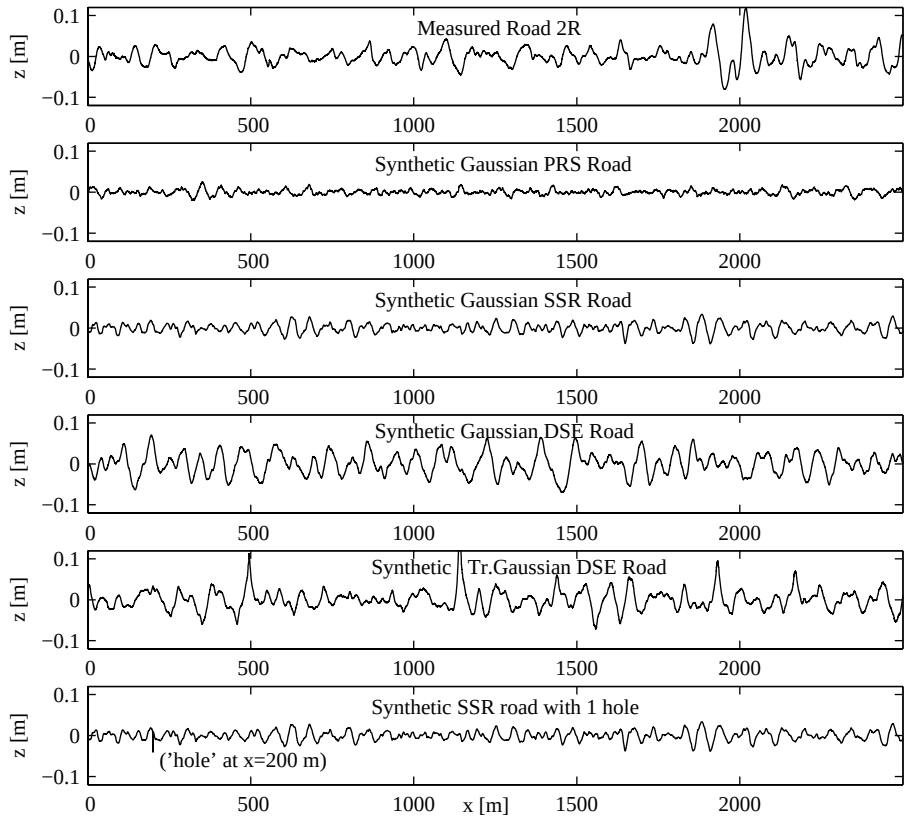

Figure 5: Measured road and synthetic roads.

Realizations of synthetic road profiles are given the same length as the measured profiles, 5.8, 5 and 25 km, respectively. Figure 5 is limited to the first 2.5 km to improve readability.

The Gaussian PRS and SSR road realizations appear different from the measured road. The Gaussian DSE and transformed Gaussian DSE roads are more similar to the measured profile, but still give a different impression, although they have the same variance, similar spectrum and similar upcrossing intensity as the actual road. Furthermore, the variance of the derivative of these processes also agrees with the measured roads'.

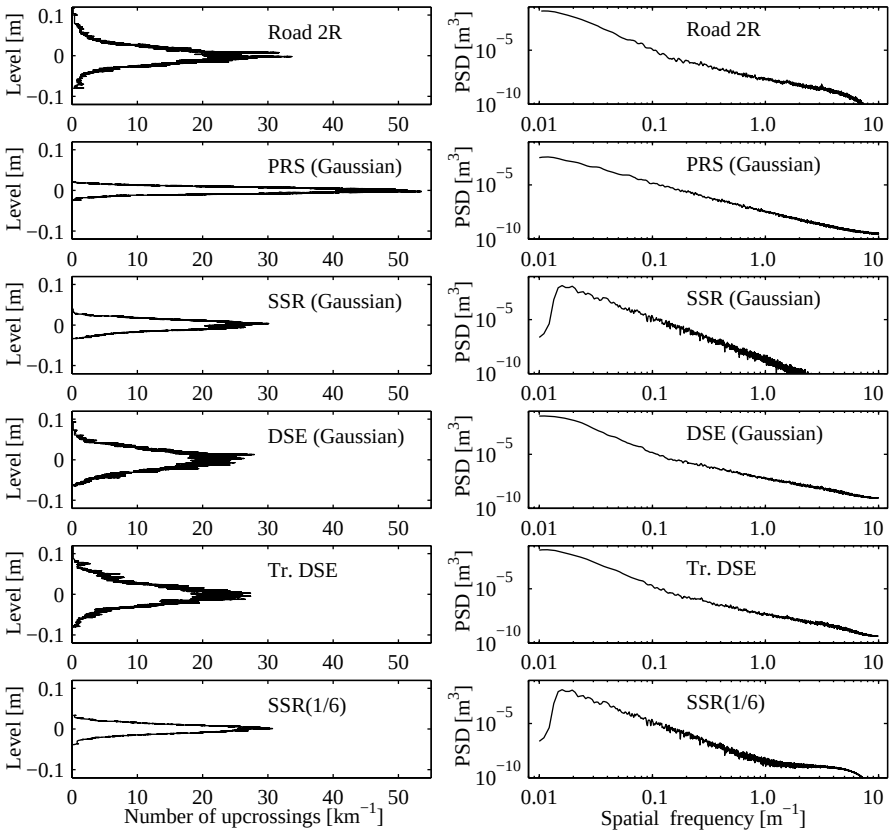

Figure 6: Upcrossing intensity and power spectral density.

Level crossings and PSD:s in Figure 6 result from analysis of one realization. Thus, they may differ somewhat from the theoretical distribution and parametrically described spectra of the corresponding road model.

4 Vehicle fatigue assessment

Fatigue damage is assessed by studying a quarter-car model travelling at constant velocity on (actual or synthetic) road profiles. This very simple vehicle model cannot be expected to predict loads on a physical vehicle exactly, but it will high-light the most important road characteristics as far as fatigue loading is concerned; it might be viewed as a 'fatigue load filter'. The utilised quarter-car model includes one non-linearity: it may lose road contact; otherwise it's linear with parameter values modelling a heavy truck.

The total force acting on the sprung mass is rainflow-counted and the resulting load cycles evaluated with Palmgren-Miners linear damage accumulation hypothesis. Fatigue strength is described by Basquin's relation, i.e. $s^\beta N = \text{constant}$, where s is load cycle amplitude, β fatigue exponent and N number of cycles to failure. For vehicle components, β is usually in the range $3 - 8$, making it most important to describe load cycles with large amplitude accurately.

5 Durability simulation results

Vehicle simulations are performed with three velocities, 15, 19 and 23 m/s. Fatigue damage is calculated for each of the resulting $3 \cdot (2400 + 6) = 7218$ load sequences, using 6 fatigue exponents, $\beta = 3, 4, \ldots, 8$. The 'Monte-Carlo' simulation result thus comprises 43308 fatigue damage values. All results are normalised with the fatigue damage indicated for the corresponding measured road profile.

The stochastic road modelling makes every realization of a road profile different, although it is based on the same model and parameter values. Naturally, the calculated fatigue damage will also vary from one road realization to the next. The mean result from a number of realizations provides an estimate of the expected fatigue damage on the studied stochastic road. Averaging all results from each input combination reduces the simulation output to 540 values and enables evaluation of the road models' performance as a function of physical road, fatigue exponent and vehicle velocity.

Figure 7 shows the relative damage of Road 1R, $v = 23$ m/s. Figure 8 shows the relative damage of Road1R, $v = 15$ m/s. Figures 7 and 8 illustrate a typical result, the PRS model underestimates the fatigue damage in all cases, the SSR(1/6) model performs quite well at 23 m/s on road 1R, but it is less satisfactory at 15 m/s. Detailed analysis indicates that this is due to a vehicle resonance, which occurs at 15 m/s on the measured road profile, but is absent at 23 m/s.

Figure 9 summarises the results of the study, the 108 mean relative damage values obtained for each road model are grouped according to calculated damage:

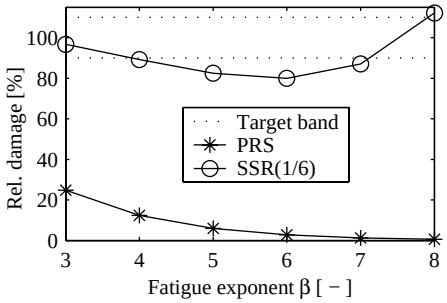

Figure 7: Road1R, v=23 m/s

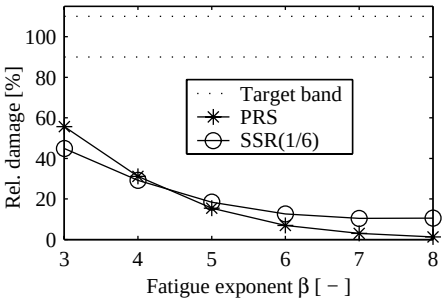

Figure 8: Road1R, v=15 m/s

- less than half the damage indicated on the measured road (unsatisfactory)
- 50 – 90 % of damage indicated on the measured road
- 90 – 110 % of damage indicated on the measured road (on target)
- 110 – 200 % of damage indicated on the measured road
- more than twice the damage indicated on the measured road (unsatisfactory)

Figure 9 shows that none of the investigated road model fulfils the ambitious target: mean relative damage 90 – 110 %, irrespective of velocity and fatigue exponent. The purely Gaussian road models underestimate the imposed fatigue damage in almost every case, while non-Gaussian TrDSE model frequently overestimate the fatigue damage, often overshooting the target grossly (relative damage 10^5 in several cases). Usually the result deteriorates with increasing fatigue exponent β, as illustrated in figures 7 and 8.

6 Conclusions

- Gaussian models PRS, SSR and DSE give non-conservative fatigue estimates.
- The PRS model coincides with the method suggested in ISO 8608 [1].
- The non-Gaussian TrDSE model produces very conservative fatigue estimates.
- Standard stochastic analysis, (transformed) Gaussian models, is insufficient.

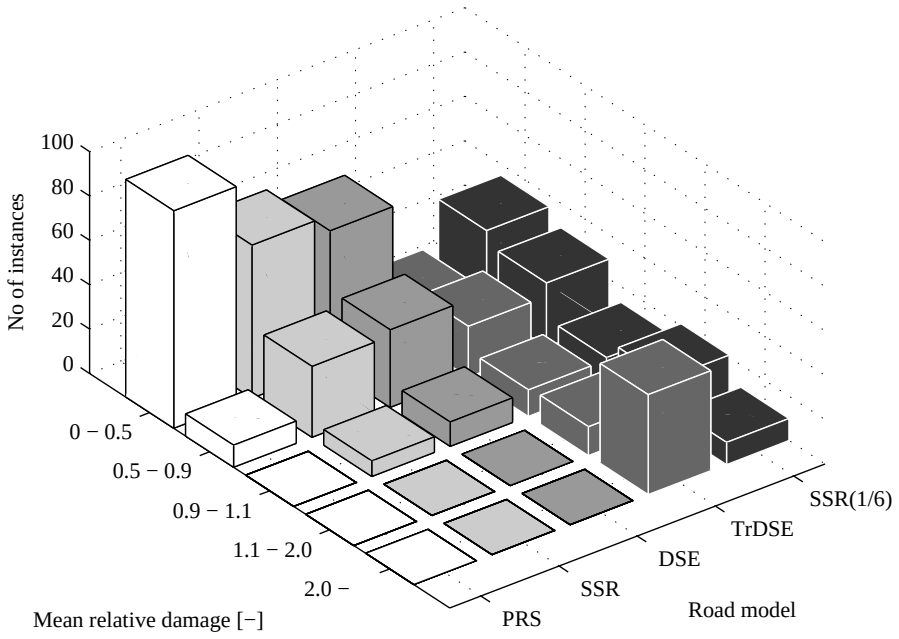

Figure 9: Monte-Carlo simulation results

- A prototype model SSRq (Gaussian 'noise' with added transients) is promising.
- It is quite difficult to create a synthetic road that causes the correct amount of fatigue damage, probably due to fatigue's sensitivity to occasional large load cycles, i.e. occasional transients in the road profile.

7 Discussion and comments

Fairly good roads, on which a 'normal' driver keeps essentially constant velocity, are investigated. Bad and inhomogeneous roads, where the driver adapts his driving to the varying conditions, may require a more sophisticated approach.

Sampling distances in road profile measurements should be quite small to catch road transients, preferably in the range 0.005 – 0.01 m, but conventional sampling distances are 0.05 – 0.1 m. This makes it difficult to investigate shape, size and frequency of transient events ('holes' and 'bumps') in actual roads.

Synthetic roads with manually added 'holes' display an interesting behaviour, especially when β is large, as illustrated in Figure 7. This suggests a

way to deal with the problem of occasional road transients and corresponding large load cycles.

The unsatisfactory performance of the transformed Gaussian DSE road model might be due to shortcomings in the transformation function, Figure 5 indicates that the TrDSE model produces too many large peaks. Another possible cause of the difficulties is that the transformation procedure assumes (strictly) stationary data. If this assumption is not fulfilled, the transformation function should be altered along the road. Longer measurements increase the likelihood of non-stationary data, thus increasing the modelling difficulty, but longer measurements also improve the chance of creating a realistic model, by decreasing the statistical uncertainty and forcing the analyst to consider the physical reality of non-stationary roads.

Acknowledgement

The support and encouragement offered by professors Georg Lindgren and Igor Rychlik, Mathematical Statistics, Lund Institute of Technology, is gratefully acknowledged.

References

[1] ISO 8608. *Mechanical Vibration — Road Surface Profiles — Reporting of Measured Data*. International Organization for Standardization, Geneva, 1995.

[2] Rice, S.O.: The mathematical analysis of random noise. *Bell Syst Techn. J.*, Vol 23 (1944), pp. 282–332.

[3] Drury, C.G. and Overton, J.A.: *Vehicle service loads. Part I: A preliminary study of stress level counting*. MIRA report No 1964/8.

[4] WAFO, a MATLAB Toolbox for Analysis of Random Waves and Loads. *http://www.maths.lth.se/matstat/wafo/*, Lund University, 2000.

[5] Wittig, L.E. and Sinha, A.K.: Simulation of multicorrelated random processes using the FFT algorithm. *Journal of Acoustical Society of America*, Vol. 58, No 3 (1975), pp. 630–634.

[6] Hudspeth, R.T. and Borgman, L.E.: Efficient FFT simulation of Digital Time Sequences. *Journal of the Engineering Mechanics Division*, ASCE, Vol 105, No EM2 (1979), pp. 223–235.

Appendix: Synthetic road realization

Two kinds of distributions are used to create synthetic roads, Gaussian and transformed Gaussian. To create a transformed Gaussian processes, a transformation function is applied to the generated Gaussian data. All calculations are performed with MATLAB and the WAFO toolbox [4]. The method to generate realizations of a Gaussian road with given spectrum is described briefly below, see [5] and [6] for a detailed explanation.

To create a Gaussian road realization with K samples, a set of K independent Gaussian random numbers $\zeta_k = \xi_k + i\eta_k$ is created, such that $\mathrm{E}(\xi_k) = \mathrm{E}(\eta_k) = 0$ and $\mathrm{E}(\xi_k^2) = \mathrm{E}(\eta_k^2) = 0.5$. Next, a vector $Z = [Z_0, \ldots, Z_{K-1}]$ is defined, where

$$Z_k = \sqrt{\frac{K}{2h} a_k}\ \zeta_k, \quad k = 0, \ldots, \frac{K}{2}.$$

The second half of vector Z is found from the property $Z_k = Z^*_{K-k+1}$, where * denotes complex conjugate. The parameter h is the sample distance in the realization and a_k is given by:

$$a_k = \frac{1}{Kh} \int_{(k-1/2)/(Kh)}^{(k+1/2)/(Kh)} R(n)\mathrm{d}n,$$

where $R(n)$ is the one-sided spectrum. The realization of the Gaussian process is obtained by taking the inverse FFT of Z:

$$z(x_j) = \frac{1}{K} \sum_{k=0}^{K-1} Z_j e^{\frac{i2\pi kj}{K}}, \quad j = 0, \ldots, K-1, \quad x_j = jh.$$

B

Paper B

Development of analysis tools and stochastic models of road profiles regarding their influence on heavy vehicle fatigue

K. Bogsjö
Lund Institute of Technology, Sweden

Road profiles are analysed with focus on road characteristics essential for heavy vehicle fatigue assessment. Road profile measurements indicate that roads contain short sections with above-average irregularity. Such rough sections are shown to cause most of the vehicle fatigue damage. An algorithm using a spatial-frequency description is developed to automatically identify rough sections. Based on the analysis a new stochastic road model, with randomly placed and randomly shaped irregularities, is proposed.

Keywords: Road roughness; stochastic road model; vehicle fatigue
2000 Mathematics Subject Classification: 62–07; 62M15; 62P30

1 Introduction

A vehicle in normal operation is exposed to occasional high loads. In vehicle durability assessment it is important to have an accurate statistical description of these high loads, which often are caused by road irregularities. A road model including such irregularities is proposed in this paper.

Stochastic modelling can be useful in several aspects. For example, the model parameters can be used to numerically quantify roughness severity. Thus, a model can be used to group roads into different roughness categories, in order to be able to comprehend large data sets. Also, the randomness described by the stochastic model enables studies of uncertainties of, for example, fatigue life.

The conventional statistical method for road profile evaluation models the road profile as a Gaussian process, with spectral density estimated from measured data [1]. However, a stationary Gaussian model is insufficient as a road model, as demonstrated in [2–6].

The proposed model is tested on records from 14 actual roads, measured in left and right wheel-path. The measure equipment is described in [12]. The total length of these roads is 370 km. The measured roads are of varying quality, ranging from smooth motorways to very rough gravel roads. The profiles are high pass-filtered prior to analysis, to remove measurement drift and hills (very long-wave 'disturbances').

In Section 2 an algorithm for automatic identification of rough road sections is presented. In Section 3 it is shown that the identified parts have a large impact on vehicle fatigue. In Section 4 the proposed road model is described. In Section 5 parameter estimation is discussed, and finally, in Section 6, the new road model is evaluated.

2 The normalised spectrogram as roughness indicator

Very rough short sections, irregularities, can be observed in the measured roads. In the literature there are several algorithms proposed to identify road profile irregularities, see for example [2–5]. The identification methods described in [2–5] are rather complex: in [2] a flowchart diagram is used, in [3–4] wavelets are used and in [5] singular value decomposition is used. Here, a simpler approach is proposed. Straight-forward evaluation according to equations (1)–(4) locates irregular sections.

2.1 The spectrogram, location dependent spectrum estimates

The function $z(x)$ describes the road elevation at spatial location x. Let $z(kh)$ denote a sampled road profile with sample distance h. The road is divided into sections $z(kh + k_i h),\ k = 0, \ldots, N_H - 1$, where $k_i h$ is the start and $x_i = k_i h + N_H h/2$ the middle point of the i:th section. Each section is multiplied with a Hanning window, $H(kh)$, with N_H samples and length $L_H = hN_H$ meters. The number of samples N_H is assumed even. (Also, as customary the window is normalised, $\sum_{k=1}^{N_H} |H(kh)|^2 = 1$.) Let $\xi_n = n/L_H, n = 0, \ldots, N_H/2$, be the Fourier frequencies. The spectrogram $R(x_i, \xi_n)$ describes frequency content of the road around location x_i,

$$R(x_i, \xi_n) = 2h \left| \sum_{k=0}^{N_H - 1} H(kh) z(kh + k_i h) \exp(-\frac{j2\pi kn}{N_H}) \right|^2, i = 1, \ldots, N_R, \quad (1)$$

where N_R is the number of analysed sections. To avoid frequency leakage from lower frequencies to higher frequencies $z(x)$ is high-pass filtered prior to the computation.

The choice of window length L_H is crucial. A long window yields a high resolution in the frequency domain, but a poor spatial resolution. Another parameter that must be chosen is the midpoint distance, $\delta = x_{i+1} - x_i$, which together with L_H decides the amount of section overlap (e.g. $\delta = L_H$ implies no overlap). The choice of the δ and L_H will be discussed in Section 2.3.

Obviously, if $z(x)$ is a random stationary process (for example Gaussian) the spectrogram $R(x_i, \xi_n)$ will vary randomly but have similar properties for different x_i. Road sections with increased roughness will be indicated by anomalies in $R(x_i, \xi_n)$. In the following subsection a criterion for identification of irregularities is suggested.

2.2 Roughness criterion

First the *normalised spectrogram* is defined as

$$R_{\text{norm}}(x_i, \xi_n) = \frac{R(x_i, \xi_n)}{\frac{1}{N_R}\sum_{i=1}^{N_R} R(x_i, \xi_n)}. \tag{2}$$

The maximum over the different frequencies ξ_n in the set A,

$$M(x_i; A) = \max_{\xi_n \in A} R_{\text{norm}}(x_i, \xi_n), \tag{3}$$

will be used to identify rough sections. More precisely, a section $[x_i - \delta/2, x_i + \delta/2]$ is marked as deviant if

$$M(x_i; A) > u, \tag{4}$$

for a suitably chosen critical level u and spatial frequency set A.

2.3 Parameter choices for identification of rough road sections

To use $M(x_i; A)$ for identification of rough road sections values of the following parameters must be chosen: window length L_H, midpoint distance δ, threshold level u and frequency interval A. Road vehicle characteristics need to be considered in order to choose A appropriately.

Frequency analysis of strain measurements in heavy vehicles usually displays a peak at approximately 1 Hz and another in the 10–15 Hz range. Specific, local, resonances add to this general pattern. In the considered velocity range, 40–90 km h^{-1} (typical truck velocities on the measured roads) road irregularities with spatial frequencies from 0.04–0.20 m^{-1}, will excite the low-frequency (ca 1 Hz) resonance. Similarly, road irregularities at higher spatial frequencies, up to 1.0 m^{-1}, will excite the 10–15 Hz resonance.

Thus, road irregularities are divided in two classes: short-wave and long-wave. The first type has high spectral density in the range 0.04–0.20 m^{-1}. The second type has a high spectral density in the range 0.20–1.0 m^{-1}. The two types are identified separately, by means of two sets A, see Table 1. Parameter values in the table are chosen by studying typical values of peaks in the normalised spectrogram. The thresholds are chosen so that only extreme peaks

are identified. In the short-wave region, the extreme peaks are higher than in the long-wave region, hence the threshold is higher in the short-wave region.

Irregularity type	A [m^{-1}]	L_H [m]	δ [m]	u
Long-wave	[0.04, 0.20]	64	16	7.6
Short-wave	[0.20, 1.0]	10	2.5	50

Table 1: Parameter values for identification of long-wave and short-wave irregularities

2.4 Examples from measured roads

The spectrogram provides information about roughness variation along the road. It is easy to visualise the difference between a measured road and a stationary Gaussian road. Figure 1 shows a normalised spectrogram of one km of the second measured road, left wheel path: road 2L. High values of R_{norm} are indicated by the black areas. Three irregularities are indicated by the thick lines in the bottom plot.

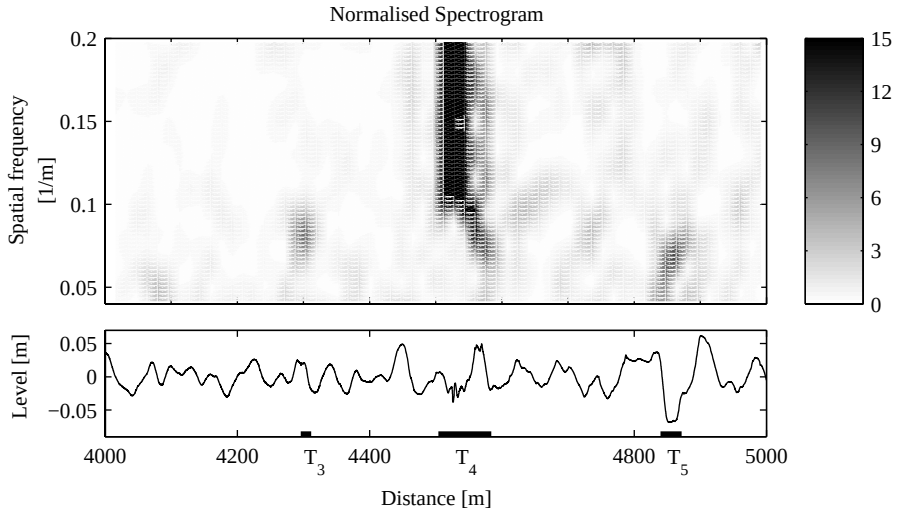

Figure 1: Normalised spectrogram of one km of a measured profile. The sections T_3, T_4 and T_5 identify deviant sections.

For comparison Figure 2 shows a normalised spectrogram of a Gaussian process with a spectral density equal to the estimated spectral density of road 2L.

One can see that the normalised spectrogram of the Gaussian process does not contain any high peaks.

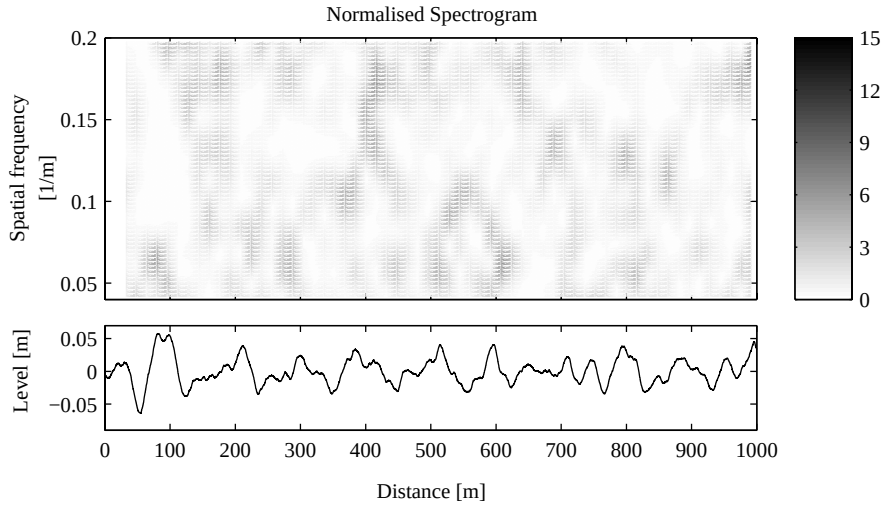

Figure 2: Normalised spectrogram of a synthetic (computer simulated) Gaussian road.

Figure 3 shows two examples of identified irregularities, high-lighted by the thick lines above the horizontal axis.

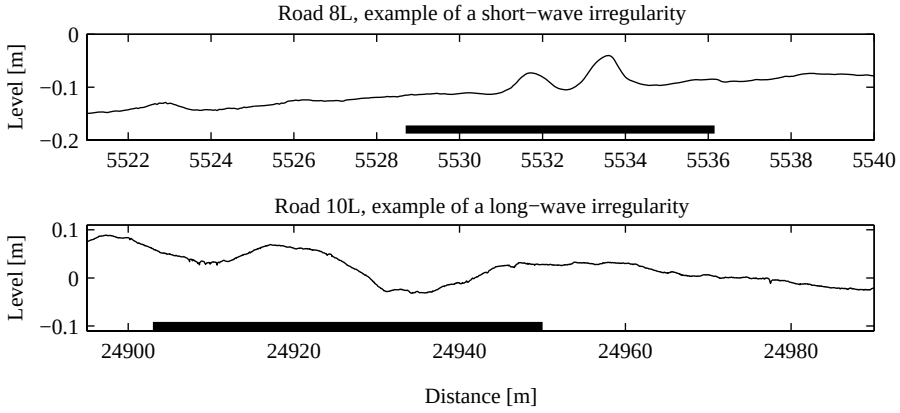

Figure 3: A short-wave irregularity (top) and a long-wave irregularity (bottom).

3 Impact of irregularities on fatigue damage

Fatigue damage is assessed by studying a quarter-vehicle model travelling at constant velocity on road profiles. This very simple vehicle model can not be expected to predict loads on a physical vehicle exactly, but it will high-light the most important road characteristics as far as fatigue damage accumulation is concerned; it might be viewed as a 'fatigue load filter'. In this study the model comprises masses, linear springs and linear dampers; the only non-linearity is the ability to loose road contact. The parameters are set so that the dynamics of the model resembles a heavy vehicle. Velocities in the range 40–90 km/h, the typical velocities on the measured roads, are studied.

The total force acting on the sprung mass of the quarter-vehicle model is rainflow-counted [7]. The resulting load cycles are evaluated with Palmgren-Miner's linear damage accumulation hypothesis. Fatigue strength is described by Basquin's relation, i.e. $s^\beta N_F = C$, where s is load cycle amplitude, β fatigue exponent, C is a constant and N_F number of cycles to failure. Here, the value of C is unimportant, since only relative damage values will be studied, i.e. damage values will be given in percent. For vehicle components, β is usually in the range 3–8 [13], making it most important to describe load cycles with large amplitude accurately.

With the suggested criterion, roughly 5–10 % of the roads are marked as irregular. However, this small portion causes most of the fatigue damage in the vehicle!

For each road, rough sections are detected using the criterion $M(x_i; A) > u$. The identified sections are removed and replaced by smooth sections to give a modified smoothened road. A Gaussian process with parameters estimated from the 'non-rough' parts of the road is used to design a smooth replacement for the removed section, conditioned on the surrounding 'known' observations. Computations of the conditional expected profiles are performed with the WAFO toolbox [8]. An example of a conditional expected Gaussian process is given in Figure 4 (solid line).

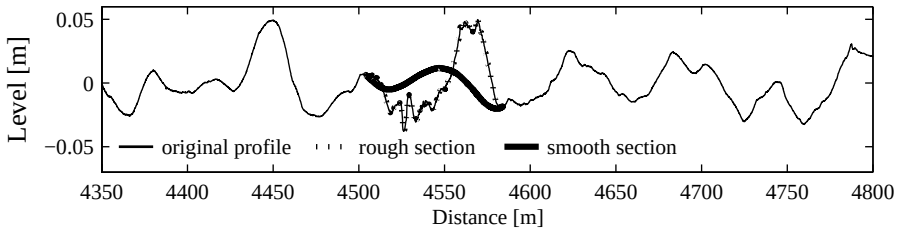

Figure 4: An identified irregularity (dotted) in road 2L replaced by a smooth road section (solid).

Vehicle damage is assessed: D_{orig} is the damage caused by the original road and D_{smooth} is the damage caused by the smoothed road. The effect of the irregularities is $100(D_{\text{orig}} - D_{\text{smooth}})/D_{\text{orig}}$ %. If all sections caused the same amount of damage, then one would expect smoothing 5 % of the road to reduce damage by about 5 %. But, as Figure 5 shows, this is not the case.

The identified rough sections cover on average 6.8 % of the total length of the road. The irregularities contribute to a large portion of the vehicle fatigue damage. How significant the impact of the irregularities is, depends mainly on the fatigue exponent β but also on vehicle velocity. Figure 5 shows the result when $\beta = 6$ and $v = 60$ km/h for each road, left and right track; the mean portion is then 87 %. For other choices of β, the mean vehicle fatigue is given by the left plot in Figure 6. Increased impact of the irregularities for increased β is due to a property of fatigue; large β gives more weight to large load cycles. The mean vehicle fatigue as a function of velocity is shown in the right plot. A slight decrease in the damage proportion caused by the irregularities is observed when the velocity increases.

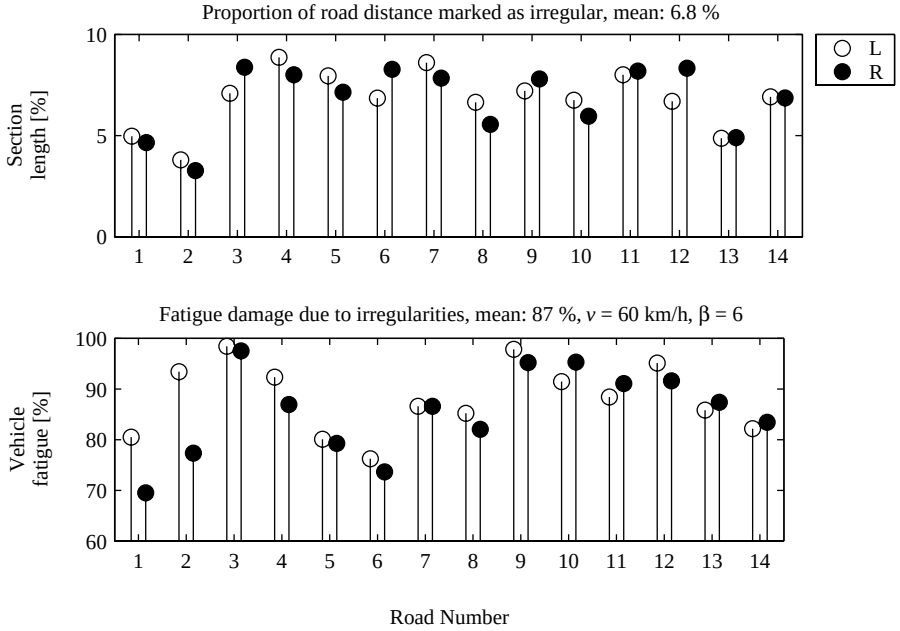

Figure 5: Fatigue relevance of identified irregularities. L = left wheel-path, unfilled dot. R = right wheel-path, filled dot.

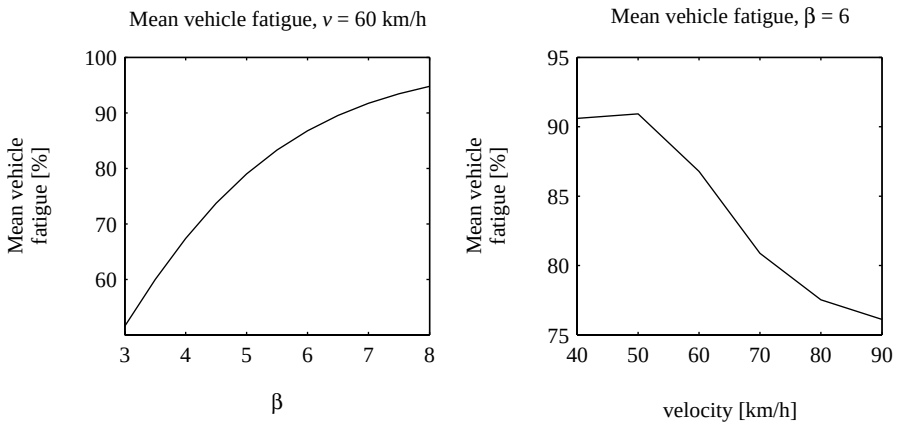

Figure 6: Mean vehicle fatigue caused by irregularities as a function of β (left) and velocity (right).

4 Synthetic road profile generation — The Roughness summation model

In Section 3 it was shown that the measured roads contain rough parts, which cause most of the vehicle fatigue. Therefore the method to generate synthetic roads should include such rough parts.

The main variability in the road profile is described by the stationary Gaussian process $Z(x)$, with spectrum

$$R(\xi) = \begin{cases} 10^{\mathrm{a}} \left(\frac{\xi}{\xi_0}\right)^{-w}, & 0.01 \leq \xi \leq 10, \\ 0, & \text{otherwise}, \end{cases} \tag{5}$$

where $\xi_0 = 0.1$ m^{-1}. In order to add rough parts, irregularities of two types, long-wave and short-wave, are superimposed to $Z(x)$. The two types occur independently of each other. To exemplify, a 2 km long road is generated with two irregularities of each type added in the interval 100 – 400 meters, see Figure 7. Note that, as the example shows, long-wave and short-wave irregularities may overlap. Moreover, the i:th long-wave irregularity and the k:th short-wave irregularity are described by the processes $Z_L^i(x)$ and $Z_S^k(x)$.

To avoid discontinuities at the start and end of a rough section, the added irregularity starts and ends with two values equal to zero. Thus, the irregularities are non-stationary and hence it is impossible to assign a spectral density to them. However, an irregularity reaching from $-\infty$ to $+\infty$ is stationary. The spectral densities of such infinite length long-wave and short-wave irregularities

are of the same form as the full road spectrum (5) but restricted in frequencies and described by three parameters b, c and w (i.e. the spectrum 'slope' w is unchanged),

$$\text{Long-wave:} \qquad R_L(\xi) = \begin{cases} 10^{\mathrm{b}} \left(\frac{\xi}{\xi_0}\right)^{-w}, & 0.04 \le \xi \le 0.20, \\ 0, & \text{otherwise}, \end{cases} \tag{6}$$

$$\text{Short-wave:} \qquad R_S(\xi) = \begin{cases} 10^{\mathrm{c}} \left(\frac{\xi}{\xi_0}\right)^{-w}, & 0.20 \le \xi \le 1.0, \\ 0, & \text{otherwise}. \end{cases} \tag{7}$$

For finite length irregularities see Appendix A.

Furthermore, the location and length of the sections with added roughness is random. More precisely, the distance between the end of a long-wave irregularity and the start of the next is exponentially distributed with mean θ_L. Similarly, the distance between end and start of short-wave irregularities is exponentially distributed with mean θ_S. The length of long-wave and the length of short-wave irregularities are exponentially distributed with mean d_L and d_S, respectively.

In Figure 8 the function $M(x; A)/u$ is plotted for the two choices of spatial frequency regions A with corresponding threshold u, recall Table 1. Obviously, when $M(x; A)/u$ exceeds 1 an irregular section is identified. As shown in Figure 8, both types of irregularities in Figure 7 are accurately identified.

All model parameters are compiled in Table 2.

Symbol	*Description*
a	Severity level, 'regular' road
b	Severity level, LW-irregularities
c	Severity level, SW-irregularities
w	Spectral parameter, spectrum 'slope'
θ_L	Mean distance between LW-irregularities
θ_S	Mean distance between SW-irregularities
d_L	Mean length of LW-irregularities
d_S	Mean length of SW-irregularities

Table 2: Parameters in the road model, LW = long-wave, SW = short-wave.

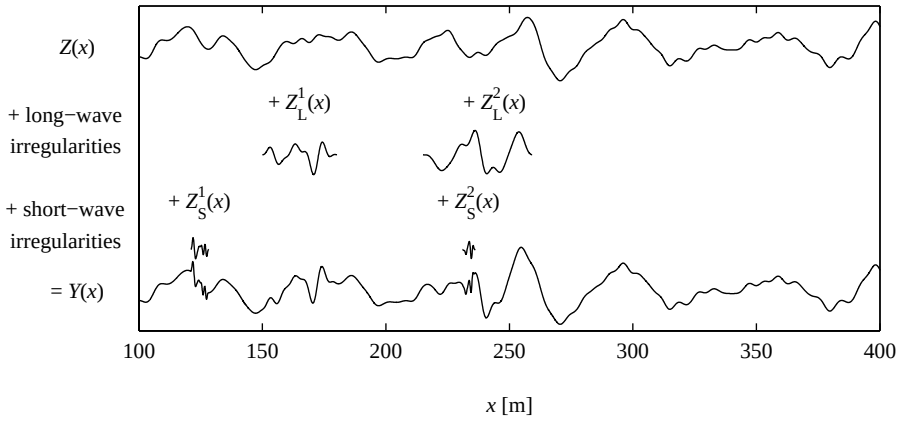

Figure 7: Superposition of irregularities to generate rough road sections.

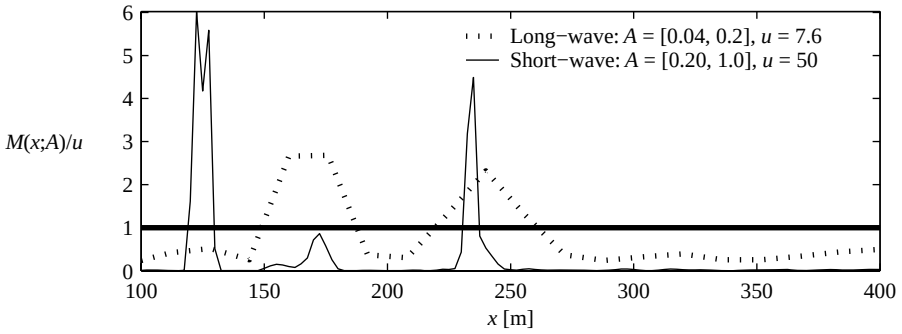

Figure 8: The test functions $M(x;A)/u$ for long-wave and short-wave irregularity identification.

5 Parameter estimation

5.1 Spectral parameters

The road model comprises four spectral parameters a, b, c and w. The parameters a and w are estimated from smooth non-irregular road sections. The parameters b and c are estimated from long- and short-wave irregularities, respectively.

The method, as described in Section 2, identifies road sections belonging to the three roughness classes: smooth sections, long-wave irregularities and short-wave irregularities.

A periodogram of each section estimates spectral density. The periodogram of a road section starting at $k_i h$ and ending at $(k_i + N_i - 1)h$, i.e. $z(kh + k_i h)$, $k = 0, \ldots, N_i - 1$, is an estimation of the one-sided spectral density and is defined by

$$I_i(\xi) = \frac{2h}{N_i} \left| \sum_{k=0}^{N_i-1} z(kh + k_i h) \exp(-j2\pi kh\xi) \right|^2 , \tag{8}$$

where N_i is the number of samples in the i:th section and h the sample distance. In order to improve the estimate a modified periodogram is used,

$$I_i^H(\xi) = 2h \left| \sum_{k=0}^{N_i-1} H(kh) z(kh + k_i h) \exp(-j2\pi kh\xi) \right|^2 , \tag{9}$$

where H is the normalised Hanning window, see Section 2.1. The modified periodogram is evaluated at the Fourier frequencies, $\xi_n = n/(N_i h), n = 0, \ldots, N_i/2$ (assuming N_i even).

To simplify notation the subscript i in I_i and I_i^H is omitted if not important. The theoretical properties of $I(\xi)$, (when z is Gaussian) can be found in [10]. Since the spectra, given by equations (5)–(7), are linear in logarithmic scale, the parameters are estimated from the least square fit of values of the logarithm of I^H. Here the base-10 logarithm is used. Fitting in logarithmic scale demands carefulness: The expectation of the logarithm $I(\xi)$ does not equal the logarithm of the true spectral density. Under the assumption that z is Gaussian this bias is computed in [11]. The bias-correction is the reversed sign of the expected value of the logarithm of a standard exponential random variable, which is +0.25068. Here, it is assumed that the result in [11] holds approximately also when the $I^H(\xi)$ is used instead of $I(\xi)$.

Since there usually are many road sections belonging to the same roughness class, several modified periodograms are computed, which estimate the same spectral density. Therefore the least-square fit is a fit of several I^H:s.

To exemplify, a 10 km long synthetic road was simulated according to the model assumptions stated in Section 4. The identification algorithm was used to

group the road sections into the different classes. Modified periodograms were computed for each section belonging to one of the three the roughness classes. In Figure 9 values of I^H are shown as dots. Bias-corrected least square fits of the logarithm of the I^H:s are given by the broken lines, which almost coincide with the true spectra given by the solid lines. (As discussed in Section 4 the irregularities are non-stationary, so their spectral densities are not defined. But if we neglect this and assume piecewise stationarity b and c may be estimated.)

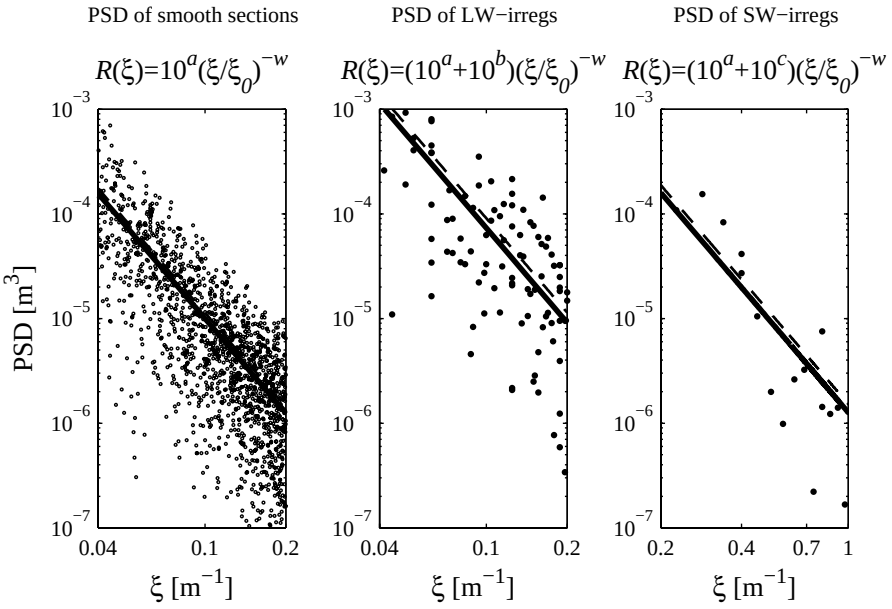

Figure 9: Power spectral densities: true spectra (solid lines), I^H-values (dots), bias corrected LS-fit of I^H-values (broken lines).

5.2 Distance parameters

The average of the empirical lengths of identified sections is used to estimate θ_L, θ_S, d_L and d_S.

6 Simulation results

Vehicle simulations are performed with six velocities, $v = 40, 50, \ldots, 90$ km/h. For each measured road profile, parameters in the Roughness summation model are estimated. 100 synthetic roads of equal length as the corresponding measured road are realised with the estimated parameter values. The mean vehicle fatigue damage per kilometre is assessed for $\beta = 3, 4, \ldots, 8$.

Since the number of measured road profiles is 14×2 (2 wheel paths for each actual road), the number of velocities is 6 and the number of studied values of β is 6, there are totally $14 \times 2 \times 6 \times 6 = 1008$ assessed mean fatigue damage values. All results are normalised with respect to the fatigue damage assessed for the corresponding measured road profile.

The vehicle fatigue damage caused by a measured road can be approximated by a sum of the damage of each individual kilometre. This division makes it possible to analyse the variability of the vehicle fatigue damage. The conclusion is that a relative damage of 50–200 % is a reasonable target. However, one may argue that it is wiser to use different targets for different roads and different values of β. But here, for sake of simplicity, a fixed target is used.

Figure 10 shows that the addition of irregularities gives a more accurate damage estimate. For example, the black dot at 64 % in the 'Damage region' 50–200 % means that, with irregularities, 64 % of the 1008 mean damages are between 50 % and 200 % compared to the damage caused by the corresponding measured road. Without irregularities only 12 % of the 1008 damages falls into that damage region.

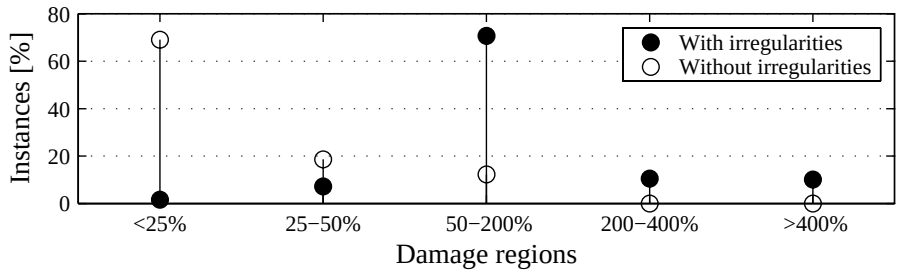

Figure 10: Mean damage values for the Roughness summation model and the stationary Gaussian model, on roads 1–14.

7 Conclusions

A large portion, 90–95 %, of the measured road length can be treated as having the same degree of unevenness. The remaining 5–10 % of the road consists of rough sections. With the proposed identification method it is possible to detect these rough sections. The detected sections cause the major part of the vehicle fatigue damage.

The general roughness is modelled by a stationary Gaussian process. To model occurrence of unusually rough parts, random irregularities are superimposed to the stationary process at random locations. The added irregularities are of two types: long-wave and short-wave. A road with such added rough parts gives a better description of measured roads than the stationary Gaussian model.

Acknowledgements

Scania and The Programme Council for Vehicle Research within The Swedish Agency for Innovation Systems (PFF/VINNOVA) have supported this work. The author is grateful to Prof. Igor Rychlik and Dr Anders Forsén for their helpful assistance.

A Simulation of a road irregularity

Here an algorithm is presented on how to simulate a road irregularity described by the random sequence $\tilde{Y}$. Let $Z(x)$ be a mean zero stationary Gaussian sequence with spectral density as Equation (6) or (7). To simplify notation, let the sampled process $Z(kh) = Z[k], k = 1, \ldots, N$. Furthermore, it is convenient to define the two column vectors $Y_1 = (Z[3] \ \ldots \ Z[N-2])^T$ and $Y_2 = (Z[1] \ Z[2] \ Z[N-1] \ Z[N])^T$, where ^{T} denotes matrix transpose. We want to simulate $Y_1|Y_2 = 0$ (i.e. condition on zero start and zero end values). Define

$$\tilde{Y} = Y_1 - \Sigma_{12}\Sigma_{22}^{-1}Y_2, \tag{A.1}$$

where $\Sigma_{12} = \mathrm{cov}(Y_1, Y_2)$ and $\Sigma_{22} = \mathrm{cov}(Y_2, Y_2)$. The expectation and covariance of $\tilde{Y}$ are

$$\begin{aligned} &\mathrm{E}[\tilde{Y}] = 0, \\ &\mathrm{cov}(\tilde{Y}, \tilde{Y}) = \Sigma_{11} - \Sigma_{12}\Sigma_{22}^{-1}\Sigma_{21}. \end{aligned} \tag{A.2}$$

This coincides with the expectation and covariance of the conditional Gaussian process of Y_1 given $Y_2 = 0$, thus $\tilde{Y}$ represents $Y_1|Y_2 = 0$. In order to compute $\tilde{Y}$ we need Σ_{12} and Σ_{22}. The (one-sided) spectral density $R(\xi)$ is used to obtain

the covariance matrices. The covariance function is

$$r(x) = \int_0^\infty R(\xi)\cos(2\pi\xi x)\mathrm{d}\xi \tag{A.3}$$

and the sampled covariance function $r(kh) = r[k]$. This gives the covariance matrices

$$\mathrm{cov}(Y_2, Y_2) = \Sigma_{22} = \begin{pmatrix} r[0] & r[1] & r[N-2] & r[N-1] \\ r[1] & r[0] & r[N-3] & r[N-2] \\ r[N-2] & r[N-3] & r[0] & r[1] \\ r[N-1] & r[N-2] & r[1] & r[0] \end{pmatrix} \tag{A.4}$$

and

$$\mathrm{cov}(Y_1, Y_2) = \Sigma_{12} = \begin{pmatrix} r[2] & r[1] & r[N-4] & r[N-3] \\ r[3] & r[2] & r[N-5] & r[N-4] \\ \vdots & \vdots & \vdots & \vdots \\ r[N-3] & r[N-4] & r[1] & r[2] \end{pmatrix}. \tag{A.5}$$

To realize a conditional Gaussian process: Simulate the unconditional process Z, identify Y_1 and Y_2, calculate covariance matrices and compute $\tilde{Y}$. Simulation of unconditional Gaussian processes is described in [9]. Conditional multivariate Gaussian vectors are described in (e.g.) [10].

References

[1] ISO 8608, 1995, *Mechanical vibration — Road surface profiles — Reporting of measured data*. International organization for standardization, Geneva.

[2] Rouillard, V., Sek, M.A. and Bruscella, B., 2001, Simulation of road surface profiles. *Journal of Transportation Engineering*, Vol. 127, No. 3, 247–253.

[3] Steinwolf, A., Giacomin, J.A. and Staszewski, W.J., 2002, On the need for bump event correction in vibration test profiles representing road excitations in automobiles. *Journal of automobile engineering*, Proc. of the Institution of mechanical engineers, Part D, Vol. 216, 279–295.

[4] Öijer, F. and Edlund, S., 2003, Identification of Transient Road Obstacle Distributions and Their Impact on Vehicle Durability and Driver Comfort. *Supplement to Vehicle System Dynamics*, Vol. 41, 744–753.

[5] Frinkle, M., Weir, R. and Ferris, J.B., 2004, A graphical representation of road profile characteristics. *SAE World Congress and Exhibition*, Detroit, Michigan, USA, 8–11 March.

[6] Bogsjö, K. and Forsén, A., 2003, Fatigue relevant road surface statistics. *Supplement to Vehicle System Dynamics*, Vol. 41, 724–733. (Paper A in this thesis.)

[7] Rychlik, I., 1987, A new definition of the rainflow cycle counting method. *International J. of fatigue*, Vol. 9, 119–121.

[8] WAFO, A MATLAB Toolbox for analysis of random waves and loads. *http://www.maths.lth.se/matstat/wafo/*, Lund University, 2000.

[9] Wittig, L.E. and Sinha, A.K., 1975, Simulation of multicorrelated random processes using the FFT algorithm. *Journal of acoustical society of America*, Vol. 58, No. 3, 630–634.

[10] Brockwell, P.J. and Davis, R.A., 1991, *Time series: Theory and methods*, Second edition. Springer-Verlag, New York.

[11] Vaughan, S., 2004, A simple test for periodic signals in red noise. *Astronomy & Astrophysics*, v.431, 391–403.

[12] Ahlin, K., Granlund, J. and Lindström, F., 2004, Comparing road profiles with vehicle perceived roughness, *Int. J. Vehicle Design*, Vol. 36, Nos. 2/3, 270–286.

[13] Unpublished vehicle component test results.

[14] Blackman, R. B. and Tukey, J. W., 1959, Particular Pairs of Windows. In The Measurement of Power Spectra, From the Point of View of Communications Engineering, New York: Dover.

C

Paper C

Accuracy of stochastic road models

KLAS BOGSJÖ

Road roughness literature suggests numerous stochastic road models. To evaluate their accuracy, a new method is proposed. Accuracy is assessed by comparison of a measured profile and a corresponding synthetic profile, realized from a stochastic model. A model is accurate if synthetic and measured profiles induce a similar amount of fatigue damage to a vehicle. A lack-of-fit measure is assigned to the evaluated models, facilitating quick and simple comparison. The uncertainty of the vehicle fatigue indicated for the measured profile is considered in the definition of the lack-of-fit measure. A bootstrap technique is applied to estimate the uncertainty.

Keywords: Road profile; road roughness; stochastic models; model evaluation; vehicle fatigue; lack of fit; bootstrap.

1 Introduction

Road surface roughness is a major source of dynamic loads in travelling vehicles. These dynamic loads cause fatigue damage. Thus, road roughness is an essential input for prediction of vehicle fatigue.

One-dimensional road profiles are modelled as stochastic processes. Stochastic modelling can be useful in several aspects. For example, the model parameters can be used to numerically quantify roughness severity. Thus, a model can be used to group roads into different roughness categories, in order to be able to comprehend large data sets. Also, the randomness described by the stochastic model enables studies of uncertainties of, for example, fatigue life.

Several stochastic road models are proposed in the literature, a few papers are listed in the references. However, there is no generally accepted method to evaluate the vehicle fatigue relevance of road models. Thus, an objective method to compare accuracy of these models is needed. This paper describes such a method.

Vehicle fatigue evaluations are used to assess the accuracy. More precisely, vehicle fatigue indicated for synthetic roads realized from the model is compared to vehicle fatigue indicated for the actual measured road. Obviously, the synthetic profiles should indicate a similar amount of vehicle damage as the measured profile. Note that it is not sufficient to estimate, say, the power spectral density (PSD) or crossing intensity of the synthetic and measured roads to

assess the induced vehicle fatigue damage.

A central idea of the evaluation method is to take into account the uncertainty of the vehicle fatigue damage caused by the actual measured road. A large uncertainty, due to (for example) a very short measured distance, allows for larger discrepancy between model and measurement than when the uncertainty is small. The uncertainty is estimated using the bootstrap algorithm.

As always, there is a trade-off between model accuracy and model simplicity. However, this paper focuses only on accuracy. Since the evaluation method is general — any model can be evaluated — it is difficult to penalise for model complexity. A lack-of-fit measure is defined, which gives a quantitative measure of inaccuracy.

The proposed evaluation method is tested on records from 14 actual roads, with a total length of 370 km. The measured roads are of varying quality, ranging from smooth motorways to very rough gravel roads. The profiles are high pass-filtered prior to analysis, to remove measurement drift and hills (very long-wave 'disturbances').

The outline of the paper is as follows: In Section 2 vehicle fatigue damage is introduced. In Section 3 the studied models are presented: the Gaussian, the transformed Gaussian and the Roughness summation (RS) model. In Section 4 the lack-of-fit measure is introduced. In Section 5 the choice of target interval for the lack-of-fit measure is discussed. In Section 6 the lack of fit is assessed for the three studied stochastic road models.

2 From road profile to vehicle fatigue

Fatigue damage is assessed by studying a quarter-vehicle model travelling at constant velocity on road profiles, see Figure 1. This very simple model cannot be expected to predict loads on a physical vehicle exactly, but it will high-light the most important road characteristics as far as fatigue damage accumulation is concerned; it might be viewed as a 'fatigue-load filter'. In this study the model comprises masses, linear springs and linear dampers; the only non-linearity is the ability to loose road contact. The parameters are set to mimic heavy vehicle dynamics, see Table 1.

The total force acting on the sprung mass of the quarter-vehicle model is rainflow-counted (Rychlik, 1987). The resulting load cycles U_j are evaluated with Palmgren-Miners linear damage accumulation hypothesis, and fatigue strength is described by Basquin's relation. The fatigue damage is

$$D = k \sum_j U_j^\beta, \tag{1}$$

where k and β are treated as deterministic constants. For vehicle components, β is usually in the range 3–8, making it most important to describe load cycles

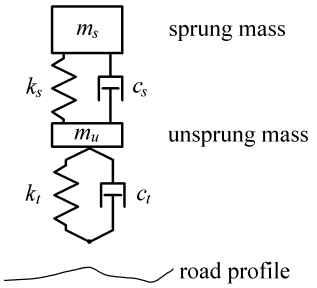

Figure 1: Quarter vehicle model

Description	Symbol	Value	Unit
sprung mass	m_s	3400	kg
suspension spring stiffness	k_s	270 000	N/m
suspension damper stiffness	c_s	6000	Ns/m
unsprung mass	m_u	350	kg
tire spring stiffness	k_t	950000	N/m
tire damper stiffness	c_t	300	Ns/m

Table 1: Quarter vehicle parameters.

with large amplitude accurately.

A physical tire on a heavy vehicle has a road contact length of approximately 0.15 m. Hence, short wavelengths (of order 0.01 m) in the road profile are attenuated by a real tire. In this study, sample distance in the measured roads is 0.05 m, all signal content with shorter wavelength than 0.10 m is neglected.

3 Stochastic road models

There is an extensive set of proposed road models in the literature, some examples are given in the references. In this study, three models are used to illustrate how the proposed lack-of-fit measure works: the Gaussian, the transformed Gaussian and the Roughness summation model.

3.1 The Gaussian model

A Gaussian process is uniquely described by its spectrum, R_1, which is a function of spatial frequency ξ. Here, it is defined by two parameters, κ and w,

$$R_1(\xi) = \begin{cases} \kappa \left(\frac{\xi}{\xi_0}\right)^{-w}, & 0.01 \leq \xi \leq 10, \\ 0, & \text{otherwise}, \end{cases} \tag{2}$$

where $\xi_0 = 0.1$ m^{-1} is the reference spatial frequency. This is the parametric form suggested in the standard ISO 8608. The parameters κ and w are estimated from the real road measurements according to ISO 8608.

3.2 The transformed Gaussian model

Gaussian distributions are convenient in statistical analysis, but real roads are often non-Gaussian. The transformed Gaussian model takes this into account. The road profile $Y_2(x)$ is assumed to be a function of a stationary Gaussian process $Z_2(x)$,

$$Y_2(x) = G(Z_2(x)). \tag{3}$$

The spectral density of $Z_2(x)$ is $R_2(\xi)$. Hence, the model is uniquely described by G and $R_2(\xi)$.

The functions G and $R_2(\xi)$ are estimated from data. More precisely, the inverse $g = G^{-1}$ is estimated by non-parametric means from the measured road, $y(x)$, according to Rychlik (1997). The spectral density $R_2(\xi)$ is estimated from $z_2(x) = g(y(x))$, also by non-parametric means.

Steinwolf and Connon (2005) propose the transformed Gaussian model to describe test course profiles, with a parametric description of the transformation function, G.

3.3 The Roughness summation (RS) model

The Roughness summation (RS) model was introduced by Bogsjö (2005). This section presents a brief description of the model.

The main variability in the road profile is described by the stationary Gaussian process $Z(x)$, with spectral density

$$R(\xi) = \begin{cases} 10^a \left(\frac{\xi}{\xi_0}\right)^{-w}, & 0.01 \leq \xi \leq 10, \\ 0, & \text{otherwise}, \end{cases} \tag{4}$$

where $\xi_0 = 0.1$ m^{-1}. In order to add rough parts, irregularities of two types, long-wave and short-wave, are superimposed to $Z(x)$. The two types occur independently of each other. Figure 2 shows 300 meters of a realized road. Note

that, as the example shows, long-wave (LW) and short-wave (SW) irregularities may overlap. Moreover, the i:th long-wave irregularity and the k:th short-wave irregularity are described by the processes $Z_L^i(x)$ and $Z_S^k(x)$.

To avoid discontinuities at the start and end of the rough sections, the added irregularities start and end with two values equal to zero. Thus, the irregularities are non-stationary and hence it is impossible to assign a spectral density to them. However, an irregularity reaching from $-\infty$ to $+\infty$ is stationary. The spectral densities of such infinite length long-wave and short-wave irregularities are of the same form as the full road spectrum (4) but restricted in frequencies and described by three parameters b, c and w (i.e. the spectrum slope w is unchanged),

$$\text{Long-wave:} \qquad R_L(\xi) = \begin{cases} 10^{\mathrm{b}} \left(\frac{\xi}{\xi_0}\right)^{-w}, & 0.04 \le \xi \le 0.20, \\ 0, & \text{otherwise}, \end{cases} \tag{5}$$

$$\text{Short-wave:} \qquad R_S(\xi) = \begin{cases} 10^{\mathrm{c}} \left(\frac{\xi}{\xi_0}\right)^{-w}, & 0.20 \le \xi \le 1.0, \\ 0, & \text{otherwise}. \end{cases} \tag{6}$$

For finite length irregularities see Bogsjö (2005).

Locations and lengths of added rough sections are random. More precisely, the distance between the end of a long-wave irregularity and the start of the next is exponentially distributed with mean θ_L. Similarly, the distance between end and start of short-wave irregularities is exponentially distributed with mean θ_S. The length of long-wave and the length of short-wave irregularities are exponentially distributed with mean d_L and d_S, respectively. All model parameters are compiled in Table 2.

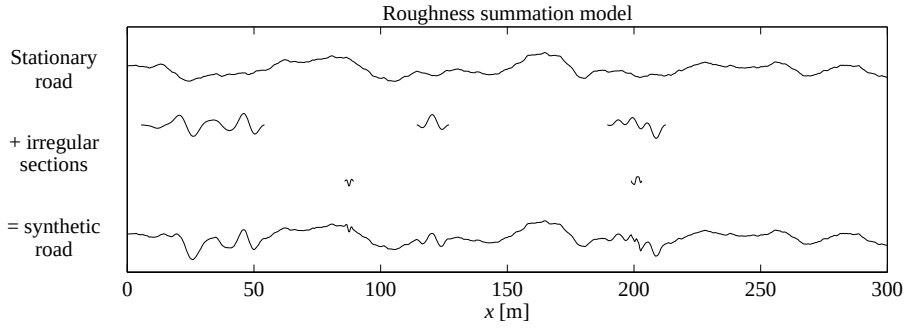

Figure 2: Generation of a synthetic road according to the RS-model.

Symbol	*Description*
a	Severity level, 'regular' road
b	Severity level, LW-irregularities
c	Severity level, SW-irregularities
w	Spectral parameter, spectrum 'slope'
θ_L	Mean distance between LW-irregularities
θ_S	Mean distance between SW-irregularities
d_L	Mean length of LW-irregularities
d_S	Mean length of SW-irregularities

Table 2: Parameters in the RS-model, LW = long-wave, SW = short-wave.

4 Road model accuracy

To study the vehicle fatigue relevance of a road model, roads are realized according to the model assumptions. Such artificial roads are called 'synthetic'. The vehicle fatigue indicated for a synthetic road is labelled a synthetic damage. The damage indicated for a measured road is labelled an observed damage.

A usual statistical hypothesis test can be used to analyse if the observed damage could come from the same distribution as the synthetic damages. However, since almost any observed damage could come from a model with extremely high variance of damage, such a test is not particularly discriminating. Here, a slightly different approach is used, in that a function $\delta(v, \beta)$ is introduced that measures discrepancy between the synthetic damages and the observed damage for each velocity v and fatigue exponent β.

The hypothesis that a road model is 'correct' means that the measured road cannot be distinguished (statistically) from a road realized from the model. This assumption is denoted by H_0, the null-hypothesis. Naturally, the discrepancy should be low when H_0 is true, but, due to randomness the discrepancy will always deviate slightly from zero. To decide a reasonable acceptance region it is necessary to know the distribution of $\delta(v, \beta)$ under H_0.

The distribution of $\delta(v, \beta)$ under H_0 is denoted by F_0. It is convenient if F_0 is independent of the velocity v, the fatigue parameter β and specific properties of the actual road (such as measured distance). It is then possible to compare discrepancies computed in different situations. Furthermore, if a model fails to describe the essential properties of a measured road, then ideally the discrepancy should have a distribution clearly deviating from F_0, see the artificial example in Figure 3.

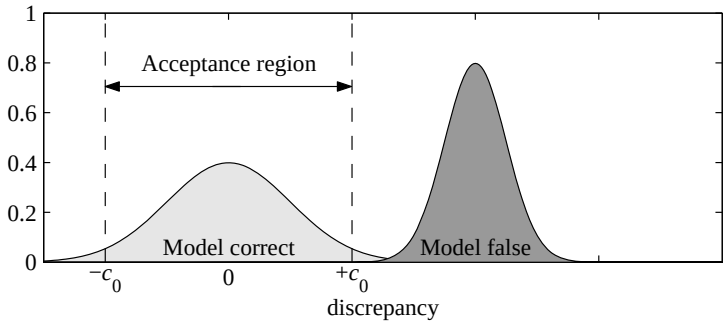

Figure 3: Probability densities of a $\delta(v, \beta)$.

4.1 Logarithmic transformation of the damage

The transformed damage Q is a function of the damage D. Subscripts s and o denote synthetic value (from model) and observed value (from measurement), respectively. The transformation is defined as

$$Q = \frac{1}{\beta} \ln(D). \tag{7}$$

The variables D and Q are treated as random variables. Outcomes of these random variables are denoted by lower-case letters. For example, q_o is the observed transformed damage obtained from the measured road, an outcome of the random variable Q_o. The following two subsections show examples where the randomness of the transformed damage is accurately described by the Gaussian probability distribution.

4.1.1 Distribution of Q_s

Synthetic Gaussian roads are realized with spectral parameters $\kappa = 10^{-4}$ m^3 and $w = 2$. Figure 4 shows the assessed damage for 100 Gaussian roads, when the road length is 5 km (left plot) and 50 km (right plot). The damage is normalised so that the average damage is 1. The figure displays two obvious properties of the damage. The relative spread around the average value decreases with road length but increases with β. Figure 5 shows the transformed damage Q_s. The variance of the transformed variable Q_s is almost constant as a function of β. Moreover, Q_s is symmetrically distributed around zero, and in fact, the distribution is approximately Gaussian, see Figure 6.

A similar study is performed for the RS-model, to ensure that the result (Figure 6) is valid also for other models than the Gaussian. Figure 7 shows two examples of Gaussian probability plots of the transformed damage of the

RS-model, when $\beta = 3$ and $\beta = 8$. The fit is very good for both values of β. The number of simulated roads is 1000 and the road length is set to 5 km. The parameters are set to $a = -4.0$, $b = -3.5$, $c = -2.7$, $w = 3.3$, $\theta_L = 220$ m, $\theta_S = 1000$ m, $d_L = 42$ m and $d_S = 4$ m.

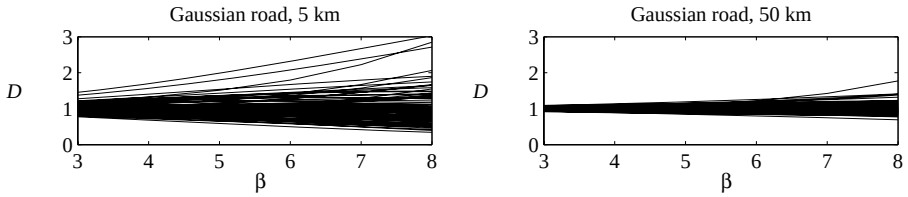

Figure 4: Damage (normalised), $v = 60$ km/h, $\kappa = 10^{-4}$ m^3 and $w = 2$.

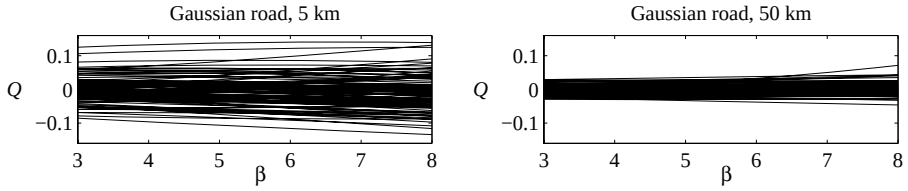

Figure 5: Logarithmic transformation of the damage, $v = 60$ km/h.

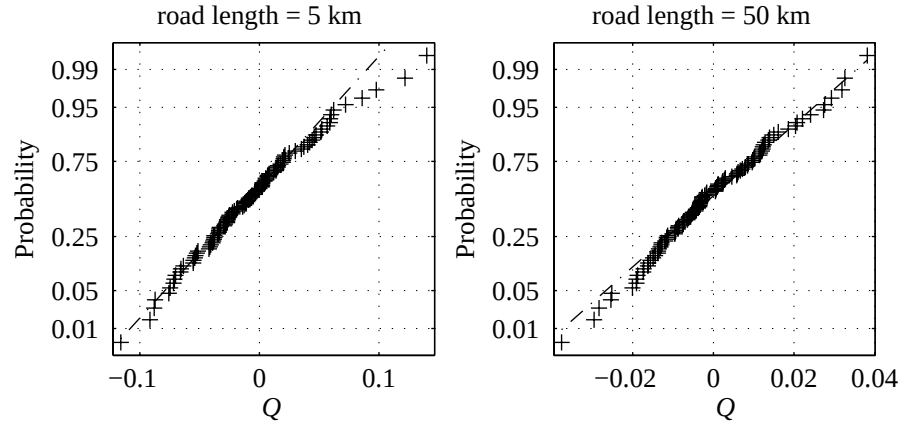

Figure 6: Gaussian probability plots of Q_s from Gaussian roads, $v = 60$ km/h, $\beta = 6$.

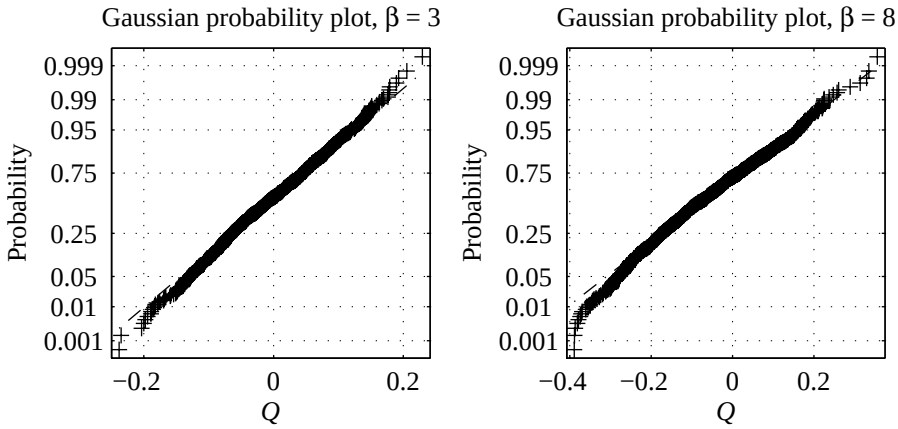

Figure 7: Probability plots of Q_s from the RS-model, $v = 80$ km/h, length = 5 km.

4.1.2 Distribution of Q_o

In the specific examples, in the previous subsection, Q_s is Gaussian distributed both when road profiles are generated from the Gaussian model and the RS-model. However, it has been shown in several different studies that Gaussian processes are not adequate to model road profiles (e.g. Rouillard et al, 2002; Bogsjö and Forsén, 2003; Öijer and Edlund, 2003). The RS-model has been shown to give more accurate results than the Gaussian model (Bogsjö, 2005). A bootstrap study is performed to investigate the distribution of Q_o. An introduction to bootstrap is given by Davison and Hinkley (1997).

In the bootstrap study, the observed damage d_o is expressed as a sum of partial damages. The load history from the measured road is divided into N equally long sequences. Here, the minimum sequence length is set to 1 km, (e.g. if the road length is 8.8 km, the load history is divided into 8 sequences of 1.1 km). All load sequences are rainflow-counted to obtain the partial damages $\tilde{d}_j$, $j = 1, \ldots, N$. The partial damages are normalised to ensure that the sum of the partial damages is equal to the total damage d_o,

$$d_j = \frac{d_o}{\sum_{k=1}^{N} \tilde{d}_k} \tilde{d}_j. \tag{8}$$

The partial damages $d_j, j = 1, \ldots, N$, are assumed to be outcomes of independent and identically distributed random variables. Thus, interaction between

segments is neglected. The transformed damage is

$$q_o = \frac{1}{\beta} \ln(\sum_{j=1}^{N} d_j). \tag{9}$$

Now, the non-parametric bootstrap algorithm is used: Sampling at random with replacement from the original sample $d_1, \ldots, d_N$ gives a bootstrap sample $d_1^*, \ldots, d_N^*$. Applying the transformation to the bootstrap sample gives,

$$q^* = \frac{1}{\beta} \ln(\sum_{j=1}^{N} d_j^*). \tag{10}$$

Repeating the algorithm m times generates bootstrap replications q_b^*, $b = 1, \ldots, m$. The idea of bootstrap is that the empirical distribution of $q_b^* - q_o$ approximates the distribution of $Q_o - \mathrm{E}[Q_o]$. The empirical distribution of $q_b^* - q_o$ is compared to the Gaussian distribution in Figure 8 and 9. The plots show that the Gaussian assumption is reasonable.

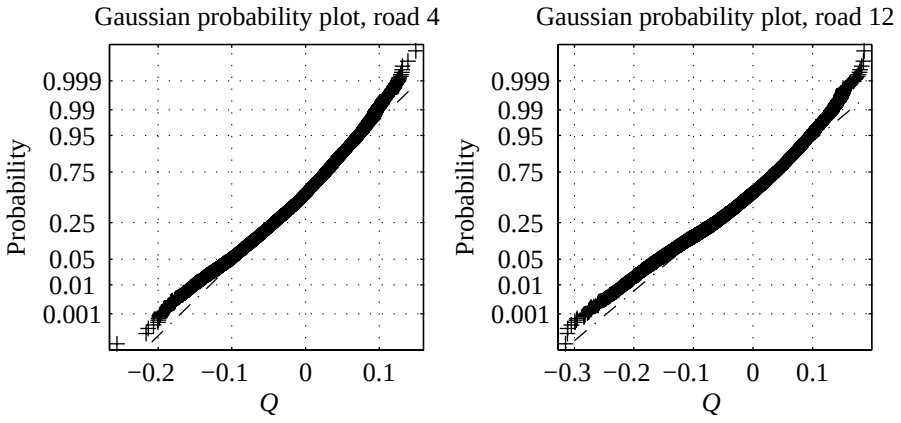

Figure 8: Gaussian probability plots of the transformed damage, $\beta = 6$.

Note that, in the examples above, the transformed damage Q is Gaussian distributed but the damage D is lognormally distributed. Also note that in general

$$\mathrm{E}[Q] \neq \frac{1}{\beta} \ln(\mathrm{E}[D]). \tag{11}$$

4.2 Discrepancy and lack of fit

To measure discrepancy between model and measurement, the transformed synthetic damage Q_s is compared to the transformed observed damage Q_o.

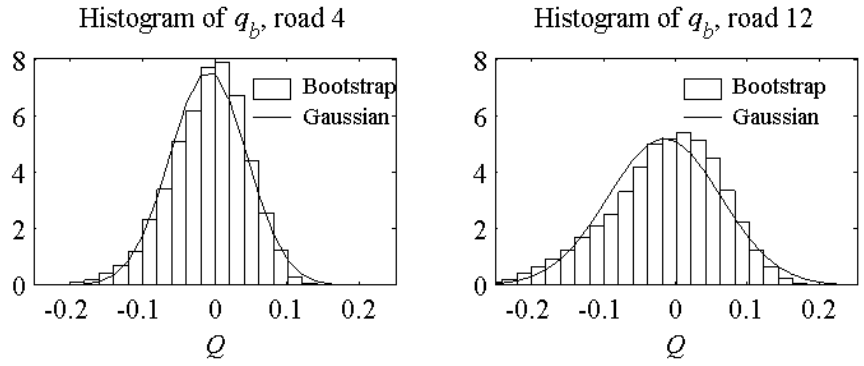

Figure 9: Histogram of bootstrap replicates compared to the Gaussian density function.

The discrepancy is given by

$$\delta = \frac{\mathrm{E}[Q_s] - Q_o}{\sigma_o}, \tag{12}$$

where σ_o is the standard deviation of Q_o and E[ ] is the expectation of the random variable. Note that under H_0 the expectation $\mathrm{E}[Q_s] = \mathrm{E}[Q_o]$. So under H_0, δ is approximately a standard Gaussian variable (zero mean, unit variance). In general, it is expected that damage assessed from shorter roads are more uncertain than damage assessed from longer roads, recall Figure 4 and 5. Note that the uncertainty of Q_s is not included in the denominator in (12), since then models with extremely high variance would always obtain a small discrepancy.

By Monte-Carlo simulation, i.e. generation of synthetic roads according to the model assumptions and assessing fatigue damages as described in Section 2, all information about Q_s can be obtained. In particular the expectation, $\mathrm{E}[Q_s]$ is estimated by the empirical average

$$\bar{q}_s = \frac{1}{n_{mc}} \sum_{j=1}^{n_{mc}} q_s^{(j)}, \tag{13}$$

where n_{mc} is the number of Monte-Carlo simulations and $q_s^{(j)}$ is the transformed damage caused by the j:th synthetic road; i.e. the j:th observation of the random variable Q_s. By increasing n_{mc} the estimate of $\mathrm{E}[Q_s]$ can be made arbitrarily accurate.

Recall that q_o denotes the transformed damage caused by the measured road. Since q_o is the only observation of the random variable Q_o it is difficult

to estimate the standard deviation of Q_o. However, dividing the measured road into subsections as in Section 4.1.2 makes it possible to analyse variability of Q_o. More precisely, employment of the bootstrap algorithm enables estimation of σ_o. The computations can be found in Appendix A. The estimated standard deviation is denoted by s_o. The empirical discrepancy is

$$\hat{\delta} = \frac{\bar{q}_s - q_o}{s_o}. \tag{14}$$

An empirical discrepancy $\hat{\delta}$ can be obtained for any vehicle velocity v and fatigue exponent β. Let the vehicle velocities on the studied road belong to a set V and fatigue exponents belong to a set B. Then the road model lack-of-fit is defined as the largest deviation from zero,

$$\Delta = \hat{\delta}(v_0, \beta_0), \tag{15}$$

where $v_0 \in V$ and $\beta_0 \in B$ are such that $|\hat{\delta}(v_0, \beta_0)| \geq |\hat{\delta}(v, \beta)|$ for all $v \in V$ and $\beta \in B$. Hence, the lack of fit of a model is decided by its worst fit, for all studied velocities and fatigue exponents. To clarify, if the empirical discrepancies equal $(-3, 4, -6)$ then $\Delta = -6$. A negative value indicates that the model gives non-conservative fatigue damage estimates, and vice versa for a positive value.

To ensure that the road model is suitable for a wide range of velocities and fatigue exponents the following sets are proposed:

$$B = \{3, 4, 5, 6, 7, 8\} \tag{16}$$

and

$$V = \{40, 50, 60, 70, 80, 90\}, \tag{17}$$

where the velocities are expressed in km/h.

5 Lack of fit rejection level

The purpose of this section is to define a target interval for the lack-of-fit measure Δ. The distribution of Δ is investigated in the case when H_0 is true, i.e. when the synthetic roads and the observed road originate from the same model. More precisely, the quantile λ is searched for, which satisfies $\mathrm{P}(-\lambda \leq \Delta \leq \lambda) = 0.95$.

The measure Δ is, with the proposed sets B and V, the maximum deviation from zero of $n = 36$ (approximately) Gaussian variables, here denoted by $\hat{\delta}_i$, $i = 1, \ldots, n$. If we assume that H_0 is true then $\mathrm{E}[Q_o] = \mathrm{E}[Q_s]$. Also, if we assume that $\mathrm{E}[Q_s]$ and σ_o are accurately estimated by $\bar{q}_s$ and s_o, respectively, then $\hat{\delta}_i$, $i = 1, \ldots, n$ is a standard Gaussian variable. Now, if the $\hat{\delta}_i$:s are assumed independent then the probability density of Δ is

$$f_{\Delta}^{(1)}(z) = n \left(2\Phi(|z|) - 1\right)^{n-1} \dot{\Phi}(z), \tag{18}$$

where $\Phi(z)$ and $\dot{\Phi}(z)$ are the standard Gaussian distribution and density, respectively. On the other hand, if the $\hat{\delta}_i$:s are strictly dependent, then the probability density is simply the Gaussian density,

$$f_{\Delta}^{(2)}(z) = \dot{\Phi}(z). \tag{19}$$

A 95 %-interval of Δ is $[-3.2, 3.2]$ in the independent case and $[-2.0, 2.0]$ in the dependent case. This gives an idea on how to choose the interval. However, it was assumed that the standard deviation was accurately estimated. But the estimation of σ_o is not exact, which makes the variability of Δ larger than indicated by equations (18) and (19).

Simulation studies are performed in order to aid the choice of the target interval. Two studies are presented below. The first simulation study uses a stationary Gaussian model to simulate both 'observed' and synthetic roads. The spectral parameters are $\kappa = 10^{-4}$ m^3 and $w = 2$, see Equation (2). The second study uses the RS-model to generate 'observed' and synthetic roads. The parameters are set to $a = -4.0$, $b = -3.5$, $c = -2.5$, $w = 3.0$, $\theta_L = 200$ m, $\theta_S = 1000$ m, $d_L = 40$ m and $d_S = 4$ m. Hence, in these studies, the correct model and its parameters are known in advance.

To show how road distance influences the distribution of Δ, two different road lengths are studied: 10 and 50 km. Also, Δ is computed for both known and unknown σ_o, in order to show how estimation of σ_o influences the distribution. For each road length, 1000 synthetic roads are realized. Then, one of the synthetic roads is set to be the 'observed' road, and a lack-of-fit measure is computed. Repeating this for every road enables 1000 lack-of-fit measures to be computed. Figures 10 and 11 display the resulting histograms of Δ.

In the case when the true value of σ_o is used to compute Δ the distribution is insensitive to a change of road length and road model, see the right-hand-side plots in Figures 10 and 11. However, in practical situations, σ_o is unknown and has to be estimated. The left-hand-side plots show, as expected, that the estimation of σ_o increases the variability of Δ. Note especially that the spread is larger for the shorter distance, since then the estimation of σ_o is more uncertain.

A comparison of the left-hand-side plots of Figures 10 and 11 shows that the spread of Δ is larger for the RS-model. This is natural since there is more variability in the RS-model, which implies that the road must be long in order to obtain an accurate estimate of σ_o.

Note also the skewness of the distributions, clearly visible in the left-hand-side plots of Figure 11. There are several outcomes above $+4$ but very few below -4. This is due to the positive correlation between the observed transformed damage q_o and the estimated standard deviation s_o, see (14). A large lack of fit occurs when the 'observed' road causes, by chance, an unusually low damage. Unfortunately, this unusually low damage q_o is likely to give an unusually

large underestimation of the standard deviation, s_o. Recall that the standard deviation is estimated using only the observed road. Thus, (14) with a low q_o and a small s_o, implies that the empirical discrepancy becomes largely positive.

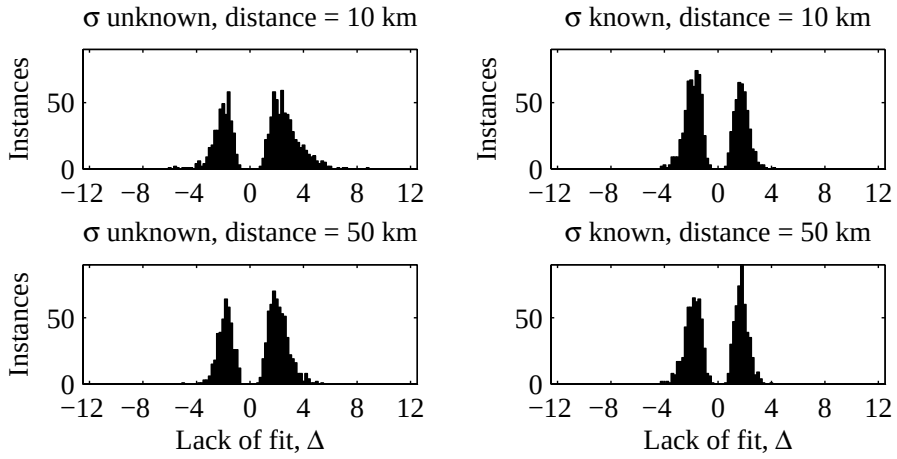

Figure 10: Histograms of the lack-of-fit measure. Roads realized from the Gaussian model, $\kappa = 10^{-4}$ and $w = 2$.

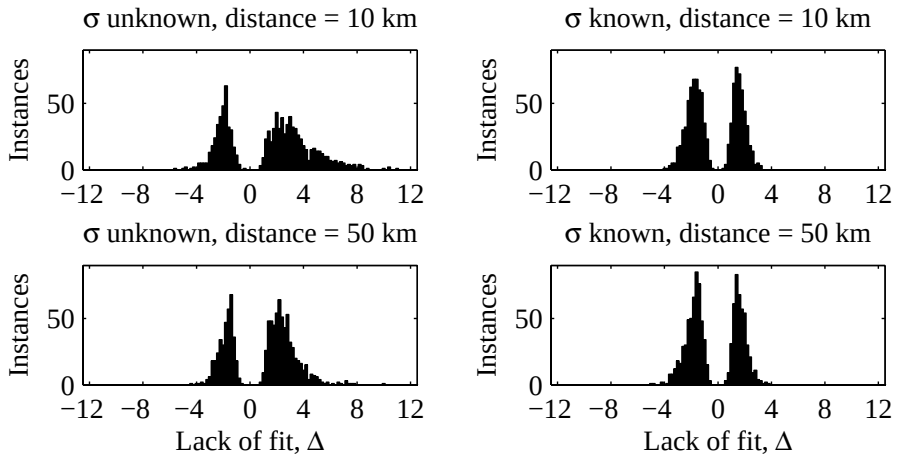

Figure 11: Histograms of lack-of-fit measure. Roads realized from the RS-model.

Judging from the simulation studies the 0.025-quantile of Δ is higher than 3.2, due to estimation uncertainty of σ_o. The results indicate that a reasonable level is 4. Thus, lack-of-fit measures in the interval $[-4, 4]$ are deemed satisfactory.

There is one matter that has not been discussed in this section. When a road has been measured, the parameters in the road model have to be estimated. The estimated parameters are uncertain. This uncertainty will lead to an increased spread of the lack-of-fit measure, even if the road model is correct. In this section all parameters are known in advance, and hence no parameter estimation was needed. However, it is difficult to take this into account since different models are associated with different parameter uncertainties. Therefore, the effect of parameter uncertainties is not treated here.

6 Evaluation of three road models

In this section the three road models presented in Section 3 are compared to 14 measured profiles. For each measured road and road model the lack of fit is computed. The actual roads range from newly paved smooth motorways to very rough gravel roads. The measured distances vary in the interval 5–45 km.

For parameter estimation of the Gaussian model, see ISO 8608, for estimation of the transformation function used in the transformed Gaussian model, see Rychlik (1997), and for parameter estimation of the RS-model, see Bogsjö (2005). The lack of fit is presented in Figure 12.

The target is reached in 1 out of 14 roads for the Gaussian and the transformed Gaussian model. The Gaussian model underestimates the damage whereas the transformed Gaussian overestimates the damage. The RS-model reaches the target in 11 out of 14 studied roads. If we compare the absolute values of the lack-of-fit measures, the RS-model has the smallest lack of fit for all roads.

7 Conclusions

This paper explains how to evaluate any stochastic road model given a measured profile. The lack-of-fit measure quantifies discrepancy between model and measurement. It facilitates quick and simple comparison of different road models.

8 Comments

The results presented in Section 6 show that the Roughness summation model is more accurate than the Gaussian model and the transformed Gaussian model.

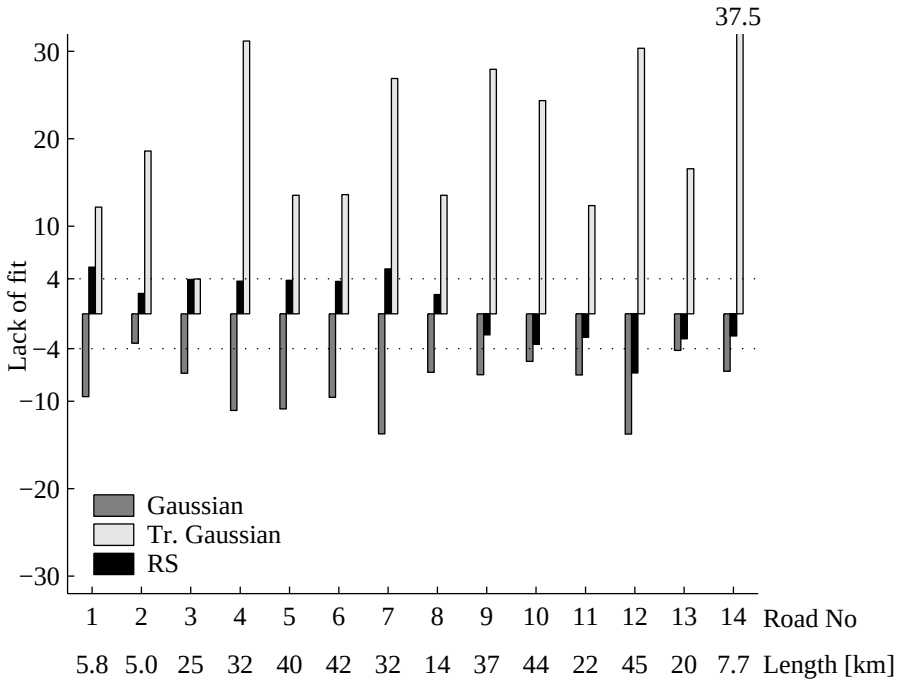

Figure 12: Lack of fit, for each measured road, for the three models.

The Gaussian model gives non-conservative fatigue estimates. The transformed Gaussian model gives too conservative fatigue estimates. The transformed Gaussian model should be used with caution. The Gaussian and the transformed Gaussian model assumes strictly stationary roads, which is a very strong assumption.

References

[1] Bogsjö, K. and Forsén, A. (2004) 'Fatigue relevant road surface statistics', *Supplement to Vehicle System Dynamics*, Vol. 41, pp. 724–733. (Paper A in this thesis)

[2] Bogsjö, K. (2005), 'Development of analysis tools and stochastic models of road profiles regarding their influence on heavy vehicle fatigue', *Supplement to Vehicle System Dynamics*, Vol. 44, pp. 780–790. (Paper B in this thesis.)

[3] Davison, A. C. and Hinkley, D. V. (1997), 'Bootstrap methods and their applications', Cambridge: Cambridge University Press.

[4] Ferris, J. B. (2004) 'Characterising road profiles as Markov Chains', *Int. J. Vehicle Design*, Vol. 36, Nos. 2/3, pp. 103–115.

[5] Frinkle, M., Weir, R. and Ferris, J. B. (2004), 'A graphical representation of road profile characteristics' *SAE technical paper series*, 2004-01-0769.

[6] Heath, A.N. (1989) 'Modelling and simulation of road roughness', *Proc. of 11th IAVSD symposium. The Dynamics of vehicles on roads and on tracks*, pp. 275–284.

[7] Howe, J.G., Lee, D-C, Chrstos, J.P. Myers, T.T. Allen, R.W., Gorsich, D.J. and Reid, A. (2004) 'Analysis of potential road/terrain characterization rating metrics' *SAE technical paper series*, 2004-01-2640.

[8] ISO 8608 (1995) '*Mechanical Vibration — Road Surface Profiles — Reporting of Measured Data*', International Organization for Standardization, Geneva.

[9] Öijer, F. and Edlund, S. (2003) 'Identification of Transient Road Obstacle Distributions and Their Impact on Vehicle Durability and Driver Comfort', *Supplement to Vehicle System Dynamics*, Vol. 41, pp. 744–753.

[10] Robson, J.D. and Dodds, C.J. (1973) 'The description of road surface roughness', *J. Sound and vibration*, Vol. 31, pp. 175–183.

[11] Rouillard, V. and Sek, M.A. (2002) 'A statistical model for longitudinal road topography', *Road and Transport Research, ARRB*, Vol. 11, No. 23, pp. 17–23.

[12] Rychlik, I. (1987) 'A new definition of the rainflow cycle counting method', *Int. J. Fatigue* Vol. 9, pp. 119–121.

[13] Rychlik, I., Johannesson, P. and Leadbetter M.R. (1997) 'Modelling and statistical analysis of Ocean-Wave Data using transformed Gaussian processes', *Marine structures*, Vol. 10, pp. 13–47.

[14] Šprinc, J., Kropác, O. and Šprinc, M. (2002) 'Characterization of Longitudinal Road Unevenness in the Light of the International PIARC - EVEN Experiment 1998', *Vehicle System Dynamics*, Vol. 37, No. 4, pp. 263–281.

[15] Steinwolf, A., Giacomin, J.A. and Staszewski, W.J. (2002) 'On the need for bump event correction in vibration test profiles representing road excitations in automobiles', *J. Automobile engineering*, Proc. of the institution of mechanical engineers, Part D, Vol. 216, pp. 279–295.

[16] Steinwolf, A. and Connon, W.H. (2005) 'Limitations on the use of Fourier transform approach to describe test course profiles', *Sound and Vibration, the noise and vibration control magazine*, Vol. 39, No. 2, Acoustical Publications Inc, pp. 12–17.

[17] Sun, Lu and Su, Jie (2001) 'Modeling random fields of road surface irregularities', *Int. J. Road Materials and Pavement Design*, Vol. 2, No. 1, pp. 49–70.

[18] Szöke, D. and Kuti, I. (2004), 'A new development in the numerical description of road profile realisations', *Int. J. Vehicle Design*. Vol. 34, No. 2, pp. 183–190.

[19] Zhu, J. Jim and Zhu, Wenli (1996), 'Stochastic modeling of pavement roughness', *28th Southeastern Symposium on System Theory*, pp. 28–32.

A Estimation of σ_o

To compute the empirical discrepancy an estimation of the standard deviation σ_o is needed. Due to the logarithmic transformation (7) it is difficult to estimate the standard deviation. Hence, bootstrap is employed.

As in Section 4.1.2 the observed transformed damage is expressed as a function of partial damages,

$$q_o = \frac{1}{\beta} \ln(\sum_{j=1}^{N} d_j), \tag{A.1}$$

where the partial damages $d_j, j = 1, \ldots, N$, are assumed to be outcomes of independent and identically distributed random variables.

The following stepwise procedure computes the estimate of σ_o:

1. The original sample is $d_1, \ldots, d_N$.
2. Sample at random with replacement from the original sample to obtain a bootstrap sample $d_1^*, \ldots, d_N^*$.
3. Compute $q^* = \frac{1}{\beta} \ln(\sum_{j=1}^{N} d_j^*)$.
4. Repeat step 2–3 M times to generate bootstrap replications: q_b^*, $b = 1, \ldots, M$.
5. Compute s_o, the empirical standard deviation of q_b^*,

$$s_o = \sqrt{\frac{1}{M-1} \sum_{b=1}^{M} (q_b^* - \overline{q^*})^2}, \quad \overline{q^*} = \frac{1}{M} \sum_{b=1}^{M} q_b^*.$$

D

Paper D

Evaluation of stochastic models of parallel road tracks

KLAS BOGSJÖ

ABSTRACT

In road roughness literature different stochastic models of parallel road tracks are suggested. A new method is proposed to evaluate their accuracy, by comparison of measured parallel tracks and synthetic parallel tracks, realized from a stochastic model. A model is judged accurate if synthetic and measured roads induce a similar amount of fatigue damage to a vehicle. A lack-of-fit measure is assigned to the evaluated models, facilitating quick and simple comparison. The uncertainty of the vehicle fatigue indicated for the measured profile is considered in the definition of the lack-of-fit measure. A bootstrap technique is applied to estimate the uncertainty.

Keywords: Road roughness; vehicle fatigue; stochastic processes; model evaluation.

1 Introduction

Long road profile measurements reveal what operating vehicles can be exposed to. However, such measurements give very large data quantities, which are difficult to comprehend. A stochastic model of the road data is appropriate, due to the random nature of such measurements. If the stochastic model is uniquely defined by a few parameters, these parameters summarise the large data quantities. Moreover, synthetic roads can be generated from the model, with parameter values estimated from a measured road. If synthetic and measured roads are equivalent, in the sense that they induce the same amount of vehicle fatigue damage, then it can be concluded that the road model and the estimated parameters are relevant.

A four-wheeled vehicle is subjected to excitations due to road roughness in the left and right wheel paths. Hence, to describe the excitations we need a stochastic model of parallel road tracks. The model shall describe variation within each track and the covariation between the tracks. In this paper, an evaluation method is proposed, which assesses accuracy of such 'parallel track' models.

Several parallel track models were evaluated and the most accurate one is described and compared to the isotropic Gaussian model. In previous work [1]

a single-track road model was proposed. The parallel track model proposed in this paper is an extension of that single-track model. The parallel track model includes irregular sections with above-average roughness. These irregularities have random shape, length and location.

This paper focusses on evaluation of stochastic road models, rather than accurate estimation of vehicle fatigue damage. Hence, the vehicle model is simple and its fatigue properties are described with low complexity. A two-wheeled vehicle model (half-vehicle) is used to simulate vehicle response. A measure of lack-of-fit is derived, which quantifies the discrepancy between indicated vehicle fatigue damage on synthetic and measured roads.

In Section 2 information regarding the road measurements are given. In Section 3, vehicle fatigue assessment is discussed. In Section 4, two road models are defined, referred to as Models A and B. In Section 5, computation of the lack-of-fit measure is described, and in Section 6, a rejection region of the lack-of-fit is defined. In Section 7, Models A and B are evaluated utilising the lack-of-fit measure.

2 Road measurements

The proposed road model and the evaluation method is tested on records from 20 Swedish roads, measured in left and right wheel path. The total length of these roads is 520 km. The measured roads are of varying quality, ranging from very smooth motorways to very rough gravel roads.

The profile of the left and right wheel-path is measured by laser/inertial profilometers. The measurement equipment is described in [2]. Here, laser number 3 and 15, as numbered in [2], represent the left and right wheel-path, respectively.

3 Vehicle fatigue

Fatigue damage is assessed by studying a half-vehicle model travelling at constant velocity on road profiles, see Figure 1. This simple model cannot be expected to predict loads on a physical vehicle exactly, but it will high-light the most important road characteristics as far as fatigue damage accumulation is concerned; it might be viewed as a 'fatigue-load filter'. The parameters of the vehicle model are set to mimic heavy vehicle dynamics. In this study the model comprises masses, linear springs and linear dampers; the only non-linearity is the ability to loose road contact. For an analysis of a vehicle-model with non-linear damping excited by stochastic road profiles, see [3].

The vertical accelerations of the left and the right side of the sprung mass are denoted by $\ddot{u}_{\mathrm{L}}(x;v)$ and $\ddot{u}_{\mathrm{R}}(x;v)$, where x is the position of the vehicle along

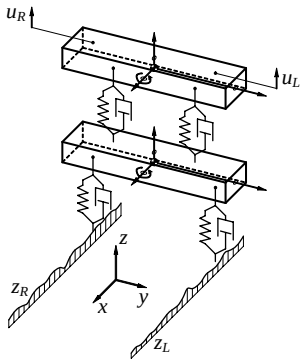

Figure 1: The half-vehicle

the road and v is the (constant) velocity of the vehicle. Linear combination of $\ddot{u}_{\mathrm{L}}$ and $\ddot{u}_{\mathrm{R}}$ forms a one-dimensional acceleration sequence, which is used to assess fatigue damage [4], [5]. In this general setting, where we do not study a specific critical location in a vehicle component of a particular vehicle exposed to deterministic loads, the appropriate linear combination is unknown. Hence, several linear combinations are studied,

$$\ddot{u}(x;v;n) = c_1(n)\ddot{u}_{\mathrm{L}}(x;v) + c_2(n)\ddot{u}_{\mathrm{R}}(x;v), \tag{1}$$

where

$$c_1(n) = \cos(\frac{n\pi}{N+1}),\ c_2(n) = \sin(\frac{n\pi}{N+1}), \tag{2}$$

and where $n = 0, 1, \ldots, N$. Obviously, $c_1^2 + c_2^2 = 1$ for all n.

Rainflow cycles, $U_j,\ j = 1, \ldots N_c$, are identified in $\ddot{u}(x;v;n)$, where N_c is the total number of rainflow cycles. For a simple definition of the rainflow cycle, see [6]. The rainflow cycles U_j are evaluated with Palmgren-Miner's linear damage accumulation hypothesis, and fatigue strength is described by Basquin's relation. The fatigue damage is

$$D(v;n;\beta) = \kappa \sum_{j=1}^{N_c} U_j^{\beta}, \tag{3}$$

where κ and β are treated as deterministic constants. For vehicle components, β is usually in the range 3–8, making it most important to describe load cycles with large amplitude accurately. Here, the value of κ is unimportant, since only relative damage values are studied. This also justifies that acceleration

can be used as the 'fatigue-load', since the acceleration is proportional to the dynamic load.

To sum up, $D(v; n; \beta)$ is the fatigue indicated by a certain road at velocity v, 'left-right unit' n and fatigue parameter β. A reliable stochastic road model should be accurate for all realistic values of v, n and β.

4 Stochastic models

Two stochastic models will be evaluated in this paper. But first some general properties of stationary stochastic processes are discussed. Let the zero mean stationary processes $Z_{\mathrm{L}}(x)$ and $Z_{\mathrm{R}}(x)$ describe the road elevation at position x along the left and right wheel path. Furthermore, it it is assumed that $Z_{\mathrm{L}}(x)$ and $Z_{\mathrm{R}}(x)$ are statistically equivalent, so that the auto-covariance function $r(x) = \mathrm{E}[Z_{\mathrm{L}}(x + x_0)Z_{\mathrm{L}}(x_0)] = \mathrm{E}[Z_{\mathrm{R}}(x + x_0)Z_{\mathrm{R}}(x_0)]$. Also, the cross-covariance functions $r_{\mathrm{RL}}(x) = \mathrm{E}[Z_{\mathrm{R}}(x + x_0)Z_{\mathrm{L}}(x_0)]$ and $r_{\mathrm{LR}}(x) = r_{\mathrm{RL}}(-x)$.

The one-sided spectrum and cross-spectrum are defined by

$$R(\xi) = \begin{cases} 2\int_{-\infty}^{\infty} r(x)e^{-i2\pi\xi x}\mathrm{d}x, & \xi > 0, \\ \int_{-\infty}^{\infty} r(x)\mathrm{d}x, & \xi = 0, \\ 0, & \xi < 0, \end{cases} \tag{4}$$

$$R_{\mathrm{LR}}(\xi) = \begin{cases} 2\int_{-\infty}^{\infty} r_{\mathrm{LR}}(x)e^{-i2\pi\xi x}\mathrm{d}x, & \xi > 0, \\ \int_{-\infty}^{\infty} r_{\mathrm{LR}}(x)\mathrm{d}x, & \xi = 0, \\ 0, & \xi < 0, \end{cases} \tag{5}$$

where ξ is spatial frequency.

Inversely, the auto-covariance function is given by the one-sided spectrum,

$$r(x) = \int_0^{\infty} R(\xi)\cos(2\pi\xi x)\mathrm{d}x. \tag{6}$$

If the road profiles Z_{L} and Z_{R} are (correlated) Gaussian processes, then their spectrum and cross-spectrum fully define the model. Simulation of correlated Gaussian processes with given spectrum and cross-spectrum is described in [7]. Alternatively, a Gaussian model is fully defined by the spectrum, coherence and phase function. Here, we will assume a zero phase function and focus on the spectrum and coherence function, where the coherence is defined by $\gamma(\xi) = |R_{\mathrm{LR}}(\xi)|/R(\xi)$.

4.1 Model A (Isotropy)

Often (e.g. [8]–[12]) roads are assumed to be ergodic, homogeneous, isotropic Gaussian surfaces. Homogeneity and isotropy imply that all profiles following a

straight-line on the road surface have the same statistical properties, irrespectively of direction and position of the line. Specifically, the covariance between two values of a field at points A and B is a function only of the distance between them. Isotropy and Gaussianity imply that a spectrum of any profile on the isotropic surface uniquely describes the surface model. However, the spectrum cannot be chosen arbitrarily, it has to satisfy certain conditions. The conditions are stated in [9].

Kamash and Robson [9] propose the following spectrum, which is compatible with the isotropic assumption,

$$R_A(\xi) = \begin{cases} c\xi_a^{-w}, & 0 \le \xi \le \xi_a, \\ c\xi^{-w}, & \xi_a \le \xi \le \xi_b, \\ 0, & \text{otherwise.} \end{cases} \tag{7}$$

Here, the boundary constants ξ_a and ξ_b are set to 0.01 and 10 m^{-1}, respectively.

Isotropy implies that $r_{\mathrm{RL}}(x) = r_{\mathrm{LR}}(x) = r_{\mathrm{LR}}(-x)$, i.e. the cross-covariance functions are symmetric. This symmetry implies that the cross-spectra are real, thus $R_{\mathrm{RL}} = R_{\mathrm{LR}}$.

In Figure 2 three points are marked, points A and C on the right track and point B on the left track. The covariance between the road levels in points A and B is $r_{\mathrm{LR}}(x)$ and the covariance between the road levels in points A and C is $r(\sqrt{x^2 + t_w^2})$. Since the distance between A and B equals the distance between A and C, a consequence of isotropy is that

$$r_{\mathrm{LR}}(x) = r(\sqrt{x^2 + t_w^2}). \tag{8}$$

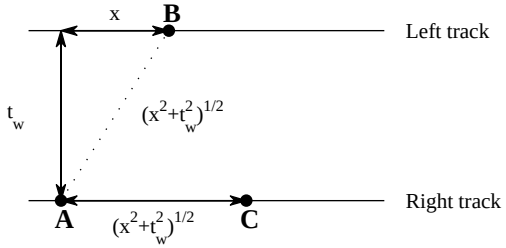

Figure 2: Two parallel road tracks

The cross-spectrum can be computed from $R_A(\xi)$ using (6), (8) and (5). Thus, the coherence function $\gamma_A(\xi)$, is also given by $R_A(\xi)$. In Figure 3, a spectrum and corresponding coherence function is plotted for different track widths.

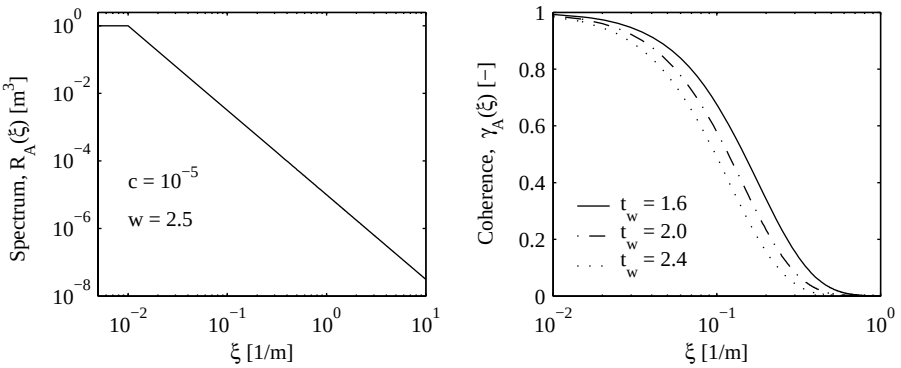

Figure 3: Spectrum and coherence of Model A, when t_w=[1.6, 2.0, 2.4].

The two model parameters are gathered in the vector $\mathbf{p}_A = [c, w]$. The two parameters fully define the model, since the track width t_w is known a priori and ξ_a and ξ_b are fixed constants.

4.2 Model B

The left and right wheel paths are assumed to be statistically equivalent. Moreover, the main variability in the road is described by the two-dimensional process, $\mathbf{Z}^{(0)}(x)$, which consists of two stationary Gaussian processes, corresponding to the left and right wheel path,

$$\mathbf{Z}^{(0)}(x) = \begin{bmatrix} Z_{\mathrm{L}}^{(0)}(x) \\ Z_{\mathrm{R}}^{(0)}(x) \end{bmatrix}. \tag{9}$$

The spectrum and coherence of $\mathbf{Z}^{(0)}(x)$ is given later on.

Irregularities of two types, long-wave (LW) and short-wave (SW), are superimposed to $\mathbf{Z}^{(0)}(x)$. The two irregularity types, LW and SW, occur independently of each other. To illustrate this, a 240 m long road is generated with two superimposed irregularities of each type, see Figure 4. As the example shows, the left and right irregularities have different shape, but occur simultaneously. Also, long-wave and short-wave irregularities may overlap. The j:th long-wave irregularity and the k:th short-wave irregularity are described by the processes $\mathbf{Z}_j^{(1)}(x)$ and $\mathbf{Z}_k^{(2)}(x)$. The road with superimposed irregularities is denoted by $\mathbf{Z}_{\mathrm{B}}(x)$.

The irregularities are modelled as (non-stationary) conditional Gaussian processes. To avoid discontinuities at the start and end of the rough sections, the added irregularities start and end with two values equal to zero, in both left and right track. The irregularities are simulated conditioning on the zero

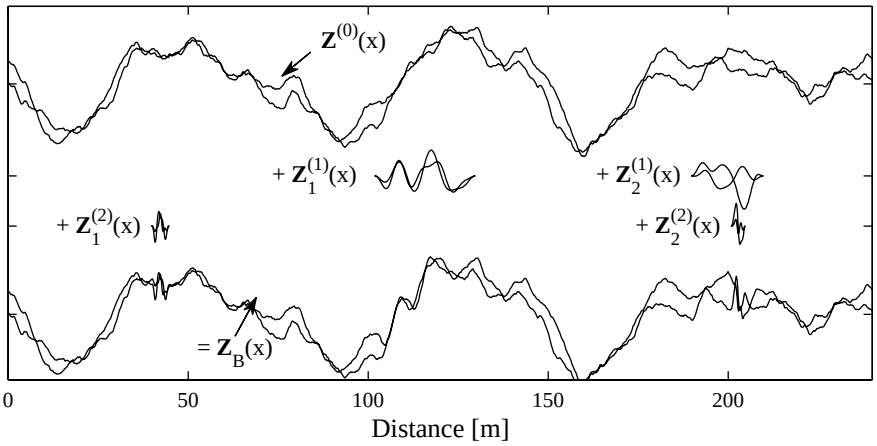

Figure 4: A realization from Model B: $\mathbf{Z}^{(0)}(x)$ = two-dim. stationary Gaussian process, $\mathbf{Z}_j^{(1)}(x)$ = long-wave irregularities, $\mathbf{Z}_k^{(2)}(x)$ = short-wave irregularities. The realized road $\mathbf{Z}_{\mathrm{B}}(x)$ equals the stationary Gaussian process plus simulated irregularities.

boundary levels, for more details see [14]. The irregularity simulation technique is similar to the technique in [15], where the algorithm to realize single-track irregularities is presented. Since the irregularities are non-stationary, it is incorrect to assign a spectral density to them. However, an irregularity reaching from $-\infty$ to $+\infty$ is stationary.

We need to define spectrum, coherence and phase functions for the main process, $\mathbf{Z}^{(0)}(x)$, and infinite length irregularities. As usual, it is a assumed that all cross-spectra are real, hence, the phase functions are zero (see for example [13]). The spectrum and coherence associated with $\mathbf{Z}^{(\eta)}(x)$, for $\eta = 0, 1, 2$ are denoted by $R_{\mathrm{B}}^{(\eta)}$ and $\gamma_{\mathrm{B}}^{(\eta)}$, correspondingly. Many different parametric functions have been proposed for the description of road profile spectrum, see [16] and [17]. Here, the shape in [8] is used for the spectrum of $\mathbf{Z}^{(0)}(x)$,

$$R_{\mathrm{B}}^{(0)}(\xi) \quad = \quad \begin{cases} 10^{a_0}\left(\frac{\xi}{\xi_0}\right)^{-w_1}, & \xi \in [0.01, 0.20], \\ 10^{a_0}\left(\frac{\xi}{\xi_0}\right)^{-w_2}, & \xi \in [0.20, 10], \\ 0, & \text{otherwise}, \end{cases} \tag{10}$$

and for (infinite length) LW- and SW-irregularities,

$$R_{\mathrm{B}}^{(\eta)}(\xi) \quad = \quad \begin{cases} (10^{a_\eta} - 10^{a_0})\left(\frac{\xi}{\xi_0}\right)^{-w_\eta}, & \xi \in \Xi_\eta, \\ 0, & \text{otherwise}, \end{cases} \qquad \eta = 1, 2. \tag{11}$$

As suggested in [18] the coherence is exponentially decreasing,

$$\gamma_{\mathrm{B}}^{(\eta)}(\xi) \quad = \quad \begin{cases} e^{-\rho t_w \xi}, & \xi \in \Xi_\eta, \\ 0 & \text{otherwise}, \end{cases} \quad \eta = 0, 1, 2. \tag{12}$$

The intervals Ξ_η, $\eta = 0, 1, 2$, are given in Table 1 and the reference spatial frequency $\xi_0 = 0.2$ m^{-1}. Note also that these spectra and coherence functions are not compatible with the isotropic assumption used in the previous model.

Symbol	Ξ_0	Ξ_1	Ξ_2
Interval [m^{-1}]	[0.01, 10]	[0.03, 0.2]	[0.2, 2.0]

Table 1: Spatial frequency intervals

Furthermore, the location and length of the sections with added roughness are random. More precisely, the distance between the end of a long-wave irregularity and the start of the next is exponentially distributed with mean θ_1. Similarly, the distance between short-wave irregularities is exponentially distributed with mean θ_2. The length of long-wave and the length of short-wave irregularities are exponentially distributed with mean τ_1 and τ_2, respectively.

All model parameters are gathered in the vector

$$\mathbf{p}_B = [a_0, a_1, a_2, w_1, w_2, \rho, \theta_1, \theta_2, \tau_1, \tau_2], \tag{13}$$

where the spectral parameters a_0, a_1, a_2, w_1, w_2 and ρ are dimensionless and the distance parameters $\theta_1, \theta_2, \tau_1$ and τ_2 are given in meters.

Remark: Analysis of measured single road tracks indicates that actual roads contain short sections with above-average irregularity. Such irregularities are shown to cause most of the vehicle fatigue damage [1]. The single track model, proposed in [1], comprises a stationary Gaussian process and superimposed irregularities of random shape, length and location. An alternative naive first choice of a parallel track model is to use two independent single tracks, modelled as in [1]. However, this gives, as expected, very inaccurate results. A slightly more realistic model use two *correlated* Gaussian processes and superimposed irregularities, where the irregularities are still independently superimposed in left and right track. However, this also gives very inaccurate results. As mentioned, in the proposed Model B, correlated irregularities occur simultaneously in left and right side. The simplifying assumption of simultaneousness is realistic, because when an irregularity is detected in a measured track, the other parallel track is usually also irregular.

5 The lack-of-fit measure

The stochastic models described in the previous section may be used to realize synthetic roads, with parameter values estimated from a measured road. A model is accurate if the synthetic roads and the measured road induce a similar amount of fatigue damage to the half-vehicle. In Section 5.1 the logarithm of the fatigue damage is used to construct a lack-of-fit measure. The measure quantifies dissimilarity between a road model and a measurement. Firstly, an introductory example is discussed, motivating the usefulness of the transformation of the damage to a logarithmic scale.

When we use standard statistical tools to test whether the mean damage from the measured road equals the mean damage from a model, we encounter problems, due to the highly skewed and non-Gaussian distribution of the damage values. More precisely, the measured road is divided into shorter sections, roughly 1 km long. Then damage d_i caused by each section is computed, and treated as independent and identically distributed observations of a random variable, D, where in general D is non-Gaussian.

The standard approach to test if $\mathrm{E}[D]$ equals the expected damage $\mathrm{E}[D_{\mathrm{mod}}]$ caused by a road realised from the stochastic model, would be to construct the statistic

$$\nu = \frac{\bar{d} - \mathrm{E}[D_{\mathrm{mod}}]}{s_d},$$

where $\bar{d} = 1/K \sum_{k=1}^{K} d_i$ is the observed sample mean and s_d the empirical standard deviation, and compare ν to quantiles of the standard Gaussian distribution. Naturally, this test is only valid if K is large enough so that $\bar{d}$ is approximately Gaussian, by the central limit theorem.

As a numerical example, road 11 (which is 21.5 km long) is divided into $K = 21$ equally long sections. With $n = 3$, $\beta = 4$, $v = 50$ km/h, the damage values of the K sections are approximately distributed like a log-normal variable with $\mathrm{E}[\ln D] = -12.25$ and $\mathrm{Var}[\ln D] = 2.13$. With these parameters, 1000 simulations of the sample mean of K log-normal variables, are plotted on a normal probability paper in Figure 5. As illustrated by the figure, the sample mean $\bar{d}$ can not be approximated by a Gaussian variable.

5.1 Transformed fatigue damage

First of all, v, n and β are fixed and $D(v, n, \beta) = D$. The vehicle fatigue D indicated for a stochastic road is a non-negative random variable (r.v.), $D \geq 0$. Generally, the distribution is highly asymmetric, as discussed above. It is therefore more convenient to study the transformation,

$$Q = \frac{\ln D}{\beta}. \tag{14}$$

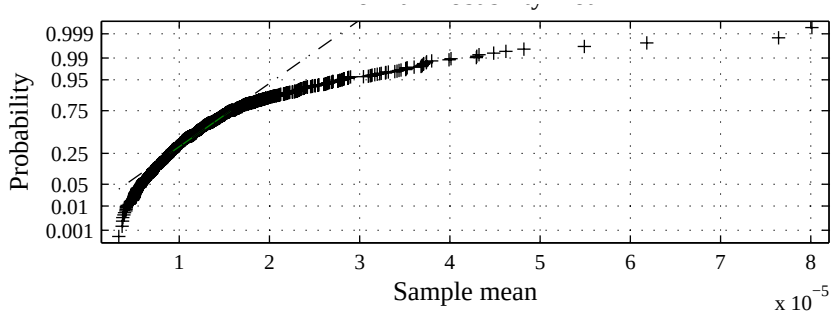

Figure 5: Normal probability plot of the sample mean, $\bar{d} = 1/K \sum_{k=1}^{K} d_i$

A Monte-Carlo study is performed to empirically study the distribution of D and Q. From Model B, 300 synthetic roads of length 5 km are realized with $\mathbf{p}_B = [-5.4, -4.3, -3.2, 3.4, 2.6, 3.3, 300, 900, 30, 4]$. In this specific example, the empirical distribution of Q closely matches the Gaussian distribution, whereas the distribution of D is non-symmetric and non-Gaussian, see Figure 6. This is the same result as obtained in earlier studies [1].

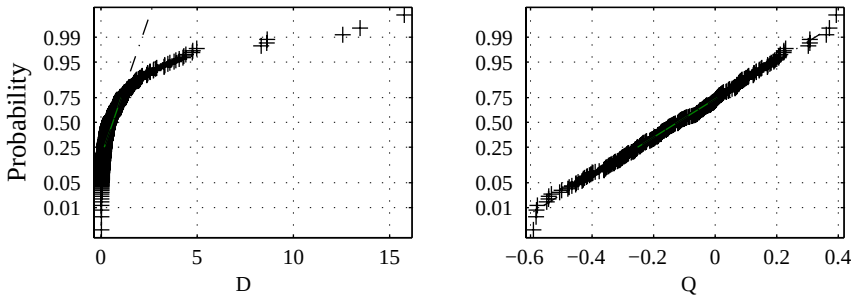

Figure 6: Normal probability plots of D and Q, $v = 70$ km/h, $n = 0$ and $\beta = 7$.

The nomenclature of fatigue damage values indicated by measured and synthetic roads are compiled in Table 2.

We wish to test if synthetic roads induce the same amount of damage (on average) as the measured road. The expected damage values are denoted by $m_o = \mathrm{E}[Q_o]$ and $m_s = \mathrm{E}[Q_s]$. The following hypothesis is tested,

$$\begin{cases} H_0: & m_o = m_s, \\ H_1: & m_o \neq m_s. \end{cases} \tag{15}$$

If H_0 is true, then the road model and the actual road induce the same amount

Road	*Damage*		*Tr. Damage*		*Uncertainty*	
	(r.v)	(outcome)	(r.v)	(outcome)	(True)	(Estim.)
Measured	D_o	d_o	Q_o	q_o	$\sigma_o^2 = \mathrm{Var}(Q_o)$	s_o^2
Synthetic	D_s	d_s	Q_s	q_s		

Table 2: Nomenclature of fatigue related values

of fatigue (on average). If $Q_o \sim N(m_o, \sigma_o^2)$, then the usual test-statistic is

$$\frac{q_o - m_s}{\sigma_o}. \tag{16}$$

In this application σ_o is unknown and has to be estimated. Here, we use a similar test statistic, but with changed sign,

$$\delta = \frac{\bar{q}_s - q_o}{s_o}, \tag{17}$$

where $\bar{q}_s$ estimates m_s, s_o estimates σ_o and q_o is the outcome of the random variable Q_o. With this definition, a negative δ indicates that the model underestimates the damage, and vice versa for a positive δ. The fact that we only have one outcome of Q_o complicates the estimation of the standard deviation σ_o. The standard deviation is estimated by means of bootstrap and described in Section 5.2. Estimation of m_s is easier: it is obtained by Monte Carlo simulation. Synthetic roads are realized from the model and the transformed damage is assessed for each road. The average transformed damage estimates the expected transformed damage,

$$\bar{q}_s = \frac{1}{N_r} \sum_{j=1}^{N_r} q_s^{(j)}, \tag{18}$$

where $q_s^{(j)}$ is the transformed damage from synthetic road j and where N_r is the total number of synthetic roads.

A discrepancy, δ, is computed for each v, n and β. Finally, the lack-of-fit is defined as

$$\delta_{\max} = \delta(v_0, n_0, \beta_0), \tag{19}$$

where $v_0 \in \Psi_v, n_0 \in \Psi_n$ and $\beta_0 \in \Psi_\beta$ are such that $|\delta(v_0, n_0, \beta_0)| \geq |\delta(v, n, \beta)|$ for all $v \in \Psi_v, n \in \Psi_n$ and $\beta \in \Psi_\beta$. To ensure that the road model is validated for a wide range of parameter values the following sets are proposed:

$$\Psi_n = \{0, 1, 2, 3, 4, 5\},\ (N = 5), \tag{20}$$

$$\Psi_\beta = \{3, 4, 5, 6, 7, 8\}, \tag{21}$$

and

$$\Psi_v = \{40, 50, 60, 70, 80, 90\}, [\text{km/h}]. \tag{22}$$

Note that

$$|\delta_{\max}| = \max_{v\in\Psi_v, n\in\Psi_n, \beta\in\Psi_\beta} |\delta(v; n; \beta)|. \tag{23}$$

Note also that there are 6 elements in each of the three sets, which gives in total $6^3 = 216$ combinations. Thus, $\delta_{\max}$ corresponds to the *worst* model fit of these 216 combinations. A negative value of $\delta_{\max}$ indicates that the model gives non-conservative fatigue damage estimates, and vice versa for a positive value.

5.2 Estimation of σ_o using bootstrap

To compute the discrepancy $\delta(v; n; \beta)$ the standard deviation σ_o has to be estimated for each v, n and β. This section describes the estimation procedure for fix values of v, n and β.

The load sequence $\ddot{u}(x)$, obtained by simulation of the half-vehicle response on the measured road, is divided into K equally long subsequences. Each subsequence is at least 1 km long, for example, if the measured road is 8.8 km, the road is divided into 8 subsequences, 1.1 km long. The rainflow damage of the subsequences are $\tilde{b}_k$ for $k = 1, \ldots, K$. The partial damage values are normalised to ensure that the sum of the partial damage values equal the total observed damage d_o,

$$b_k = \tilde{b}_k \frac{d_o}{\sum_{j=1}^{K} \tilde{b}_j}. \tag{24}$$

Then, the transformed damage can be expressed as

$$q_o = \frac{1}{\beta} \ln\left(\sum_{k=1}^{K} b_k\right). \tag{25}$$

Note that $d_o = \sum_{k=1}^{K} b_k$. The purpose of expressing q_o as a function of the partial damage values is to enable estimation of $\sigma_o = \sqrt{\text{Var}(Q_o)}$. It is assumed that the partial damage values b_k are outcomes from independent and identically distributed random variables. This assumption is questionable, but used here for simplicity. By employment of the Bootstrap algorithm it is possible to obtain bootstrap observations,

$$q^* = \frac{1}{\beta} \ln\left(\sum_{k=1}^{K} b_k^*\right), \tag{26}$$

where b_k^* is a bootstrap sample from $\{b_j\}_{j=1,\ldots,K}$. Thus, q^* can be treated as an additional outcome of the random variable Q_o. The bootstrap algorithm is

repeated N_{boot} times, producing the bootstrap observations q_l^*, $l = 1, ..., N_{\text{boot}}$. For more details about bootstrap, see (e.g.) [19]. Finally, an estimate of the standard deviation σ_o is simply the empirical standard deviation of the bootstrap samples,

$$s_o = \sqrt{\frac{1}{N_{\text{boot}} - 1} \sum_{l=1}^{N_{\text{boot}}} \left(q_l^* - \bar{q}^*\right)^2} \tag{27}$$

where $\bar{q}^* = \frac{1}{N_{\text{boot}}} \sum_{l=1}^{N_{\text{boot}}} q_l^*$.

An estimate s_o is obtained for each v, n and β. It measures the uncertainty of the observed (transformed) damage $Q_o(v; n; \beta)$.

Naturally, the accuracy of the bootstrap estimate improves with increasing road length. Figure 7 shows the result of a Monte-Carlo simulation of 50 synthetic roads of length 100 km. The roads are realized from Model B, with $\mathbf{p}_B = [-5.6, -4.4, -3.7, 3.4, 1.7, 3.2, 350, 1000, 30, 5]$. The transformed damage $Q(x)$ is computed as function of travelled distance x, for each road, with $n = 3$, $\beta = 4$ and $v = 70$ km/h. The empirical standard deviation of $Q(x)$ (solid line) and corresponding confidence interval of $\sigma_o(x)$ (dotted lines) are plotted in Figure 7. For comparison a bootstrap estimate of σ_o is computed for each road, for $x = 10, 20, \ldots, 100$ km. As illustrated by the figure, the bootstrap estimate approaches the true standard deviation as length increases. Note also the uncertainty of the bootstrap estimate for distances between 10 and 50 km. This will influence the uncertainty associated with the lack-of-fit measure and is discussed in Section 6.

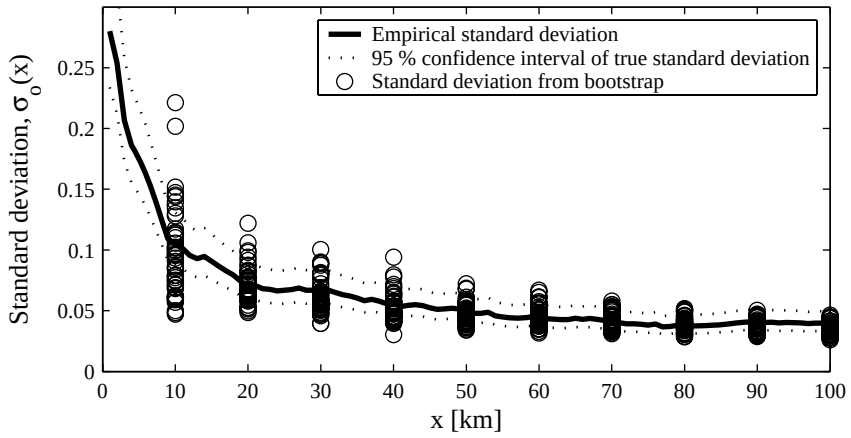

Figure 7: Convergence of bootstrap estimate, $n = 3$, $\beta = 4$ and $v = 70$ km/h.

Remark: In Section 3 it was claimed that κ is unimportant. Now, this is verified by observing that δ is not a function of κ. First of all, note that a difference between two transformed damage values can be rewritten as

$$q_1 - q_2 = \frac{\ln d_1}{\beta} - \frac{\ln d_2}{\beta} = \frac{1}{\beta} \ln \left(\frac{d_1}{d_2} \right). \tag{28}$$

The parameter κ cancels in the ratio $\frac{d_1}{d_2}$, which implies that $q_1 - q_2$ is not a function of κ. Moreover, since the numerator of δ is $\bar{q}_s - q_o$ and the denominator of δ is a function of $q_b^* - \bar{q}^*$, it follows that δ is not a function of κ.

6 Rejection region

If $\delta_{\max}$ belong to the *rejection region*, the hypothesis H_0 should be rejected. The probability to reject H_0 when H_0 is true (Type I error) is α_I. In this section an approximate rejection region when $\alpha_I = 0.05$ is searched for. The region where H_0 cannot be rejected is referred to as the *acceptance region*.

First of all, the lack-of-fit $\delta_{\max}$, is treated as the outcome of the random variable which satisfies

$$|\Delta_{\max}| = \max_{v,n,\beta} \left| \frac{\bar{Q}_s(v;n;\beta) - Q_o(v;n;\beta)}{S_o(v;n;\beta)} \right|, \tag{29}$$

where $\bar{Q}_s$ is the (random) average transformed damage from the model and S_o is the estimator of the standard deviation. We want to study the probability density function (PDF) of $\Delta_{\max}$. In particular, the quantile λ is of interest,

$$\mathrm{P}(-\lambda \leq \Delta_{\max} \leq \lambda \,|H_0 \text{ true}) = 1 - 0.05. \tag{30}$$

Note that $\Delta_{\max}$ is a function of the random variables Q_o and S_o, which are obtained from the observed road. Hence, to compute the PDF of $\Delta_{\max}$ it is necessary to know the true model of the observed road. By 'true model' we mean that roads realized from this model are statistically equivalent to the observed (measured) road. However, this model is of course unknown, so it is neither possible to exactly compute the PDF of $\Delta_{\max}$ nor the quantile λ.

The road models defined in Section 4, are used to empirically study the PDF of $\Delta_{\max}$ under H_0. First, $J = 500$ roads are realized from one of the models. Then each of the J synthetic roads is treated as the observed road. The 'observed' road is then compared to the other $J - 1$ synthetic roads, by computation of $\delta_{\max}$. Thus, lack-of-fit measures, $\delta_{\max,i},\ i = 1, \ldots J$, are computed, when we know that H_0 is true. Two different road lengths are studied: 10 and 50 km. The left-hand-side histograms in Figures 8 and 9 estimate the PDF of $\Delta_{\max}$. A straight-forward estimation of λ satisfies $\frac{\#\{|\delta_{\max,i}| > \tilde{\lambda}\}}{J} = 0.05$.

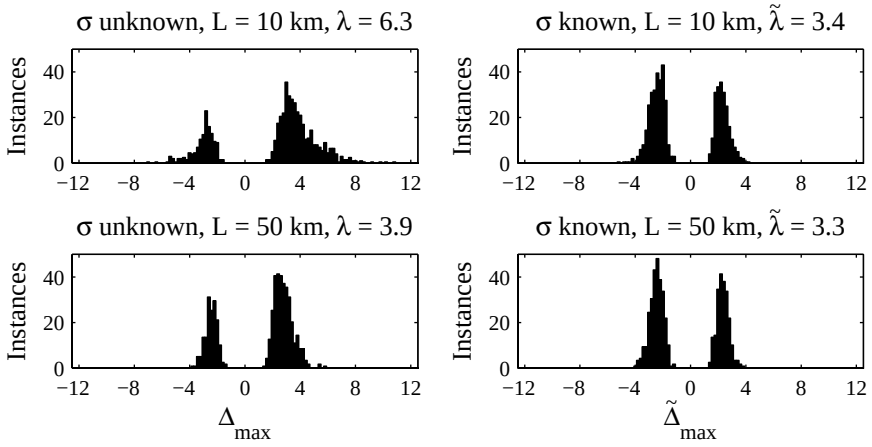

Figure 8: Histogram of $\Delta_{\max}$ and $\tilde{\Delta}_{\max}$, when $L = 10,\ 50$ km. The synthetic roads are realized from model A, with $\mathbf{p}_A = [10^{-5}, 2]$ and $t_w = 2$ m.

In this theoretical context, when we have several realizations from the true model, the standard deviation can be accurately estimated. Hence, the following random variable can be accurately computed,

$$|\tilde{\Delta}_{\max}| = \max \left| \frac{\bar{Q}_s(v; n; \beta) - Q_o(v; n; \beta)}{\sigma_o(v; n; \beta)} \right|. \tag{31}$$

The standard deviation, σ_o, is replaced by the empirical standard deviation,

$$\tilde{s}_o = \sqrt{\frac{1}{J-1} \sum_{j=1}^{J} \left(q_s^{(j)} - \bar{q}_s \right)^2}. \tag{32}$$

Since J is large, $\tilde{s}_o$ is accurate and we can consider σ_o as known. The affect of estimating σ_o is studied by comparison of $\Delta_{\max}$ and $\tilde{\Delta}_{\max}$. In particular, it is interesting to compare the quantiles λ and $\tilde{\lambda}$, where $\tilde{\lambda}$ satisfies

$$\mathrm{P}(-\tilde{\lambda} \leq \tilde{\Delta}_{\max} \leq \tilde{\lambda} \,|H_0 \text{ true}) = 1 - 0.05. \tag{33}$$

The right-hand-side histograms in Figures 8 and 9 show that $\tilde{\Delta}_{\max}$ is insensitive to changes of measurement length and change of true road model. Hence if we could compute σ_o accurately a reasonable acceptance region would be, say, $[-3.3, 3.3]$. But, in practical situations σ_o has to be estimated. This implies that the acceptance region has to be wider than [-3.3,3.3], since the estimation of σ_o increase the variability of the lack-of-fit measure. Note especially the higher variability of $\Delta_{\max}$ in the top left histogram in Figure 9. This

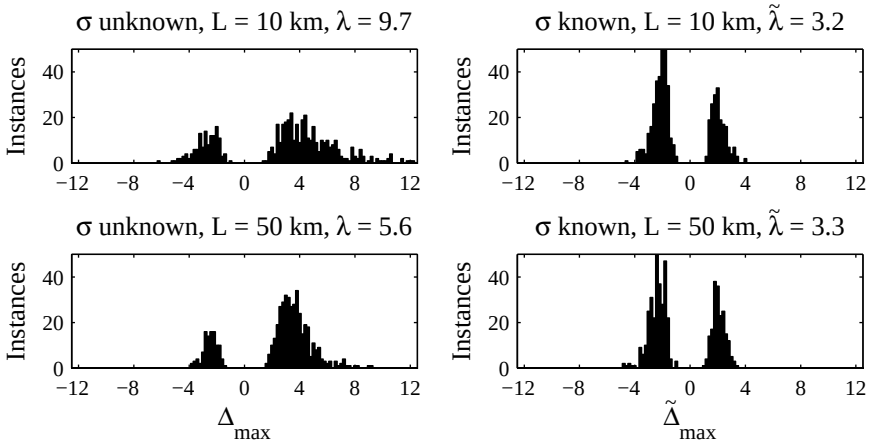

Figure 9: Histogram of $\Delta_{\max}$ and $\tilde{\Delta}_{\max}$, when $L = 10$, 50 km. The synthetic roads are realized from model B, with $t_w = 2$ m and $\mathbf{p}_B = [-5.3, -4.2, -2.9, 3.4, 3.4, 2.3, 320, 1000, 34, 4.5]$.

is due to short road length (10 km). Hence, the measurement length is crucial, the measurement has to be long enough to enable accurate estimation of σ_o. Thus, results presented in Section 7 (Figure 10) should be considered together with the provided measurement length information. Finally, the analysis and discussion above cannot provide unequivocal rejection and acceptance regions, a bit of judgement is also required. In the present work, the following three regions are selected: $|\delta_{\max}| > 7$, $5 < |\delta_{\max}| \leq 7$, $0 \leq |\delta_{\max}| \leq 5$ indicating unsatisfactory model accuracy (rejection region), doubtful model accuracy and satisfactory model accuracy (acceptance region), respectively.

7 Model evaluation using $\delta_{\max}$

Model A and Model B are fitted to each of the 20 actual roads, by estimation of $\mathbf{p}_A$ and $\mathbf{p}_B$ from the measurements. Estimation of $\mathbf{p}_B$ is described in detail in [14]. Twenty lack-of-fit values are computed for each model. The number of synthetic roads, N_r, to compute $\bar{q}_s$ is set to 100. Hence $20 * 100$ synthetic roads are simulated from each model.

The results are presented in Figure 10. Model A is inaccurate: It has 0 satisfactory, 2 doubtful and 18 unsatisfactory values of $\delta_{\max}$. Model B performs better: It has 7 satisfactory, 9 doubtful and 4 unsatisfactory values of $\delta_{\max}$.

Recall that each computed $\delta_{\max}$ corresponds to the worst fit, obtained from 216 discrepancies $\delta(v, n, \beta)$. Thus, Figure 10 presents these worst case fits.

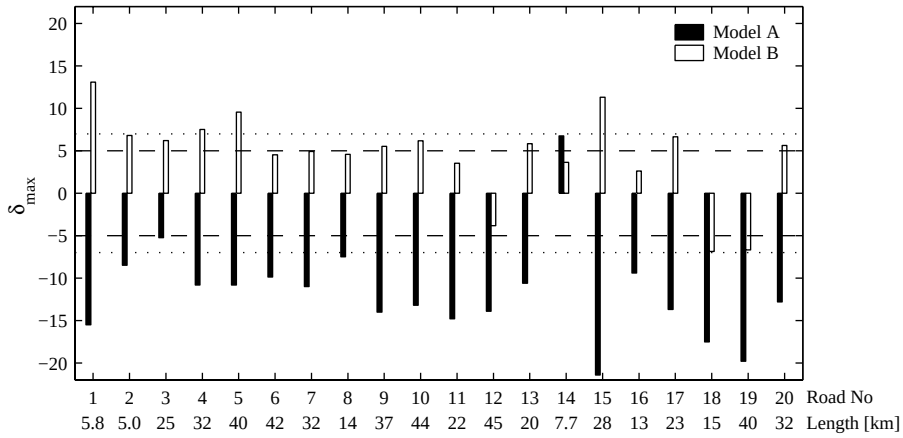

Figure 10: Lack of fit of Models A and B.

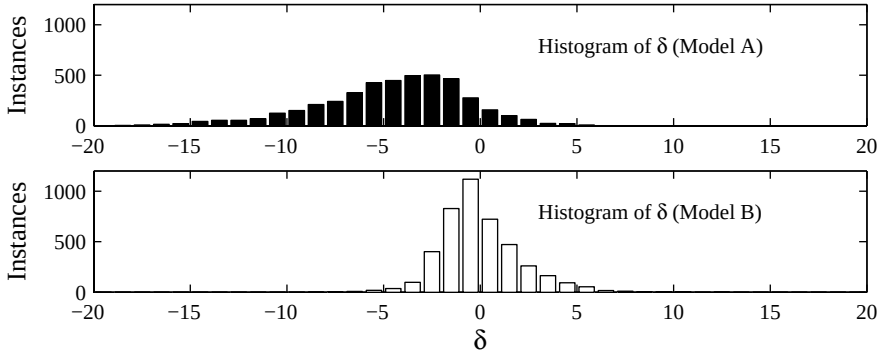

Figure 11: Histograms of δ, for Models A and B.

In Figure 11 all discrepancies from the 20 actual roads are presented in a histogram. There are in total $20 * 216 = 4320$ computed discrepancies. Hence, Figure 11 displays the general behaviour of Models A and B. Model A obtains in most cases discrepancies from -10 to 0, (i.e. underestimated fatigue damage values), due to the lack of inclusions of irregularities. Model B obtains in most cases discrepancies from -5 to $+5$.

8 Conclusions

The lack-of-fit measure $\delta_{\max}$ quantifies discrepancy between a stochastic model and two measured parallel road tracks. The accuracy of different models is easily compared when presented as in Figures 10 and 11. The lack-of-fit measure is calculated by scanning a lot of different parameter settings (i.e. different combinations of the vehicle velocity v, the left-right unit n and the fatigue parameter β). The combination of v, n and β which gives the largest discrepancy defines the lack-of-fit. Hence, to receive a low lack-of-fit a model has to be general, accurate in many different settings.

9 Comments

The isotropic Gaussian model (Model A) is a convenient model to use, since it is simple and, here, uniquely defined by only two parameters. However, the results in Section 7 clearly show that Model A is inaccurate. Model B is a more complex model, it includes irregularities of random length, shape and location. Model B is a more accurate road roughness model. Other models were also studied but Model B was the most accurate.

10 Acknowledgements

Scania and The Programme Council for Vehicle Research within The Swedish Agency for Innovation Systems (PFF/VINNOVA) have supported this work. The author is grateful to Prof. Igor Rychlik and Dr Anders Forsén for their valuable comments.

References

[1] Bogsjö K. Stochastic modelling of road roughness, Licentiate of engineering thesis, Lund Institute of Technology, Lund Sweden, 2005.

[2] Ahlin K, Granlund J, Lindström F. Comparing road profiles with vehicle perceived roughness, *Int. J. Vehicle Design*, Vol. 36, Nos. 2/3, pp. 270–286, 2004.

[3] Wedig W.V. Vertical dynamics of riding cars under stochastic and harmonic base excitations, IUTAM Symposium on Chaotic Dynamics and Control of Systems in Mechanics, 371–381, 2005.

[4] Beste A, Dreßler K, Kötzle H, Krüger W, Maier B, Petersen J. Multiaxial rainflow: A consequent continuation of Professor Tatsuo Endo's work, The rainflow method in fatigue (ed. by Y. Murakami), Oxford, 1992.

[5] Dreßler K, Köttgen VB, Kötzle H. Tools for fatigue evaluation of non-proportional loading, Fatigue Design 95, Vol. 1, 261-279, VTT, Espoo 1995.

[6] Rychlik I. A new definition of the rainflow cycle counting method, *Int. J. of fatigue* Vol. 9, pp. 119–121, 1987.

[7] Wittig LE, Sinha AK, Simulation of multicorrelated random processes using the FFT algorithm. *Journal of acoustical society of America*, 58(3), 630–634, 1975.

[8] Robson JD, Dodds CJ. The description of road surface roughness', *J. Sound and vibration*, Vol 31, pp. 175–183, 1973.

[9] Kamash KMA, Robson JD. The application of isotropy in road surface modelling. *J. Sound and Vibration*, Vol 57, No 1, pp. 89–100, 1978.

[10] ISO 8608. *Mechanical Vibration — Road Surface Profiles — Reporting of Measured Data*', International Organisation for Standardisation, Geneva, 1995.

[11] Szöke D, Kuti I. A new development in the numerical description of road profile realisations. Int. J. Vehicle Design, Vol 34, No. 2, pp. 183–190, 2004.

[12] Sun L, Kenis W, Wang W, Stochastic spatial excitation induced by a distributed contact on homogenous Gaussian random fields. *J. Engineering Mechanics* Vol 132, No 7, July 1, 2006.

[13] Yonglin Z, Jiafan Z, Numerical simulation of stochastic road process using white noise filtration, *Mechanical Systems and Signal Processing*, Vol 20, No 2, pp. 363–372, 2006.

[14] Bogsjö K, Evaluation of stochastic models of parallel road tracks, Technical report, Lund University, Centre for Mathematical Sciences, Mathematical Statistics, LUTFMS-5066-2007, 2007:16.

[15] Bogsjö K, Development of analysis tools and stochastic models of road profiles regarding their influence on heavy vehicle fatigue, *Suppl. Vehicle System Dynamics*, Vol 44, pp. 780-790, 2006. (Paper B in this thesis.)

[16] Andrén P, Power spectral density approximations of longitudinal road profiles, *Int. J. Vehicle Design*, Vol 40, No 1/2/3, pp. 2–14, 2006.

[17] Wedig WV, Parameter identification of road spectra and nonlinear oscillators, In *Analysis and estimation of stochastic mechanical systems (Udine, 1987)*, CISM Courses and Lectures, 303, Springer, Vienna, 217–242, 1988.

[18] Bogsjö K, Coherence of road roughness in left and right wheel-path, Accepted for publication in *Suppl. Vehicle System Dynamics*. (Paper E in this thesis.)

[19] Davison AC, Hinkley DV, Bootstrap methods and their applications, Cambridge: Cambridge University Press, 1997.

[20] Gustafsson F, Determining the initial states in forward-backward filtering, IEEE Transactions on Signal Processing, Vol 44, No 4, 1996.

[21] Brockwell PJ, Davis RA, *Time series: Theory and methods*, Second edition. Springer-Verlag, New York, 1991.

[22] Welch PD, The use of the fast fourier transform for the estimation of spectra: A method based on time averaging over short modified periodograms, IEEE Trans. Audio Electroacoust., AU-l5, 2, pp. 70–73, 1967.

[23] Carter GC, Coherence and time delay estimation, Proceedings of the IEEE, Vol 75, No 2, pp. 236–255, 1987.

Technical details

This section covers technical details which are not part of the paper in press. Here they are added in order to clarify how irregularities are simulated (Appendix A) and how parameters in Model B are estimated (Appendix B).

A Simulation of a road irregularity

Here an algorithm is presented on how to simulate a road irregularity in left and right wheel path. The algorithm is based on the well-known theory of conditional Gaussian vectors. However, since this technique has not been used before in this application, and that the irregularities are very important for the results, a detailed description of the simulation algorithm follows.

Let $Z_{\mathrm{L}}(x)$ and $Z_{\mathrm{R}}(x)$ be two correlated, identically distributed, mean zero, stationary Gaussian sequences. Their one-sided spectrum is given by (11), their cross-spectrum is given by the coherence function (12) and the zero phase function. To simplify notation, let the sampled process $Z_\nu(kh) = Z_\nu[k]$, for $k = 1, \ldots, N$, and $\nu = L, R$. Furthermore, it is convenient to define the two column vectors

$$\mathbf{Y}_1 = (Z_{\mathrm{L}}[3],\ \ldots\ Z_{\mathrm{L}}[N-2],\ Z_{\mathrm{R}}[3],\ \ldots\ Z_{\mathrm{R}}[N-2])^T \tag{34}$$

and

$$\mathbf{Y}_2 = (Z_{\mathrm{L}}[1],\ Z_{\mathrm{L}}[2],\ Z_{\mathrm{L}}[N-1],\ Z_{\mathrm{L}}[N],\ Z_{\mathrm{R}}[1],\ Z_{\mathrm{R}}[2],\ Z_{\mathrm{R}}[N-1],\ Z_{\mathrm{R}}[N])^T, \tag{35}$$

where ^{T} denotes matrix transpose. We want to simulate $\mathbf{Y}_1|\mathbf{Y}_2 = \mathbf{0}$, (i.e. condition on zero start and end levels). Define

$$\tilde{\mathbf{Y}} = \mathbf{Y}_1 - \mathbf{\Sigma}_{12}\mathbf{\Sigma}_{22}^{-1}\mathbf{Y}_2, \tag{36}$$

where $\mathbf{\Sigma}_{12} = \mathrm{cov}(\mathbf{Y}_1, \mathbf{Y}_2) = \mathrm{E}[\mathbf{Y}_1\mathbf{Y}_2^T]$ and $\mathbf{\Sigma}_{22} = \mathrm{cov}(\mathbf{Y}_2, \mathbf{Y}_2) = \mathrm{E}[\mathbf{Y}_2\mathbf{Y}_2^T]$. The expectation and covariance of $\tilde{\mathbf{Y}}$ are

$$\begin{aligned} &\mathrm{E}[\tilde{\mathbf{Y}}] = \mathbf{0}, \\ &\mathrm{cov}(\tilde{\mathbf{Y}}, \tilde{\mathbf{Y}}) = \mathbf{\Sigma}_{11} - \mathbf{\Sigma}_{12}\mathbf{\Sigma}_{22}^{-1}\mathbf{\Sigma}_{21}. \end{aligned} \tag{37}$$

This coincides with the expectation and covariance of the conditional Gaussian process of $\mathbf{Y}_1$ given $\mathbf{Y}_2 = \mathbf{0}$, thus $\tilde{\mathbf{Y}}$ represents $\mathbf{Y}_1|\mathbf{Y}_2 = \mathbf{0}$. In order to compute $\tilde{\mathbf{Y}}$ we need the covariance matrices $\mathbf{\Sigma}_{12}$ and $\mathbf{\Sigma}_{22}$. Firstly, the sampled covariance function is denoted by $r_{\mu\nu}[k] = r_{\mu\nu}(kh)$, for $\mu, \nu = L, R$. And, secondly, to simplify notation, if $\mathbf{A}$ is an integer-valued matrix,

$$\mathbf{A} = \begin{pmatrix} a_{11} & \ldots & a_{1p} \\ \vdots & \ddots & \vdots \\ a_{j1} & \ldots & a_{jp} \end{pmatrix} \tag{38}$$

then

$$r_{\mu\nu}[\mathbf{A}] = \begin{pmatrix} r_{\mu\nu}[a_{11}] & \dots & r_{\mu\nu}[a_{1p}] \\ \vdots & \ddots & \vdots \\ r_{\mu\nu}[a_{j1}] & \dots & r_{\mu\nu}[a_{jp}] \end{pmatrix}. \tag{39}$$

Moreover, let

$$\mathbf{A}_1 = \begin{pmatrix} 0 & -1 & 2-N & 1-N \\ 1 & 0 & 3-N & 2-N \\ N-2 & N-3 & 0 & -1 \\ N-1 & N-2 & 1 & 0 \end{pmatrix} \tag{40}$$

and

$$\mathbf{A}_2 = \begin{pmatrix} 2 & 1 & 4-N & 3-N \\ 3 & 2 & 5-N & 4-N \\ \vdots & \vdots & \vdots & \vdots \\ N-3 & N-4 & -1 & -2 \end{pmatrix}. \tag{41}$$

Then

$$\mathbf{\Sigma}_{22} = \begin{pmatrix} r_{\mathrm{LL}}[\mathbf{A}_1] & r_{\mathrm{LR}}[\mathbf{A}_1] \\ r_{\mathrm{RL}}[\mathbf{A}_1] & r_{\mathrm{RR}}[\mathbf{A}_1] \end{pmatrix} \tag{42}$$

and

$$\mathbf{\Sigma}_{12} = \begin{pmatrix} r_{\mathrm{LL}}[\mathbf{A}_2] & r_{\mathrm{LR}}[\mathbf{A}_2] \\ r_{\mathrm{RL}}[\mathbf{A}_2] & r_{\mathrm{RR}}[\mathbf{A}_2] \end{pmatrix}. \tag{43}$$

To realize a synthetic irregularity: Simulate the unconditional correlated Gaussian sequences $Z_{\mathrm{L}}[k]$ and $Z_{\mathrm{R}}[k]$, identify $\mathbf{Y}_1$ and $\mathbf{Y}_2$, calculate the auto- and cross-covariance from the spectrum and the cross-spectrum, calculate $\mathbf{\Sigma}_{22}$ and $\mathbf{\Sigma}_{12}$, and finally compute the irregularity $\tilde{\mathbf{Y}}$, according to (36). Simulation of unconditional correlated Gaussian processes is described in [7].

B Estimation of parameters in Model B

This section describes how the parameters in model B are estimated from the measurement data.

B.1 Estimation of spectral parameters a_0, a_1, a_2, w_1 and w_2

In Paper B a method is described which identifies road sections in a road profile belonging to three roughness classes: regular sections (class 0), long-wave irregularities (class 1) and short-wave irregularities (class 2). Here, left and right tracks are analysed separately, according to the method described in Paper B.

Prior to analysis the left and right road profiles are high-pass filtered to avoid leakage from lower to higher frequencies. The filtering is performed in two steps, as described in [20]: First, the original sequence is filtered in the forward direction, then the reversed filtered sequence is run back through the same filter. The resulting sequence has a zero phase shift compared to the original sequence.

The utilised filter is a high-pass Butterworth filter of order 5 and with a cut-off frequency, ξ_{cut}. The cut-off frequency defines the spatial frequency where the attenuation is $1/\sqrt{2}$ for the single filter (1/2 for the 'forward-backward' filter). The value of ξ_{cut} depends on roughness class and is stated in Table 3. Figure 12 displays a part of an original profile (road 4, right track) and its corresponding filtered profiles. In Figure 13 the same part of road 4R is plotted, where road sections have been classified.

Roughness class	η	ξ_{cut} [m^{-1}]
Regular	0	0.02
Long-wave irregularity	1	0.02
Short-wave irregularity	2	0.10

Table 3: Cut-off frequencies for different roughness classes

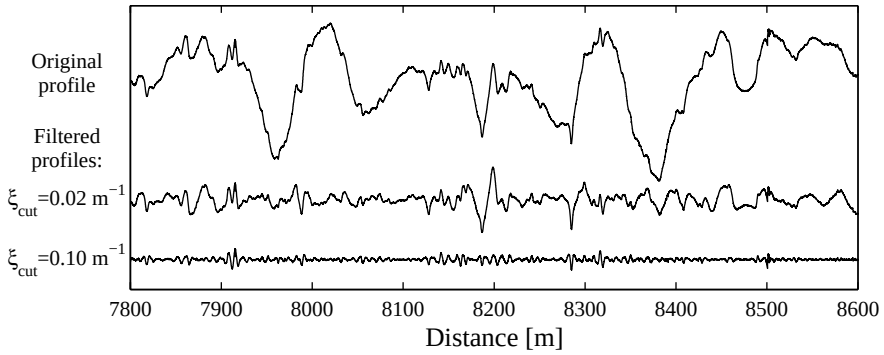

Figure 12: Original and filtered road 4R.

It is assumed that a class 0 section is a realization of the purely Gaussian process $\mathbf{Z}^{(0)}(x)$, whereas a class 1 or 2 section is composed of two independent components: the purely Gaussian process and a superimposed irregularity. Therefore the spectral density of such a section equal the sum of the spectral densities of the two components (neglecting that irregularities are non-

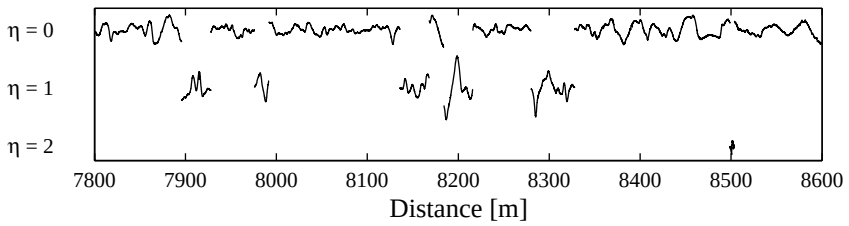

Figure 13: Classification of road sections in Road 4R.

stationary). More precisely, the spectrum of a section of class 0, 1, or 2, is

$$S_0(\xi) = R_{\mathrm{B}}^{(0)} = \begin{cases} 10^{a_0} \left(\frac{\xi}{\xi_0}\right)^{-w_1}, & \xi \in [0.03, 0.20] \\ 10^{a_0} \left(\frac{\xi}{\xi_0}\right)^{-w_2}, & \xi \in [0.20, 2.00] \end{cases} \tag{44}$$

$$S_1(\xi) = R_{\mathrm{B}}^{(0)} + R_{\mathrm{B}}^{(1)} = 10^{a_1} \left(\frac{\xi}{\xi_0}\right)^{-w_1}, \quad \xi \in [0.03, 0.20] \tag{45}$$

$$S_2(\xi) = R_{\mathrm{B}}^{(0)} + R_{\mathrm{B}}^{(2)} = 10^{a_2} \left(\frac{\xi}{\xi_0}\right)^{-w_2}, \quad \xi \in [0.20, 2.00] \tag{46}$$

correspondingly. In logarithmic scale the equations become linear, e.g.

$$\log_{10} S_1 = a_1 - w_1 \log_{10}(\xi/\xi_0). \tag{47}$$

The estimates of a_0, a_1, a_2, w_1 and w_2 are based on computations of several periodograms. The periodogram of the j:th section of roughness class η, $z(kh + k_j h)$, $k = 0, \ldots, M_j - 1$, is defined by

$$\tilde{I}_\eta^j(\xi) = \frac{2h}{M_j} \left| \sum_{k=0}^{M_j-1} z(kh + k_j h) \exp(-i2\pi kh\xi) \right|^2, \tag{48}$$

where h is the sample distance and M_j is the number of samples in section j. In order to improve the estimate the sections are detrended and windowed. The detrended section is the section with removed linear trend, denoted by $z_d(kh + k_j h)$, $k = 0, \ldots, M_j - 1$. Instead of the 'raw' periodogram (48), the modified periodogram is used,

$$I_\eta^j(\xi) = 2h \left| \sum_{k=0}^{M_j-1} H(kh) z_d(kh + k_j h) \exp(-i2\pi kh\xi) \right|^2, \tag{49}$$

where H is a Hanning window, normalised so that $\sum_{k=1}^{M_j} |H(kh)|^2 = 1$. The modified periodogram is evaluated at the Fourier frequencies, $\xi_m = m/(M_j h)$, $m = 0, \ldots, M_j/2$ (assuming M_j even).

To simplify notation the superscript j and subscript η in $\tilde{I}_\eta^j$ and I_η^j is omitted if not important. The theoretical properties of $\tilde{I}(\xi)$, (when z is Gaussian) are discussed in [21]. The periodogram is scattered around the true spectrum following a standard exponential distribution ($\mathrm{E}[\Lambda_m^j] = 1$),

$$\tilde{I}^j(\xi_m) = R(\xi_m)\Lambda_m^j. \tag{50}$$

This implies that $\tilde{I}$ is unbiased: $\mathrm{E}[\tilde{I}(\xi_m)] = R(\xi_m)$. But, in logarithmic scale this is not the case:

$$\begin{aligned}\mathrm{E}[\log_{10}(\tilde{I}(\xi_m))] &= \log_{10}(R(\xi_m)) + \mathrm{E}[\log_{10}\Lambda_m] \\ &= \log_{10}(R(\xi_m)) - 0.25068.\end{aligned} \tag{51}$$

The variance is constant in logarithmic scale,

$$\mathrm{Var}[\log_{10}(\tilde{I}(\xi_m))] = \mathrm{Var}[\log_{10}\Lambda_m] = 0.310. \tag{52}$$

The exponential random variables Λ_m^j and Λ_p^j are independent if $p \neq m$. Also, Λ_m^k and Λ_m^j can be assumed to be independent if $k \neq j$ since sections k and j usually are well separated in space. Now, it is assumed all theoretical results hold approximately when the $I(\xi)$ is used instead of $\tilde{I}(\xi)$.

Linear regression is used to fit the spectral parameters, since $\log_{10} S_\eta$ is linearly dependent of $\log_{10}(\xi)$, and the estimates $\log_{10} I_\eta^j, j = 1, 2, \ldots,$ are independent with constant variance. The periodogram values obtained from all sections of class η are denoted $I_\eta(\xi_j^{(\eta)})$, $j = 1, \ldots, n_\eta$. The parameters a_0, a_1 and w_1 is estimated from $I_0(\xi_j^{(0)})$ and $I_1(\xi_j^{(1)})$, taking only into account spatial frequencies in the range $[0.04, 0.20]$. The system of equations used to obtain the least square fitted values of a_0, a_1 and w_1 is

$$\underbrace{\begin{pmatrix} 1 & 0 & -\log_{10}(\xi_1^{(0)}/\xi_0) \\ \vdots & \vdots & \vdots \\ 1 & 0 & -\log_{10}(\xi_{n_0}^{(0)}/\xi_0) \\ 0 & 1 & -\log_{10}(\xi_1^{(1)}/\xi_0) \\ \vdots & \vdots & \vdots \\ 0 & 1 & -\log_{10}(\xi_{n_1}^{(1)}/\xi_0) \end{pmatrix}}_{=\mathbf{X}} \underbrace{\begin{pmatrix} a_0 \\ a_1 \\ w_1 \end{pmatrix}}_{=\alpha} = \underbrace{\begin{pmatrix} \log_{10}(I_0(\xi_1^{(0)})) \\ \vdots \\ \log_{10}(I_0(\xi_{n_0}^{(0)})) \\ \log_{10}(I_1(\xi_1^{(1)})) \\ \vdots \\ \log_{10}(I_1(\xi_{n_1}^{(1)})) \end{pmatrix}}_{=\mathbf{y}}. \tag{53}$$

The least square fit is $\hat{\alpha} = (\mathbf{X}^T\mathbf{X})^{-1}\mathbf{X}^T\mathbf{y}$, and

$$\mathrm{E}[\hat{\alpha}] = (\mathbf{X}^T\mathbf{X})^{-1}\mathbf{X}^T\mathrm{E}[\mathbf{y}] = \begin{pmatrix} a_0 - 0.25068 \\ a_1 - 0.25068 \\ w_1 \end{pmatrix}. \tag{54}$$

Hence, the LS-fits of a_0 and a_1 are biased and the LS-fit w_1 is unbiased. The estimates of a_0 and a_1 are therefore corrected by $+0.25068$. Moreover, $\mathrm{Var}[\hat{\alpha}] = 0.310(\mathbf{X}^T\mathbf{X})^{-1}$. The least squares estimates of a_2 and w_2 are obtained in a similar way using $I_0(\xi)$ and $I_2(\xi)$, for $\xi \in [0.20, 1.0]$.

B.2 Estimation of the coherence parameter, ρ

The coherence parameter is estimated from road sections which have no identified irregularity in any track. These sections are assumed to be observations of the purely Gaussian process $\mathbf{Z}^{(0)}$, which have an exponentially decreasing coherence function, see (12).

The computation of the empirical coherence is complicated since the smooth sections have different length. The length of each analysed segment decides the frequency sampling rate. Hence, all smooth sections are cut into 50 m long parts. Then Welch's non-overlapped averaged segment method [22] is used to estimate the (squared) non-parametric coherence function. The bias of the estimate, stated in [23], is removed. The (squared) exponential function (12) is fitted to the non-parametric estimate using least squares. The fit is made in the spatial frequency range $[0.04,\ 0.2]$.

B.3 Estimation of distance parameters

The average of the empirical lengths of identified sections is used to estimate θ_1, θ_2, τ_1 and τ_2. To exemplify, if ζ_j is the observed length of LW-irregularity j and the total number of identified LW-irregularities are N_1, then $\hat{\tau}_1 = \frac{1}{N_1}\sum_j \zeta_j$.

E

Paper E

Coherence of road roughness in left and right wheel-path

KLAS BOGSJÖ

ABSTRACT

The coherence function between road roughness in left and right wheel-path is studied. Empirical coherence functions are computed from 20 measured roads, with a total length of 520 km. It is found that the coherence estimates are similar, despite the wide range of studied road types. A one-parametric model, which describes the coherence using an exponentially decreasing function, is compared to the common isotropic model. It is found that the parametric model gives more accurate approximations of the empirical coherence functions than the isotropic model. An extensive vehicle simulation study verifies that the isotropic model is not accurate enough.
Keywords: Coherence; Road roughness; parallel tracks;

1 Introduction

Travelling vehicles are exposed to fatigue-inducing loads caused by road roughness. Hence, a description of road roughness is useful for the vehicle industry. In this work, the coherence of 20 measured roads is analysed. The total length of these roads is 520 km. The measured roads are of varying quality, ranging from very smooth motorways to very rough gravel roads.

Historically, analysis of road roughness has been focused on the Power Spectral Density, PSD. It has been observed in several studies that the PSD have a similar form irrespectively of road type, see for example [1] and [2].

While left and right track (usually) are statistically equivalent, the actual profiles are not identical. The difference between left and right track produces a roll disturbance. Information regarding this roll disturbance is not included in the PSD of the individual wheel-paths. Hence, in addition to the PSD, it is appropriate to study the coherence function. The coherence function measures linear dependence between two stochastic processes as a function of spatial frequency.

Often, the road is assumed to be isotropic. Under this assumption, the coherence function is given by the single track power spectrum. The isotropic model's accuracy is assessed by comparison of coherence obtained assuming isotropy and the coherence estimated directly from measured road profiles.

In [4], [5], [6] and [8] similar comparisons of much smaller data sets are presented (e.g. in [6] 20 km is analysed). Ammon [5] proposes a parametric model, Heath [6] proposes a modified isotropic model and Sun and Su [8] propose a non-parametric model.

Earlier work, [9] and [10], has focused on single-track analysis. It was verified that occasional irregularities cause the major part of the vehicle fatigue damage. The irregularities are identified using spectrogram analysis, which estimates local spectra along the road. Irregularities are defined where the spectrogram is significantly higher than the average level. Hence, roads can be described as stochastic processes with changing spectrum. Analogously, in Section 5 we investigate if the coherence function also varies along the road. More precisely, the coherence functions associated with the irregularities are compared to those from smooth sections.

2 Stationary stochastic processes

2.1 Spectral representation and the coherence function

The zero mean stationary processes $Z_{\mathrm{L}}(x)$ and $Z_{\mathrm{R}}(x)$ describe the road elevation over a constant mean level at position x along the left and right wheel path, with autocovariance functions $r_{\mathrm{LL}}(x) = \mathrm{E}[Z_{\mathrm{L}}(x+x_0)Z_{\mathrm{L}}(x_0)]$, and $r_{\mathrm{RR}}(x) = \mathrm{E}[Z_{\mathrm{R}}(x+x_0)\ Z_{\mathrm{R}}(x_0)]$. Moreover, it is assumed that $Z_{\mathrm{L}}(x)$ and $Z_{\mathrm{R}}(x)$ are statistically equivalent, so that

$$r_{\mathrm{LL}}(x) = r_{\mathrm{RR}}(x) \equiv r(x). \tag{1}$$

The cross-covariance functions are defined by $r_{\mathrm{RL}}(x) = \mathrm{E}[Z_{\mathrm{R}}(x+x_0)Z_{\mathrm{L}}(x_0)]$ and, similarly, $r_{\mathrm{LR}}(x) = \mathrm{E}[Z_{\mathrm{L}}(x+x_0)Z_{\mathrm{R}}(x_0)] = r_{\mathrm{RL}}(-x)$.

The Fourier transforms of the covariance functions, $r(x)$ and $r_{\mathrm{LR}}(x)$, give the double-sided spectrum and the double-sided cross-spectrum. However, here we will use the one-sided spectrum $R(\xi)$ and the one-sided crosspectrum $R_{\mathrm{LR}}(\xi)$, which is more common in practical applications,

$$R(\xi) = \begin{cases} 2\int_{-\infty}^{\infty} r(x)e^{-i2\pi\xi x}\mathrm{d}x, & \xi > 0, \\ \int_{-\infty}^{\infty} r(x)\mathrm{d}x, & \xi = 0, \\ 0, & \xi < 0, \end{cases} \tag{2}$$

$$R_{\mathrm{LR}}(\xi) = \begin{cases} 2\int_{-\infty}^{\infty} r_{\mathrm{LR}}(x)e^{-i2\pi\xi x}\mathrm{d}x, & \xi > 0, \\ \int_{-\infty}^{\infty} r_{\mathrm{LR}}(x)\mathrm{d}x, & \xi = 0, \\ 0, & \xi < 0, \end{cases} \tag{3}$$

where ξ is spatial frequency. By definition $r_{\mathrm{LR}}(x) = r_{\mathrm{RL}}(-x)$, which gives that $R_{\mathrm{RL}} = \mathrm{conj}\{R_{\mathrm{LR}}\}$, where $\mathrm{conj}\{\cdot\}$ denotes complex conjugate. The auto- and

cross-covariance functions can be obtained from the one-sided spectrum and cross-spectrum,

$$r(x) = \int_0^\infty R(\xi)\cos(2\pi\xi x)\mathrm{d}x, \tag{4}$$

$$r_{\mathrm{LR}}(x) = \int_0^\infty \mathrm{Re}\{R_{\mathrm{LR}}(\xi)\}\cos(2\pi\xi x)\mathrm{d}x, \tag{5}$$

where $\mathrm{Re}\{\cdot\}$ denotes the real part of a complex number.

When $R(\xi)$ is non-zero, the coherence is defined by the ratio,

$$\gamma(\xi) = \frac{|R_{\mathrm{LR}}(\xi)|}{R(\xi)}, \tag{6}$$

where $0 \leq \gamma(\xi) \leq 1$. For example, if Z_{L} and Z_{R} is independent then $\gamma(\xi) = 0$ or if $Z_{\mathrm{L}} = Z_{\mathrm{R}}$ then $\gamma(\xi) = 1$.

2.2 Empirical coherence

The spectrum and coherence function are estimated using Welch's method [13], also known as the weighted overlapped segment averaging (WOSA) method, described in [14]. The road is divided into L meter long overlapping segments, which are multiplied with a Hanning window prior to (FFT) analysis. The WOSA estimate is referred to as the *empirical* coherence, in order to distinguish it from other coherence estimates to be introduced in Section 4.

The empirical coherence functions from the 20 measured roads are compared. Surprisingly, the coherence functions of all roads are very similar, despite the fact that they correspond to very different road types (smooth motorways, main roads, paved country roads, gravel roads, etc). In Figure 1, the spectrum and empirical coherence of three very different Swedish roads are presented. The dotted, dashed and solid lines correspond to a gravel road, a main road and a motorway, respectively. The spectra in the left plot are estimated from both left and right track. The deviation between the spectra of left and right track is typically small, which justifies the assumption of statistically equivalent left and right tracks, recall (1).

3 The isotropic assumption

Often (e.g. [1], [3], [4], [11], [12]) roads are assumed to be ergodic, homogeneous, isotropic surfaces. Homogeneity and isotropy imply that all profiles following a straight-line on the road surface have the same statistical properties, irrespectively of direction and position of the line. Specifically, the covariance between two values of a field at points A and B is a function only of the distance between them. Also, the coherence function can be computed from a spectrum of

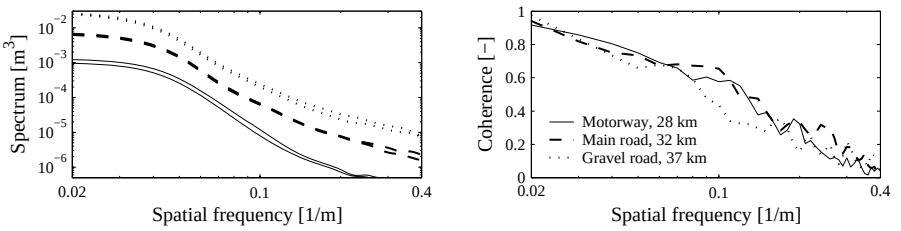

Figure 1: Spectrum and coherence functions

any profile on the isotropic surface. However, the spectrum cannot be chosen arbitrarily, it has to satisfy the conditions stated in [4]. Any monotonically non-increasing function which satisfies the boundedness condition given in [4] is admissible as a spectrum.

Isotropy implies that the cross-covariance functions are symmetric, $r_{\mathrm{LR}}(x) = r_{\mathrm{LR}}(-x)$. This symmetry implies that the cross-spectra are real, thus $R_{\mathrm{RL}} = R_{\mathrm{LR}}$.

Moreover, three points are marked in Figure 2, points A and C on the right track and point B on the left track. The covariance between the road levels in points A and B is $r_{\mathrm{LR}}(x)$ and the covariance between the road levels in points A and C is $r(\sqrt{x^2 + t_w^2})$, where t_w is the distance between the wheel-paths, the track width. Since the distance between A and B equals the distance between A and C, a consequence of isotropy is that

$$r_{\mathrm{LR}}(x) = r(\sqrt{x^2 + t_w^2}). \tag{7}$$

The coherence $\gamma(\xi)$ can be computed from the spectrum $R(\xi)$ using (4), (7), (3) and (6).

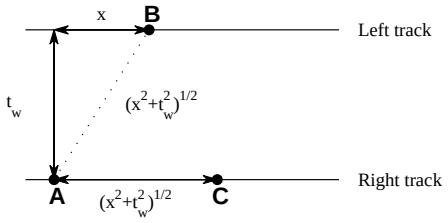

Figure 2: Two parallel road tracks

4 Coherence models

4.1 Isotropic models

To estimate the coherence for an isotropic road, it is only necessary to estimate the single-track spectrum $R(\xi)$. Furthermore, if the estimated spectrum is monotonically non-increasing and satisfies the boundedness condition in [4], then it is compatible with isotropy. A monotonically decreasing spectrum is a realistic assumption judging from estimates obtained from the measured roads.

Here, three spectrum estimates are studied. The estimates are based on a non-parametric spectrum estimate $\hat{R}(\xi)$, obtained using the WOSA method ($L = 500$ m). The estimate $\hat{R}_0(\xi) = \max_{f \geq \xi}(\hat{R}(f))$, gives a monotonically decreasing spectrum. The max-operation may appear crude, but it has an insignificant effect since $\hat{R}(\xi)$ is (with a few minor exceptions) decreasing for all relevant spatial frequencies, for all 20 roads, recall the left plot in Figure 1.

Two other spectra, which are compatible with isotropy [3], are also studied

$$R_1(\xi) = \begin{cases} c, & 0 \leq \xi \leq \xi_a, \\ c\left(\frac{\xi}{\xi_a}\right)^{-w}, & \xi_a \leq \xi \leq \xi_b, \\ 0, & \text{otherwise}, \end{cases} \tag{8}$$

(9)

$$R_2(\xi) = \begin{cases} k, & 0 \leq \xi \leq \xi_a, \\ k\left(\frac{\xi}{\xi_a}\right)^{-w_1}, & \xi_a \leq \xi \leq \xi_0, \\ k\left(\frac{\xi_0}{\xi_a}\right)^{-w_1}\left(\frac{\xi}{\xi_0}\right)^{-w_2}, & \xi_0 \leq \xi \leq \xi_b, \\ 0, & \text{otherwise}. \end{cases} \tag{10}$$

Here, the boundary constants ξ_a, ξ_0 and ξ_b are set to 0.01, 0.2 and 10 m^{-1}, respectively. The parameters $[c, w]$ and $[k, w_1, w_2]$ are set so that R_1 and R_2 optimally (in least-square sense) matches $\hat{R}(\xi)$.

The spectra $R_0(\xi), R_1(\xi)$ and $R_2(\xi)$ are fitted to the 20 measured roads. The corresponding coherence functions, computed under isotropy, are compared to the empirical coherence function. It is observed that the extended model $R_2(\xi)$ and the non-parametric model $R_0(\xi)$, are not more accurate than the simple model, $R_1(\xi)$. Thus, in Section 4.3 where coherence models are compared to measured data, results are shown only for the simple isotropic model, $R_1(\xi)$.

Remark: Numerical computation of the coherence function from a given spectrum is in principal simple, using (4), (7), (3) and (6). Indirect methods are presented by Kamash and Robson [4] in 1978 and by Heath [7] in 1987. Nowadays, a modern computer can handle larger amounts of data and compute the coherence (more or less) instantly, taking advantage of the FFT-algorithm.

However, to avoid numerical problems, it is necessary to define the spectrum for $\xi_k = 0, \Delta_\xi, 2\Delta_\xi, ..., N\Delta_\xi$, when Δ_ξ is small and N is large. Here, $N = 10^6$ and $\Delta_\xi = 0.001$ 1/m.

4.2 A parametric model

Instead of assuming isotropy in order to derive the coherence, a parametric description of the coherence function is searched for. Several parametric models were tested against the empirical coherence functions and the best fit was obtained by the exponentially decreasing function,

$$\gamma_e(\xi) = e^{-\rho t_w \xi}, \quad \rho > 0, \tag{11}$$

which is defined for positive frequencies, $\xi \geq 0$. The track width t_w is a priorly known constant. Here, it is 1.95 m for roads 1–3 and 2 m for roads 4–20.

To estimate ρ, the squared empirical coherence, $\hat{\gamma}^2(\xi)$, is computed, with $L = 100$ m. Then, the approximate bias B of the squared coherence is removed [14],

$$B(\xi) = \frac{1}{n_d}(1 - \gamma^2(\xi))^2. \tag{12}$$

where n_d is the number of non-overlapped segments. Note that, since the true coherence $\gamma(\xi)$ is unknown it is impossible to compute $B(\xi)$. An estimation of the bias, $\hat{B}(\xi)$, is computed by replacing $\gamma^2(\xi)$ by $\hat{\gamma}^2(\xi)$. Finally, the estimate of ρ is obtained by fitting (in least-square sense) $\gamma_e^2(\xi)$ to the approximately unbiased, squared coherence function, $\hat{\gamma}^2(\xi) - \hat{B}(\xi)$.

4.3 Comparison of empirical and modelled coherence

Figure 3 shows the estimated coherence of six measured roads. The isotropic model gives both accurate estimates (e.g. road 11) and inaccurate estimates (e.g. roads 17 and 19). The exponential function gives, in general, a more accurate match, which is natural since it is fitted directly to the empirical coherence.

5 Road irregularities and their coherence

In [10] a method to identify road parts with above-average roughness is presented. It is verified that these irregularities have a large impact on vehicle fatigue damage. In this section, statistical analysis is focused on these irregularities.

The detected irregularities are of two types: long-wave (LW) and short-wave (SW). The coherence function corresponding to road sections defined as

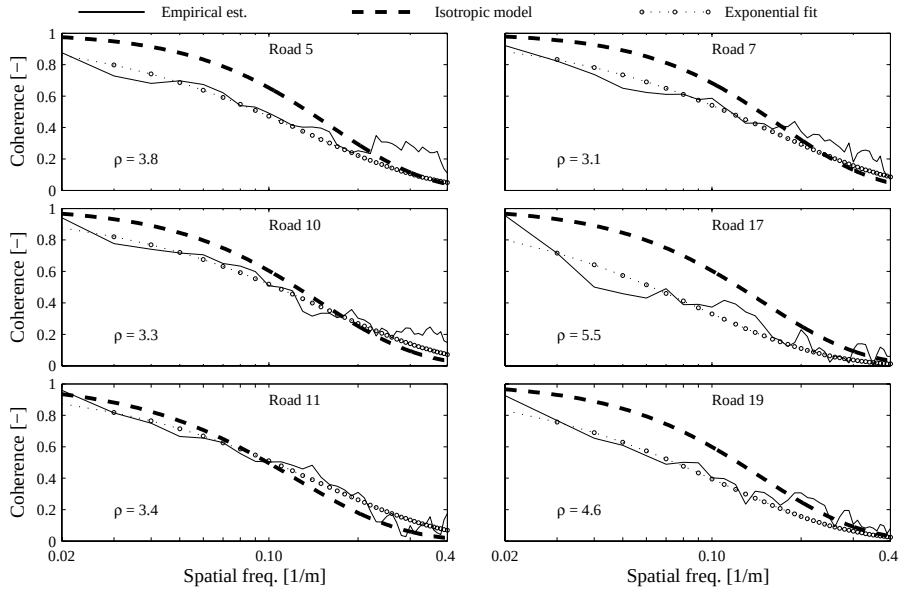

Figure 3: Estimated and fitted coherence functions

SW-irregularities, is difficult to estimate, since these irregularities are rare (on average, 1 per 2 km) and short (on average 5 m). Thus, the analysis is focused on LW-irregularities.

LW-irregularities are detected in left and right track, according to the method in [10]. Here, a road section is treated as an LW-irregularity if any LW-irregularity is detected in either left, right or both tracks.

Estimation of the coherence function is complicated by the fact that the identified LW-irregularities have different length. To overcome this problem, all identified LW-irregularities are cut into 32 m long subsections. Any section shorter than 32 m is excluded from the analysis. The coherence estimate, $\hat{\gamma}_{\mathrm{irr}}(\xi)$, is estimated from these sections, using the WOSA method (with L=32 m), but with non-overlapping segments. This estimate is then compared to similar estimates obtained from smooth sections.

Firstly, equally many sections of equal length as the LW-irregularities are randomly picked from the non-irregular road parts. Then the coherence $\gamma_{\mathrm{smt}}(\xi)$ is estimated using the same technique as for the LW-irregularities. This is done repeatedly, producing a probability distribution of the estimate $\hat{\gamma}_{\mathrm{smt}}(\xi)$. It is found that $\hat{\gamma}_{\mathrm{irr}}(\xi)$ does not differ significantly from $\gamma_{\mathrm{smt}}(\xi)$. Typical results are shown in Figure 4, where $\hat{\gamma}_{\mathrm{irr}}(\xi)$ and empirical 95%-confidence intervals

of $\gamma_{\mathrm{smt}}(\xi)$ and are plotted for two roads. This indicates that the coherence corresponding to irregular and non-irregular sections can be described by the same function.

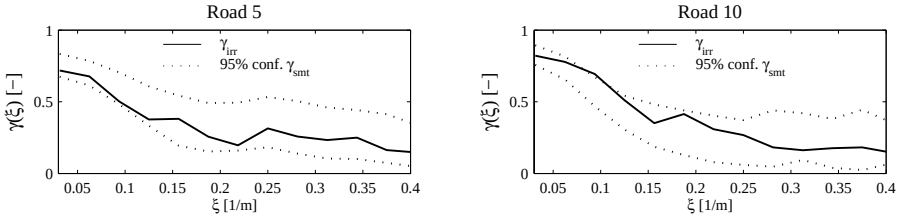

Figure 4: Coherence estimated from rough parts (solid lines) and 95% confidence intervals of the coherence estimated from non-rough road parts (dotted lines).

6 Roll disturbance and vehicle fatigue

Using only visual inspection of coherence functions (Figure 3), it is difficult to judge if the isotropic model is accurate enough. In this final section the result of a vehicle simulation study is presented.

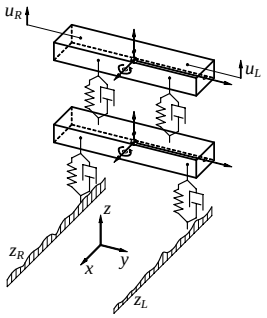

Figure 5: The half-vehicle model

The vehicle fatigue damage d is assessed by studying a two-wheeled vehicle model travelling at constant velocity v on road profiles, see Figure 5. This simple model cannot be expected to predict loads on a physical vehicle exactly,

but it will high-light the most important road characteristics as far as fatigue damage accumulation is concerned; it might be viewed as a 'fatigue-load filter'. The model comprises masses, linear springs and linear dampers; the only non-linearity is the ability to loose road contact. The parameters are set to mimic heavy vehicle dynamics. Moreover, the difference of the vertical accelerations of the left and the right side of the sprung mass, (proportional to) the roll load, is used to assess fatigue damage.

Firstly, rainflow cycles are identified in the 'roll load'. Then, the cycles are evaluated with Palmgren-Miner's linear damage accumulation hypothesis, and fatigue strength is described by Basquin's relation, i.e. $s^\beta N = \text{constant}$, where s is load cycle amplitude and β the fatigue exponent and N the number of cycles to failure.

Two stochastic models are compared, following the evaluation scheme in [15], which uses the transformed damage $q = \ln(d)/\beta$. The values q and d can be interpreted as observations of the random variables Q and D, respectively, where D is the random damage and $Q = \ln(D)/\beta$. In general the distribution of D is highly skewed and non-symmetric, while the distribution of Q can be approximated by the Gaussian distribution [9], [15].

The transformed damage indicated by measured roads and synthetic roads (computer simulated realisations from a stochastic model) are compared. The synthetic roads are realised with parameter values estimated from the corresponding measured road. Further, the discrepancy between a model and a measurement is defined as

$$\delta = \frac{\bar{q}_s - q_o}{s_o}, \tag{13}$$

where $\bar{q}_s$ is the mean transformed damage from synthetic roads, q_o the observed damage from the measured road, and s_o the estimated standard deviation of the transformed damage from the measured road. A small discrepancy indicate a good model fit (i.e. q_o is the target for $\bar{q}_s$ and s_o is the uncertainty of the target). A negative discrepancy indicates that the model underestimates fatigue damage, and vice versa for a positive damage.

A discrepancy is computed for each of the 36 combinations of the velocities $v = 40, 50, \ldots, 90$ km/h and values of $\beta = 3, 4, \ldots, 8$. Finally, the discrepancy with the largest absolute value (the worst fit) defines the lack-of-fit. A lack-of-fit outside the target region [–4,4] indicates that the model is not accurate enough [9].

The two studied road models are set up as in [15] (Model B), with one exception, the coherence function is described either by $\gamma_e(\xi)$ or obtained assuming isotropy. The model assumptions are given in Appendix A. Note that, an isotropic Gaussian model is not a realistic road surface model [15]; road irregularities have to be included. Here, the studied models include irregularities of random shape, length and location, see [15] for details. Figure 6 shows the lack-of-fit for the two models for each measured road. The parametric model is

more accurate than the isotropic model: The target region is reached in 11 and 0 out of 20 roads for the parametric model and isotropic model, respectively. As a general tendency, the isotropic model underestimates the rolling excitation due to overestimated coherence. Note, Ammon ([5], page 35) concluded the opposite: that the isotropic model overestimates rolling excitation.

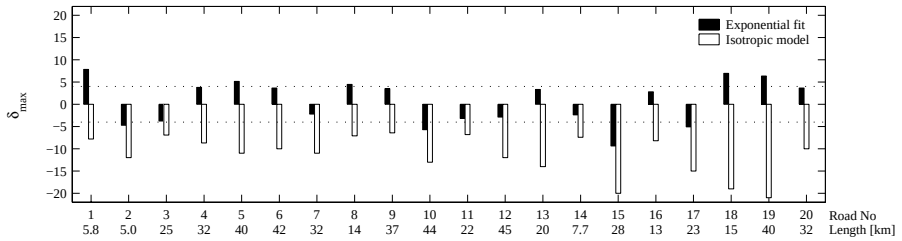

Figure 6: Lack of fit for parametric and isotropic coherence models. A negative value of $\delta_{\max}$ indicates underestimation of roll disturbance, and vice versa for positive values.

7 Conclusions

- It is difficult to distinguish between road types by coherence analysis of parallel road tracks. A motorway can have the same empirical coherence function as a very rough gravel road.
- The coherence corresponding to local irregularities and the coherence corresponding to non-irregular road sections can be described by the same function.
- Usage of the isotropic assumption to compute the coherence function gives inaccurate approximations.
- The proposed parametric model (11) gives better coherence approximations.

Acknowledgements

This work was supported by Scania and the Programme Council for Vehicle Research within The Swedish Governmental Agency for Innovation Systems. The author is grateful to Dr Anders Forsén, Scania, Prof. Igor Rychlik, Chalmers University and Prof. Georg Lindgren, Lund University for helpful comments.

A Road models

In this section the two evaluated road models in Section 6 are described. As mentioned, the two models are very similar and differ only in the description of the coherence between left and right wheel-path. First, the general assumptions are described, which are used by both models.

A.1 General assumptions

The left and right wheel paths are assumed to be statistically equivalent. Moreover, the main variability in the road is described by the two-dimensional process, $\mathbf{Z}^{(0)}(x)$, which consists of two stationary Gaussian processes, corresponding to the left and right wheel path,

$$\mathbf{Z}^{(0)}(x) = \begin{bmatrix} Z_{\mathrm{L}}^{(0)}(x) \\ Z_{\mathrm{R}}^{(0)}(x) \end{bmatrix}. \tag{A.1}$$

The spectrum and coherence of $\mathbf{Z}^{(0)}(x)$ is given later on.

Irregularities of two types, long-wave (LW) and short-wave (SW), are superimposed to $\mathbf{Z}^{(0)}(x)$. The two irregularity types, LW and SW, occur independently of each other. To illustrate this, a 400 m long road is generated with two superimposed irregularities of each type, see Figure 7. As the example shows, the left and right irregularities have different shape, but occur simultaneously. The simplifying assumption of simultaneousness is realistic, since when an irregularity is detected in one measured track, the other track is usually also irregular. Additionally, long-wave and short-wave irregularities may overlap. The j:th long-wave irregularity and the k:th short-wave irregularity are described by the processes $\mathbf{Z}_j^{(1)}(x)$ and $\mathbf{Z}_k^{(2)}(x)$. The road with superimposed irregularities is denoted by $\mathbf{Z}_{\mathrm{B}}(x)$. The irregularities are modelled as (non-stationary) conditional Gaussian processes. To avoid discontinuities at the start and end of the rough sections, the added irregularities starts and ends with two values equal to zero, in both left and right track. The irregularities are simulated conditioning on the zero boundary levels, for more details see [15]. Since the irregularities are non-stationary, it is incorrect to assign a spectral density to them. However, an irregularity reaching from $-\infty$ to $+\infty$ is stationary.

We need to define spectrum, coherence and phase functions for the main process, $\mathbf{Z}^{(0)}(x)$, and infinite length irregularities. As usual, it is a assumed that all cross-spectra are real, hence, the phase functions are zero (see for example [16]). The spectrum and coherence associated with $\mathbf{Z}^{(\eta)}(x)$, for $\eta = 0, 1, 2$ are denoted by $R_{\mathrm{B}}^{(\eta)}$ and $\gamma_{\mathrm{B}}^{(\eta)}$, correspondingly. The coherence functions are given in Section A.2.

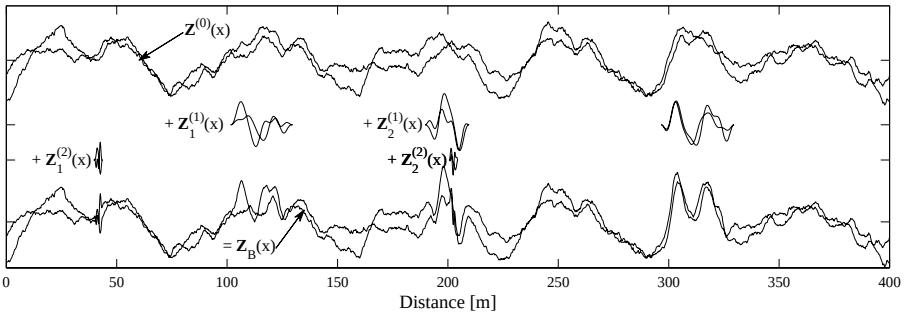

Figure 7: A simulation of two parallel road tracks: $\mathbf{Z}^{(0)}(x)$ = Two-dim. stationary Gaussian process, $\mathbf{Z}_j^{(1)}(x)$ = long-wave irregularities, $\mathbf{Z}_k^{(2)}(x)$ = short-wave irregularities. The realized road tracks $\mathbf{Z}_{\mathrm{B}}(x)$ equals the stationary Gaussian process plus simulated irregularities.

The spectra have the following parametric shape

$$R_{\mathrm{B}}^{(0)}(\xi) = \begin{cases} 10^{a_0}\left(\frac{0.01}{\xi_0}\right)^{-w_1}, & \xi \in [0, 0.01], \\ 10^{a_0}\left(\frac{\xi}{\xi_0}\right)^{-w_1}, & \xi \in [0.01, 0.20], \\ 10^{a_0}\left(\frac{\xi}{\xi_0}\right)^{-w_2}, & \xi \in [0.20, 10], \\ 0, & \text{otherwise}, \end{cases} \tag{A.2}$$

$$R_{\mathrm{B}}^{(\eta)}(\xi) = \begin{cases} (10^{a_\eta} - 10^{a_0})\left(\frac{\xi}{\xi_0}\right)^{-w_\eta}, & \xi \in \Xi_\eta, \\ 0, & \text{otherwise}, \end{cases} \quad \eta = 1, 2. \tag{A.3}$$

The intervals Ξ_η are given in Table 1 and the reference frequency $\xi_0 = 0.2\ \mathrm{m}^{-1}$.

Symbol	Ξ_0	Ξ_1	Ξ_2
Interval [m^{-1}]	[0.01, 10]	[0.03, 0.2]	[0.2, 2.0]

Table 1: Spatial frequency intervals

Furthermore, the location and length of the sections with added roughness are random. More precisely, the distance between the end of a long-wave irregularity and the start of the next is exponentially distributed with mean θ_1. Similarly, the distance between short-wave irregularities is exponentially distributed with mean θ_2. The length of long-wave and short-wave irregularities

are independent and exponentially distributed with mean τ_1 and τ_2, respectively.

A.2 Coherence models

A.2.1 Parametric model

The parametric coherence model use the parametric description introduced in Section 4.2,

$$\gamma_{\text{B}}^{(\eta)}(\xi) \quad = \quad \begin{cases} e^{-\rho t_w \xi}, & \xi \in \Xi_\eta, \\ 0, & \text{otherwise}, \end{cases} \quad \eta = 0, 1, 2. \tag{A.4}$$

Hence, the coherence parameter ρ takes the same value for the stationary process $\mathbf{Z}^{(0)}(x)$ and the irregularities $\mathbf{Z}_j^{(1)}(x)$ and $\mathbf{Z}_k^{(2)}(x)$. Note also that when ξ is outside interval Ξ_η, then the corresponding spectrum $R_{\text{B}}^{(\eta)}$ is zero, and the value of $\gamma_{\text{B}}^{(\eta)}(\xi)$ has no meaning and is set to zero.

A.2.2 Isotropic model

For the isotropic model $\gamma_{\text{B}}^{(\eta)}(\xi)$, $\eta = 0, 1, 2$, is computed from spectrum (A.2), which is a spectrum compatible with the isotropic assumption.

References

[1] ISO 8608. *Mechanical Vibration — Road Surface Profiles — Reporting of Measured Data*, International Organisation for Standardisation, Geneva, 1995.

[2] J.D. Robson and C.J. Dodds, *The description of road surface roughness*, J. Sound and vibration 31(1973), pp. 175-183.

[3] K.M.A. Kamash and J.D. Robson, *Implications of isotropy in road surfaces*, J. Sound and Vibration 54(1977), No 1, pp. 131-145.

[4] K.M.A. Kamash and J.D. Robson, *The application of isotropy in road surface modelling*, J. Sound and Vibration 57(1978), No 1, pp. 89-100.

[5] D. Ammon, *Problems in road surface modelling*, Veh Syst Dyn 20(1991), pp. 28-41.

[6] A.N. Heath, *Modelling and simulation of road roughness*, Suppl. Veh Syst Dyn 18(1989), pp 275-284.

[7] A.N. Heath, *Application of the isotropic road roughness assumption*, J. Sound and Vibration 115(1987), No 1, pp. 131-144.

[8] L. Sun and J. Su, *Modeling random fields of road surface irregularities*, Int. J. Road Materials and Pavement Design 2(2001), No. 1, pp. 49-70.

[9] K. Bogsjö, *Stochastic modelling of road roughness*, Licentiate of engineering thesis, Lund Institute of Technology, Lund Sweden, 2005.

[10] K. Bogsjö. *Development of analysis tools and stochastic models of road profiles regarding their influence on heavy vehicle fatigue*, Suppl. Veh Syst Dyn 44(2006), pp. 780-790. (Paper B in this thesis.)

[11] D. Szöke and I. Kuti, *A new development in the numerical description of road profile realisations*, Int. J. Vehicle Design 34(2004), No. 2, pp. 183-190.

[12] L. Sun, W. Kenis and W. Wang, *Stochastic spatial excitation induced by a distributed contact on homogeneous Gaussian random fields*, J. Engineering Mechanics 132(2006), No 7, pp. 714-722.

[13] P.D. Welch, *The use of the fast Fourier transform for the estimation of spectra: A method based on time averaging over short modified periodograms*, IEEE Transactions on Audio and Electroacoustics 15(1967), Issue 2, pp. 70-73.

[14] G.C. Carter, *Coherence and time delay estimation*, Proceedings of the IEEE 75(1987), No 2, pp. 236-255.

[15] K. Bogsjö, *Evaluation of stochastic models of parallel road tracks*, In press for *Probabilistic Engineering Mechanics*, 2007. (Paper D in this thesis.) doi:10.1016/j.probengmech.2007.08.002

[16] Yonglin Z, Jiafan Z, Numerical simulation of stochastic road process using white noise filtration, *Mechanical Systems and Signal Processing*, Vol 20, No 2, pp. 363–372, 2006.

F

Paper F

Vehicle fatigue damage caused by road irregularities

KLAS BOGSJÖ AND IGOR RYCHLIK

ABSTRACT

Road roughness causes fatigue-inducing loads in travelling vehicles. Road sections with a high degree of roughness are of special interest, since these have a significant impact on vehicle's fatigue life. This study is focused on the statistical description and analysis of vehicle damage caused by irregularities. Standard statistical analysis tools are not straight-forwardly applicable, due to the nonstationary property of the irregularities. However, it is found that the road irregularities influence on vehicles can be accurately described using a 'local' narrow-band approximation of the fatigue damage intensity.

Keywords: Vehicle fatigue, rainflow damage, damage intensity, road irregularities.

1 Introduction

This paper is devoted to qualitative studies of fatigue damage accumulation in vehicle components. Clearly, road roughness is a major source of fatigue-inducing vehicle loads. Properties of roads' surfaces, in scale of kilometres, are often modelled as stationary processes, often Gaussian, with a standardised type of spectrum, which may change with geographical region, age, or type of road. However, as was shown in [1], [2] and [3] most of the fatigue damage accumulated in a vehicle are consequence of short-duration oscillations caused by a local, higher degree, of road roughness. Those irregularities are sometimes called potholes and in [3] a road model was proposed that include such irregularities.

The variable stresses which may cause fatigue failure of a component are functions of road surface variability. As a first approximation, the vehicle responses (stresses) are modelled by means of linear filters having road surface profiles as input. Responses of linear filters are easy to analyse statistically if the input signal is a Gaussian process. Then the output is a Gaussian process too. Consequently, in this paper, we shall model the fatigue accumulation process for Gaussian loads with superimposed transients due to a sudden short change of surface variability. Although the true stresses acting on a component

in a vehicle will differ from the one computed using linear filters (due to the complicated and nonlinear interaction of tires and the road surface) the results of this approximate analysis can be used qualitatively to compare different design concepts at an early stage.

In addition, the problem of studying damage processes for Gaussian loads with superimposed transients is quite often met in applications. For example, responses of a sailing vessel can be modelled as a Gaussian process (responses to sea surface variability – waves) with added transients due to 'slams' which occur when a ship proceeds at certain speeds in rough seas and the front part of the hull bottom sustains large forces as the result of impact with the sea surface. Consequently, we shall first study the fatigue damage for stresses that can be described as a Gaussian process with transients, defined as follows.

Suppose that the external load $X(t)$ can be considered as a sum of a stationary Gaussian process $X_0(t)$ having mean zero and spectral density $S_0(f)$ and nonstationary Gaussian loads $X_i(t)$ such that $X_i(t) = 0$ for all t outside the interval $[t_i, t_i + \Delta_i]$, the derivatives $\dot{X}_i(t_i) = \dot{X}_i(t_i + \Delta_i) = 0$ and such that $\mathrm{E}[X_i(t)] = 0$. If the positions and length of irregularities (t_i, Δ_i) are known then the load

$$X(t) = X_0(t) + \sum_{i>0} X_i(t).$$

In this paper we shall consider random locations and durations of irregularities (t_i, Δ_i), being independent of the process $X_0(t)$. Further, suppose that the stress $Y(t)$ acting on a component, caused by the load $X(t)$, can be adequately modelled by means of a linear filter then

$$Y(t) = \int_{-\infty}^{t} h(t-s)X(s)ds = Y_0(t) + \sum_{i>0} Y_i(t), \tag{1}$$

where $h(t)$ is the impulse response. Obviously $Y_i(t) = \int_{-\infty}^{t} h(t-s)X_i(s)ds$ are all Gaussian processes, where only $Y_0(t)$ is stationary.

In this paper we shall present a general method to estimate the expected fatigue damage for the stress Y defined in (1). The paper is organised as follows: In Section 2, the rainflow counting method is reviewed and accumulated damage defined. In Section 3, a method to bound the expected damage is presented while in Section 4 the vehicle fatigue damage due to road roughness is studied. In Section 5 a minor parameter study is presented and, finally, in Section 6 the conclusions are stated.

2 Definition of rainflow damage

The rainflow method was introduced by Endo: The first paper in English can be found in [5]. Here we shall use the alternative definition given in [9], which

is more suitable for statistical analysis.

Assume $Y(t)$, $t \in [0,T]$ is a variable load having finite number of local maxima. Assume that local maximum $v_i = Y(t_i)$ in $Y(t)$ is paired with one particular local minimum u_k, determined as follows:

- From the ith local maximum (value v_i) one determine the lowest values in forward and backward directions between t_i and the nearest points at which $Y(t)$ exceeds v_i.
- The larger of those two values, denoted by u_i^{rfc}, is the rainflow minimum paired with v_i, i.e. u_i^{rfc} is the least drop before reaching the value v_i again on either side.
- Thus, the ith rainflow pair is (u_i^{rfc}, v_i), see Figure 1. The cycle amplitude is $S = v_i - u_i^{\text{rfc}}$.

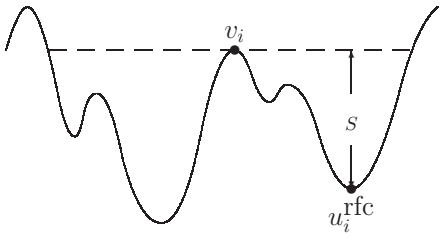

Figure 1: A rainflow pair

Note that for some local maxima v_i, the corresponding rainflow minimum u_i^{rfc} could lie outside the interval $[0,T]$. In such situations, the incomplete rainflow cycle constitutes the so called residual and has to be handled separately. In this approach, we assume that, in the residual, the maxima form cycles with the preceding minima.

The total damage $D(T)$, defined using the rainflow method and applying the linear Palmgren-Miner ([6], [7]) damage accumulation rule, leads to

$$D(T) = \sum f(u_i^{\text{rfc}}, v_i) + D^{\text{res}}, \tag{2}$$

where, $f(u_i^{\text{rfc}}, v_i)$ is the fatigue damage due to the rainflow pair (u_i^{rfc}, v_i) and D^{res} is the damage caused by cycles found in the residual. In this study, we assume that $f(u_i^{\text{rfc}}, v_i)$ is typically of the form $f(u_i^{\text{rfc}}, v_i) = \alpha(v_i - u_i^{\text{rfc}})^{\beta}$, where $\alpha > 0$ and $\beta > 1$ are experimentally defined fatigue parameters.

In this paper we study the damage accumulation for non-stationary loads $Y(t)$, defined by (1), and are particularly interested in the fatigue damage increase due to transients $Y_i(t)$, $i > 0$. Clearly, we expect that the damage will grow faster when transient stresses occur. One way of quantifying the effects of transients for the fatigue damage accumulation is to study the damage rate $\dot{D}(t)$ and the damage intensity $d(t)$ which is the expected damage rate, $d(t) = \mathrm{E}[\dot{D}(t)]$. Hence we give an alternative formula for the rainflow damage (2) employing the damage accumulation rate $\dot{D}(t)$. More precisely, as was shown in [10], one can rewrite (2) as follows

$$D(T) = \int_0^T \alpha\,\beta(Y(t) - Y^-(t))^{\beta-1}\dot{Y}(t)\,dt \equiv \int_0^T \dot{D}(t)\,dt \tag{3}$$

where $Y^-(t)$ is the lowest values in the backward direction between t and the nearest exceedence of $Y(t)$, see Figure 2. The function $\dot{D}(t)$ is interpreted as the observed damage intensity.

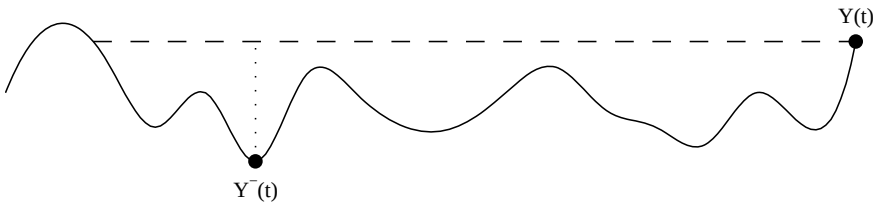

Figure 2: Definition of $Y^-(t)$

Obviously, use of the damage rate $\dot{D}(t)$ to compute the rainflow damage is practically not convenient, since the integral in (3) has to be computed numerically using a quite dense grid. The original formula (2) can be seen as a way to compute the integral by taking larger steps from local maximum to the next one. However, still $\dot{D}(t)$ can find applications for illustration purposes and for some analytical computations. On the contrary, the damage intensity $d(t)$ is a useful tool to describe the damage process for non-stationary loads, for example to describe the fatigue accumulation process for longer missions when different type of operation conditions are mixed. Clearly, when the damage intensity $d(t)$ is known the expected damage is given by

$$\mathrm{E}[D(T)] = \int_0^T d(t)\,dt \tag{4}$$

and can be efficiently computed, see the formulas in Section 3 where approximations of the intensity are given.

Note that even for stationary loads the damage intensity $d(t)$ is not constant and is not equal to $\mathrm{E}[D(t)]/t$, although the difference is negligible for larger t values. This is due to nonlinearity of the rainflow counting method, viz. the damage $D(T)$ accumulated in the interval $[0,T]$ depends also on the time T_0 when the load started to act on structure. If $T_0 \leq 0$ then the damage intensity $d(t)$ for $t \in [0,T]$, will depend on how long time it passed since the structure has been loaded for the first time (however, we suppress this dependency: $d(t,T_0) = d(t)$). Consequently, we introduce the 'stationary' damage intensity, when the influence on the initial value T_0 is not present any more, by means of the limiting value

$$d = \lim_{t\to\infty} d(t). \tag{5}$$

Suppose that $T_0 = -\infty$, which physically is not possible since the component would break before we started the experiment, then $d(t) = d$ and hence $\mathrm{E}[D(T)] = T \cdot d$.

Computations of the damage intensity $d(t)$ is a very complicated problem and exact results are known when $\beta = 1$ (practically uninteresting case). When $\beta > 1$ exact results are known for some simple periodic loads and for loads having Markov structure. For the important class of stationary Gaussian loads accurate approximations exist. In the following section we present the so called narrow-band approximation.

3 The narrow-band approximation for the stationary damage intensity d

In the early 1960s, the narrow-band approximation was presented by Bendat [4] at a time when a definition for rainflow cycle counting was not yet available. For a stationary random stress $Y(t)$, Bendat proposed that the cycle amplitude has the following probability distribution

$$P(S \leq u) = 1 - \frac{\mu(u)}{\mu(0)}, \tag{6}$$

where $\mu(u)$ is the intensity the stress $Y(t)$ crosses the level u in upward direction. He also proposed to approximate the intensity of cycles by means of the zero upcrossing intensity $\mu(0)$. For stationary loads the upcrossing intensity $\mu(u)$ is given by Rice formula [8]

$$\mu(u) = \int_0^\infty z f_{\dot{Y}(0),Y(0)}(z,u)dz. \tag{7}$$

Now, for a stationary load Y, if μ is unimodal and symmetrical around zero, i.e. $\mu(-u) = \mu(u)$, and $\mu(|u|) > \mu(|v|)$ whenever $|u| < |v|$, then the stationary

damage intensity d can be approximated by the narrow-band intensity d^{nb} defined as follows

$$d^{\mathrm{nb}} = \mu(0)\mathrm{E}[\alpha(2\cdot S)^{\beta}] = \alpha 2^{\beta}\,\beta\int_0^{\infty} u^{\beta-1}\mu(u)\,du. \tag{8}$$

Actually, as it was proven in [10], (8) is the bound for the damage intensity, i.e. one has that

$$d(t) \le d^{\mathrm{nb}},$$

which means that use of the narrow-band approximation gives conservative results since $\mathrm{E}[D(T)] \le T\cdot d^{\mathrm{nb}}$.

Finally, if in addition $Y(t)$ is a Gaussian load, then d^{nb} can be computed explicitly, viz.

$$d^{\mathrm{nb}} = \alpha\sigma_{\dot{Y}}\sigma_Y^{\beta-1}2^{3\beta/2-1}\Gamma(1+\beta/2)/\pi, \tag{9}$$

where σ_Y^2, $\sigma_{\dot{Y}}^2$ are variances of the stress $Y(t)$ and its derivative $\dot{Y}(t)$, respectively, while $\Gamma(x)$ is the gamma function.

3.1 Narrow-band approximation for non-stationary loads

For the nonstationary stress $Y(t)$ the intensity of upcrossings of level u will depend on time. Hence, by means of a generalisation of Rice formula the upcrossing intensity is given by

$$\mu_t(u) = \int_0^{\infty} z f_{\dot{Y}(t),Y(t)}(z,u)dz. \tag{10}$$

The expected number of times the stress Y passes u in upward direction in the interval $[0,T]$, $N_T(u)$, say, is given by

$$\mathrm{E}[N_T(u)] = \int_0^{T} \mu_t(u)\,du. \tag{11}$$

If $\mu_t(u)$ is unimodal and symmetrical around zero (i.e $\forall t$, $\mu_t(u) = \mu_t(-u)$ and $\mu_t(|u|) > \mu_t(|v|)$ whenever $|u| < |v|$) then, following Bendat's approach, for any t one can define a local amplitude S_t having the distribution

$$P(S_t \le u) = 1 - \frac{\mu_t(u)}{\mu_t(0)}, \tag{12}$$

and then introduce the local narrow-band damage intensity $d^{\mathrm{nb}}(t)$ as follows

$$d^{\mathrm{nb}}(t) = \mu_t(0)\mathrm{E}[\alpha(2\cdot S_t)^{\beta}] = \alpha 2^{\beta}\,\beta\int_0^{\infty} u^{\beta-1}\mu_t(u)\,du. \tag{13}$$

In a similar way, as it was done in [10] one can also prove, the simple proof is omitted, that if μ_t is unimodal and symmetrical around zero then the narrow-band approximation is conservative, viz.

$$\mathrm{E}[D(T)] = \int_0^T d(t)\,dt \leq \int_0^T d^{\mathrm{nb}}(t)\,dt. \tag{14}$$

However, it does not imply that for all t, $d(t) \leq d^{\mathrm{nb}}(t)$.

We turn now to the case of the nonstationary Gaussian load $Y(t)$ defined in (1).

Theorem 1. *Let $Y(t)$ be a zero mean Gaussian load, with derivative $\dot{Y}(t)$. If $Y(t)$ and $\dot{Y}(t)$ are uncorrelated, then (14) holds with*

$$d^{\mathrm{nb}}(t) = \alpha\Gamma(\beta/2+1)2^{3/2\beta-1}\pi^{-1}\sigma_{\dot{Y}}(t)(\sigma_{\dot{Y}}(t))^{\beta-1}. \tag{15}$$

where $\sigma_Y^2(t)$ and $\sigma_{\dot{Y}}^2(t)$ denote the variance of $Y(t)$ and $\dot{Y}(t)$, respectively.

From (43) it follows that $\mu_t(u)$ is unimodal and symmetrical around zero, which implies that (14) holds. Expression (15) is derived in the same way as (9), by insertion of (43) into (13).

Using the last theorem we have that

$$\mathrm{E}[D(T)] \leq \alpha\Gamma(1+\beta/2)2^{3\beta/2-1}\pi^{-1}\int_0^T \sigma_{\dot{Y}}(t)\sigma_Y(t)^{\beta-1}\,dt \equiv D^{\mathrm{nb}}, \tag{16}$$

say.

Now, if $\rho(t) \neq 0$ then $\mu_t(u) \neq \mu_t(-u)$ and D^{nb} in (16) may not be a conservative bound for the expected damage. In order to check if the local narrow-band approximation, i.e. assuming that $\rho(t) = 0$ even if it is not, may give non-conservative estimates of D^{nb}, we shall compare D^{nb} with the conservative bound proposed in [10] which, for completeness of the presentation, will be given next.

Let $n_T(u) = \int_0^T \mu_t(u)$ be the expected number of u upcrossings by $Y(t)$ in $[0,T]$ and let introduce $n_T^+(u,v) = \min(n_T(u), n_T(v))$ then

$$\mathrm{E}[D(T)] \leq \alpha\,\beta(\beta-1)\int_{-\infty}^{+\infty}\int_{-\infty}^{v}(v-u)^{\beta-2}n_T^+(u,v)\,du\,dv, \tag{17}$$

where, in general, the integral has to be computed numerically. For stationary Gaussian loads the integral gives the same result as the narrow-band approximation (9). The same is valid for the nonstationary Gaussian loads when $\rho(t) = 0$, then (16) and (17) give the same bound.

In the following we will present an application of the narrow-band approximation for the fatigue damage in a vehicle travelling on a road with randomly located and randomly shaped irregularities.

4 Fatigue accumulation in a vehicle

Commonly, stochastic models are used to describe the randomness of measured road profiles. Vehicle models travelling on road profiles modelled as stationary Gaussian processes have been extensively studied (see for example [12] and [13] for some recent studies). However, measured profiles are not accurately described by a stationary Gaussian model [2]. Hence, it is more interesting to study a more realistic road model. The road model used in this paper includes random non-stationary irregularities. In particular, the vehicle fatigue damage caused by such irregularities is analysed.

Fatigue damage is assessed by studying a quarter-vehicle model travelling at constant velocity on road profiles, see Figure 3. This very simple model cannot be expected to predict loads on a physical vehicle exactly, but it will high-light the most important road characteristics as far as fatigue damage accumulation is concerned; it might be viewed as a 'fatigue-load filter'. In this study the model comprises masses, linear springs and linear dampers; the only non-linearity is the ability to loose road contact. The parameters are set to mimic heavy vehicle dynamics, see Table 1. In order to assess vehicle fatigue damage, the total force, $Y(t)$, for $t \in [0, T]$, acting on the sprung mass is rainflow-counted and the damage is given by (2).

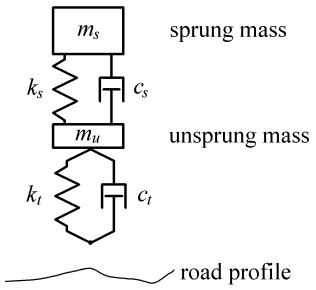

Figure 3: Quarter vehicle model

A physical tire on a heavy vehicle has a road contact length of approximately 0.15 m. Hence, short wavelengths (of order 0.01 m) in the road profile are attenuated by a real tire. In this study, sample distance in the measured roads is 0.05 m, all signal content with shorter wavelength than 0.10 m is neglected.

A vehicle travelling at the velocity v m/s will experience the road as a function of time, $t = x/v$. Thus, the vehicle load $Y(t)$ is induced by the road profile $Z(x)$, viz. $X(t) = Z(vt)$. If the 'tire' is in contact with the road, then

Description	Symbol	Value	Unit
sprung mass	m_s	3400	kg
suspension spring stiffness	k_s	270 000	N/m
suspension damper stiffness	c_s	6000	Ns/m
unsprung mass	m_u	350	kg
tire spring stiffness	k_t	950000	N/m
tire damper stiffness	c_t	300	Ns/m

Table 1: Quarter vehicle parameters.

the relationship between $Y(t)$ and $Z(vt)$ is linear, and the load is given by

$$Y(t) = \int_{-\infty}^{t} h(t-s)Z(vs)ds, \tag{18}$$

where $h(t)$ is the vehicle's impulse response.

Analysis of measured road tracks indicates that actual roads contain short sections with above-average irregularity. Such irregularities are shown to cause most of the vehicle fatigue damage [2]. The stochastic road model presented in this section is a modified version of the model in [2].

The main variability in the road is described by the stationary Gaussian process $Z_0(t)$, with spectrum $R_0(\xi)$, say. Irregularities of random shape, length and location are superimposed to $Z_0(x)$. The jth irregularity is denoted by $Z_j(x)$, $j > 0$, and the road with superimposed irregularities is denoted by $Z(x)$. To exemplify, a 400 m long road is simulated and plotted in Figure 4.

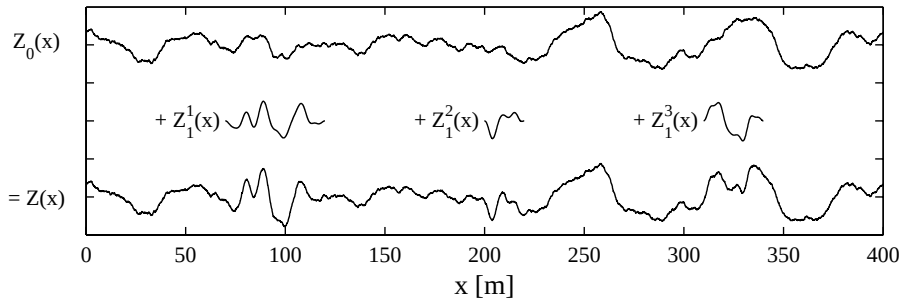

Figure 4: A synthetic (computer simulated) road profile ($a_0 = -5.2$, $a_1 = -4.1$, $w_1 = -3.1$, $w_2 = -2.2$).

The irregularities are modelled as (non-stationary) conditional Gaussian processes. To avoid discontinuities at the start and end of the rough sections,

the added irregularities starts and ends with zero slope and zero level. The irregularities are simulated conditioning on the zero boundary values, see Appendix A. Since the irregularities are non-stationary, it is incorrect to assign a spectral density to them. However, an irregularity reaching from $-\infty$ to $+\infty$ is a stationary Gaussian process with spectrum $R_j(\xi)$, say. The spectra are parametrised as follows,

$$R_0(\xi) = \begin{cases} 10^{a_0}\left(\frac{\xi}{\xi_0}\right)^{-w_1}, & \xi \in [0.01, 0.20], \\ 10^{a_0}\left(\frac{\xi}{\xi_0}\right)^{-w_2}, & \xi \in [0.20, 10], \\ 0, & \text{otherwise}, \end{cases} \tag{19}$$

$$R_j(\xi) = \begin{cases} (10^{a_j} - 10^{a_0})\left(\frac{\xi}{\xi_0}\right)^{-w_1}, & \xi \in [0.03, 0.2], \\ 0, & \text{otherwise}, \end{cases} \tag{20}$$

where the reference spatial frequency $\xi_0 = 0.2$ m^{-1}. In this paper we assume that $a_j = a_1$ for all $j > 0$, however using variable a_j allows for modelling of change in degree of roughness.

Furthermore, the location and length of the sections with added roughness are random. More precisely, the distance between the end of an irregularity and the start of the next is exponentially distributed with mean θ. The irregularity length is also exponentially distributed, but with mean τ.

4.1 Expected damage caused by an irregularity

In this section, we study the vehicle fatigue damage caused by an irregular section. The irregularity starts at $t = 0$ and ends at $t = t_0$. Its effect on the vehicle in the following t_1 seconds is also studied.

The computations of the variances $\sigma_Y^2(t)$ and $\sigma_{\dot{Y}}^2(t)$ and the correlation between $Y(t)$ and $\dot{Y}(t)$, $\rho(t)$, are rather technical and are given in Appendix B. In addition, it is easy to see that $\mathrm{E}[Y(t)] = 0$.

In our example the correlation $\rho(t)$ is small and can be set to be zero, which is verified by Figure 5, where the approximations (16) and (17) are plotted. As illustrated, the two functions (almost) overlap and hence we use the simpler of the two: the narrow-band approximation of the damage intensity (16).

In Figure 6, the observed and theoretical damage intensities are compared. The damage intensity is expressed as a function of distance using the change of variable $x = vt$,

$$\int d^{\mathrm{nb}}(t)dt = \int \underbrace{d^{\mathrm{nb}}(x/v)1/v}_{=g(x)}\, dx. \tag{21}$$

In the example, the velocity is 20 m/s and the irregularity length is 40 m. In the above plot, in Figure 6, the observed damage intensity and the local narrow-

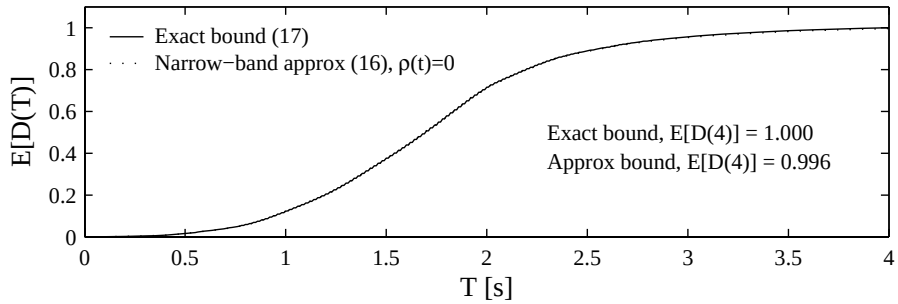

Figure 5: Accumulated damage, $a_0 = -5$, $a_1 = -4$, $w_1 = 3$, $w_2 = 2$, $v = 72$ km/h, $t_0 = 2$ s. (Normalised so that $\mathrm{E}[D(4)] = 1$ for the exact bound)

band approximation are compared. As illustrated, the observed damage due to a particular irregularity may differ significantly from the narrow-band approximation. However, in the lower plot, 1000 observed intensities are averaged, and the result resembles the narrow-band approximation.

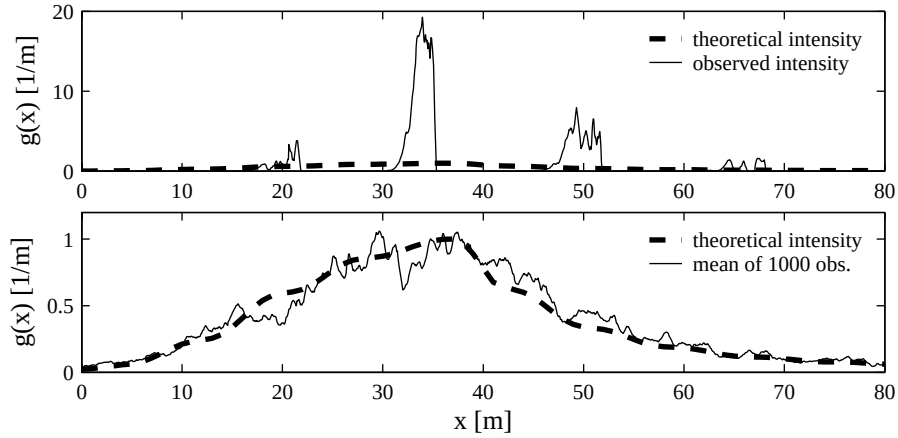

Figure 6: Damage intensity, $a_0 = -5$, $a_1 = -4$, $w_1 = 3$, $w_2 = 2$, $v = 72$ km/h, $t_0 = t_1 = 2$ s, $\beta = 4$. (Normalised so that $\max g(x) = 1$)

The theoretical expected damage $\mathrm{E}[D] = \int_0^{80} g(x)dx = 25$, where $g(x)$ is defined in (21). This result coincides with the average observed damage from simulations. From simulations, we also obtain $\mathrm{Var}(D) = 30^2$. Thus, the coefficient of variation is large, $\sqrt{\mathrm{Var}(D)}/\mathrm{E}[D] = 1.2$. Hence, if we study the damage indicated by M irregularities, the expected damage is $\mathrm{E}[\sum_{i=1}^{M} D_i] = M\mathrm{E}[D]$

and $\mathrm{Var}(\sum_{i=1}^{M} D_i) = M\mathrm{Var}(D)$, giving the coefficient of variation $1.2/\sqrt{M}$. Hence, to get a small coefficient of variation, say below 0.1, M must exceed 144. This has practical consequences, to enable accurate damage predictions one need to study around 200 irregularities, which commonly have an average separation of 400 m, resulting in a measurement length of 80 km.

4.2 Expected damage caused by a long road with several irregularities

Now, we consider a road of length L, which consists of $N+1$ stationary sections separated by N irregular nonstationary sections. The total damage is,

$$D_{\mathrm{tot}} = \sum_{j=1}^{N+1} D_j^{\mathrm{stat}} + \sum_{j=1}^{N} D_j^{\mathrm{irr}}, \tag{22}$$

where D_j^{stat} and D_j^{irr} are the damage due to stationary section j and irregularity j. Now, we wish to compute the expected damage, $\mathrm{E}[D_{\mathrm{tot}}]$.

We make a simplifying assumption, that each irregularity is well separated, so that, at the beginning of an irregularity, the effect of the previous irregularity can be neglected. More precisely, we assume that consecutive irregularities are more than $t_1 = 2$ seconds apart, and similarly, that the vehicle load is affected by an irregularity up to t_1 seconds after passing it. Then, the expected fatigue damage is

$$\begin{aligned} \mathrm{E}[D_{\mathrm{tot}}] &= \mathrm{E}[\sum_{j=1}^{N+1} D_j^{\mathrm{stat}}] + \mathrm{E}[\sum_{j=1}^{N} D_j^{\mathrm{irr}}] \\ &\approx T\frac{\theta - t_1 v}{\theta + \tau} d^{\mathrm{stat}} + \frac{L}{\theta + \tau}\mathrm{E}[D_j^{\mathrm{irr}}], \end{aligned} \tag{23}$$

where the total time $T = L/v$, $(\theta - t_1 v)/(\theta + \tau)$ is the proportion in time when the load is unaffected by any irregularities, $\frac{L}{\theta+\tau}$ is the expected number of irregularities, and d^{stat} is the damage intensity due to stationary parts, bounded using (9). We also need to compute the expected damage due to an irregularity of random length L_0. The effect of such irregularity, located at $[0, l]$, is assumed to be significant during the time interval $[0, t + t_1]$ where $t = l/v$,

$$\mathrm{E}[D(t + t_1)] = \int_0^\infty \mathrm{E}[D(l/v + t_1)|\text{irregularity length} = l] f(t) dt. \tag{24}$$

The probability density function of $T_0 = L_0/v$

$$f(t) = \frac{v}{\tau} e^{-tv/\tau}. \tag{25}$$

The conditional expected damage, $\mathrm{E}[D(l/v + t_1)|l]$ is bounded by (16), integrating from 0 to $t_0 + t_1$. The integral (24) is numerically computed using importance sampling,

$$\frac{1}{n}\sum_{j=1}^{n} \mathrm{E}[D(t_j + t_1)|l_j]\frac{f(t_j)}{w(t_j)}$$

where t_j is simulated from a gamma distribution and $w(t_j)$ is the corresponding probability density function, $w(t) = te^{-vt/\tau}(v/\tau)^2$.

In Figure 7 we compare $\mathrm{E}[D_{\mathrm{tot}}]$ with the average result $\bar{D}_{\mathrm{MC}}$ obtained from Monte-Carlo simulations. More precisely, $N = 100$ synthetic road profiles of length $L = 100$ km are generated according to model assumptions in Section 4. The observed fatigue damage induced in the quarter vehicle is computed as described in Section 4 and the average observed damage is $\bar{D}_{\mathrm{MC}}$. The road parameters are set to $a_0 = -5.4$, $a_1 = -4.3$, $w_1 = 3.4$, $w_2 = 2.2$, $\theta = 400$ m, $\tau = 32$ m, and the vehicle velocity $v = 60$ km/h. In this example (23) gives an accurate conservative estimate of the expected vehicle fatigue damage.

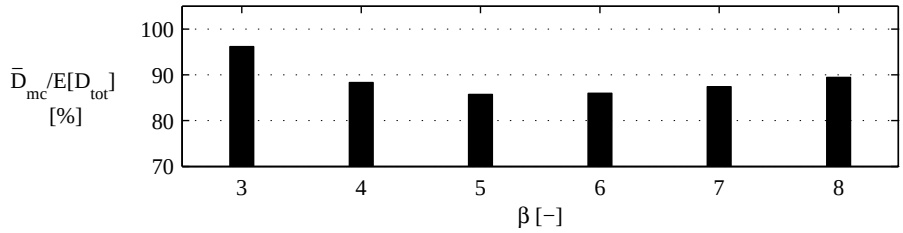

Figure 7: Verification of (23).

5 Examples

5.1 Parameter study

In this study, we assume that all irregularities in a specific road have the same properties (e.g. $a_j = a_1$), this simplification is realistic if the distance is short. However, as noted in Section 4.1, road measurements should be long (80 km) to enable accurate damage predictions. To handle these contradictory demands, one could model a_j as a random variable. In this section we will study how a change in roughness level a_1 influence the damage intensity over an irregularity. And similarly, we will also study the effect of varying the vehicle velocity and the irregularity length l.

In Figure 8 the damage intensity is plotted both when a_1 and v is changed. The irregularity length is fixed to 60 m. The total damage is given by D^{nb}, in the upper right part of each figure. We can see that, in this specific example, a change of a_1 from -4.2 to -3.8 increases the total damage more than 5 times. Similarly, in the second example, a change of velocity from 60 to 80 km/h doubles the expected damage.

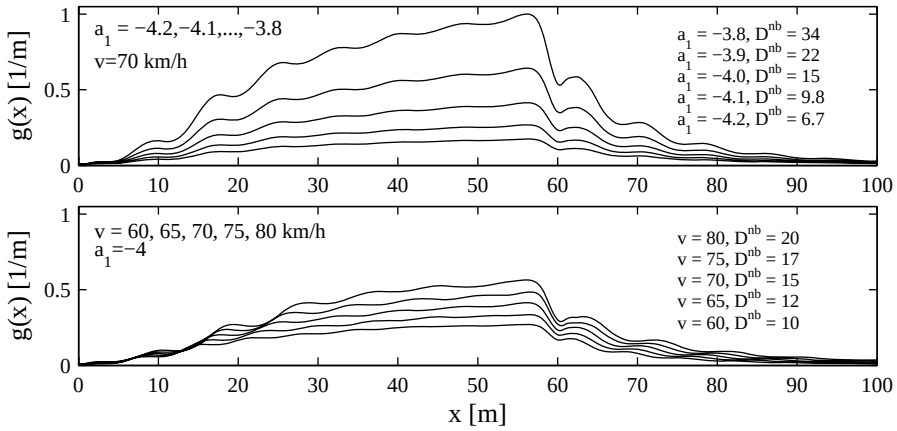

Figure 8: Damage intensity when the irregularity length is 60 m ($a_0 = -5$, $w_1 = 3$, $w_2 = 2$, $\beta = 4$). (Normalised so that maximum intensity is 1)

In the next example, a_1 and v are fixed, and irregularity length L_0 is varied. Figure 9 illustrates the effect of increasing irregularity length. The stationary level, marked by the dashed line, is the damage intensity that an infinite long irregularity would induce.

Synthetic (computer simulated) test tracks are condensed version of long road measurements. Typically, these test tracks are comprised of rough road sections connected by smooth sections. Now, Figure 9 shows the importance of irregularity length: if an irregularity is long enough, it induces vehicle vibrations that reach 'local stationarity'. More explicitly, with parameter values set as in the example in Figure 9, the expected damage of 30 irregularities of length 20 m is similar to the expected damage of one irregularity of length 60 m. This kind of length effects are important to consider when designing test sequences.

5.2 Comparison to measured data

Now we will compare the damage predicted by (23) to the observed damage induced by 520 kilometres of measured roads.

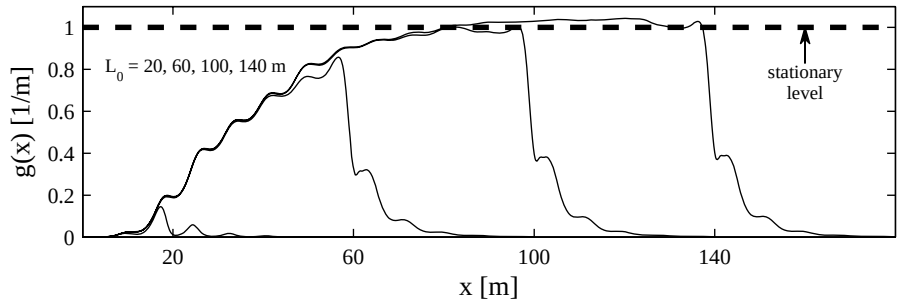

Figure 9: Damage intensity for different irregularity lengths ($a_0 = -5$, $a_1 = -4$, $w_1 = 3$, $w_2 = 2$, $\beta = 8$, $v = 72$ km/h= 20 m/s). (Normalised so that stationary level is one)

The 520 kilometres are based on 20 different road measurements. The roads are of varying quality, ranging from rough gravel roads to smooth motorways. A vehicle driver, travelling on these roads will adapt the speed to the road conditions. In this example, we group the roads into four classes and associate each road class with a constant velocity. More precisely, the velocity is set to 30, 50, 70 and 90 km/h for minor country roads, country roads, main roads and motorways, respectively. Also, for each road, we estimate the road model parameters $(a_0, a_1, w_1, w_2, \theta, \tau)$. Then the expected damage $\mathrm{E}[D_{\mathrm{tot}}^{(i)}]$ due to the ith road is computed using (23). Moreover, the observed damage caused by the ith road, $D_{\mathrm{obs}}^{(i)}$, is computed, obtained by simulation of the quarter vehicle. In Figure 10, the predicted expected total damage $\sum_{i=1}^{20} \mathrm{E}[D_{\mathrm{tot}}^{(i)}]$ is divided by the total observed damage $\sum_{i=1}^{20} D_{\mathrm{obs}}^{(i)}$. The result is plotted for $\beta = 3, 4, ..., 8$. The expected damage gives a result varying between 76 % and 128 % of the observed damage.

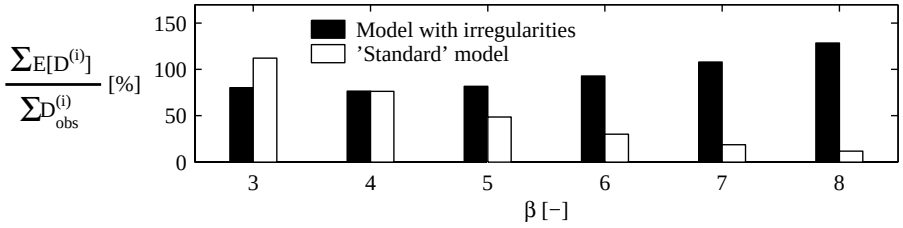

Figure 10: Comparison of theoretical expected damage and observed damage due to measured roads

As a comparison, we also use a stationary Gaussian model to predict damage. Two spectral parameters are estimated for each road, according to ISO 8608 [14], and the expected damage is computed using the narrow-band approximation (8). However, this prediction degenerates as β increases.

6 Conclusions

A method for vehicle fatigue damage prediction caused by a road with random irregularities is described. Use of the local narrow-band approximation provides insight in the accumulated vehicle fatigue damage due to road irregularities.

References

[1] Öijer F, Edlund S (2004). Identification of Transient Road Obstacle Distributions and Their Impact on Vehicle Durability and Driver Comfort, *Suppl. Vehicle System Dynamics*, **41**, 744–753.

[2] Bogsjö K (2005). Stochastic modelling of road roughness, Licentiate of engineering thesis, Lund Institute of Technology, Lund Sweden.

[3] Bogsjö K (2006). Development of analysis tools and stochastic models of road profiles regarding their influence on heavy vehicle fatigue, *Suppl. Vehicle System Dynamics*, **44**, pp. 780–790. (Paper B in this thesis.)

[4] Bendat JS (1964). Probability Functions for Random Responses: Prediction of Peaks, Fatigue damage and Catastrophic Failures. NASA technical report.

[5] Matsuishi, M and Endo, T (1968). Fatigue of metals subject to varying stress, Paper presented to *Japan Soc. Mech. Engrs, Jukvoka, Japan.*

[6] Palmgren, A (1924). Die Lebensdauer von Kugellagern, *VDI Zeitschrift*, **68**, 339–341.

[7] Miner, MA (1945). Cumulative damage in fatigue, *J. Appl. Mech.*, **12**, A159-A164.

[8] Rice, SO (1944, 1945). The mathematical analysis of random noise I and II. *Bell Syst. Tech. J.*, **23,24**.

[9] Rychlik, I (1987). A new definition of the rainflow cycle counting method, *Int. J. Fatigue*, **9**, 119–121.

[10] Rychlik, I (1993a). On the "narrow-band" approximation for expected fatigue damage. *Probabilistic Engineering Mechanics*, **8**. 1–4.

[11] Rychlik, I (1993b). Note on cycle counts in irregular loads. *Fatigue Fract. Engng Mater. and Struc.*, **16**, 377–390.

[12] Lu Sun (2001). Computer simulation and field measurement of dynamic pavement loading. *Mathematics and Computers in Simulation*, **56**, pp 297–313.

[13] Mucka P (2004), Road waviness and the dynamic tyre force, *Int. J. Vehicle Design*, **36**, Nos. 2/3, 216–232.

[14] ISO 8608 (1995) *Mechanical Vibration — Road Surface Profiles — Reporting of Measured Data*, International Organization for Standardization, Geneva.

[15] Lindgren G (1981) Jumps and bumps on random roads. *J. Sound and Vibration* **78**, 393–395.

A Simulation of an irregularity

The purpose of this section is to describe realization of an irregularity of length $L = nh$, described by the random sequence Z_r, where n is the number of values in Z_r and h is the sample step (e.g. 5 cm).

Let $W(x)$ be a zero mean stationary Gaussian sequence with spectral density given by (20), and $\dot{W}(x)$ its derivative. To simplify notation, a sampled process is denoted using brackets, e.g. $W(kh) = W[k], k = 0, \ldots, n+1$, where h is the step length. Furthermore, it is convenient to define the two column vectors $W_1 = (W[1] \ \ldots \ W[n])^T$ and $W_2 = \left(W[0] \ \dot{W}[0] \ W[n+1] \ \dot{W}[n+1]\right)^T$, where ^{T} denotes matrix transpose. We want to simulate $W_1|W_2 = 0$ (i.e. the process start and end with zero level and zero slope). Define

$$Z_r = W_1 - \Sigma_{12}\Sigma_{22}^{-1}W_2, \tag{26}$$

where $\Sigma_{12} = \mathrm{cov}(W_1, W_2)$ and $\Sigma_{22} = \mathrm{cov}(W_2, W_2)$. The expectation and covariance of Z_r are

$$\begin{aligned} \mathrm{E}[Z_r] &= 0, & (27)\\ \mathrm{cov}(Z_r, Z_r) &= \Sigma_{11} - \Sigma_{12}\Sigma_{22}^{-1}\Sigma_{21}. & (28) \end{aligned}$$

This coincides with the expectation and covariance of the conditional Gaussian process of W_1 given $W_2 = 0$, thus Z_r represents $W_1|W_2 = 0$. In order to compute Z_r we need Σ_{12} and Σ_{22}. The (one-sided) spectral density $R(\xi)$ is used to obtain the covariance matrices. The covariance function is

$$r(x) = \int_0^\infty R_1(\xi)\cos(2\pi\xi x)\mathrm{d}\xi \tag{29}$$

and the sampled covariance function $r(kh) = r[k]$. This gives the covariance matrices

$$\operatorname{cov}(W_2, W_2) = \Sigma_{22} = \begin{pmatrix} r[0] & 0 & r[n+1] & \dot{r}[n+1] \\ 0 & -\ddot{r}[0] & -\dot{r}[n+1] & -\ddot{r}[n+1] \\ r[n+1] & -\dot{r}[n+1] & r[0] & 0 \\ \dot{r}[n+1] & -\ddot{r}[n+1] & 0 & -\ddot{r}[0] \end{pmatrix} \quad (30)$$

and

$$\operatorname{cov}(W_1, W_2) = \Sigma_{12} = \begin{pmatrix} r[1] & -\dot{r}[1] & r[n] & \dot{r}[n] \\ r[2] & -\dot{r}[2] & r[n-1] & \dot{r}[n-1] \\ \vdots & \vdots & \vdots & \vdots \\ r[n] & -\dot{r}[n] & r[1] & \dot{r}[1] \end{pmatrix}. \quad (31)$$

To realize an irregularity: Simulate the unconditional sampled process $W[k]$, for $k = 0, \ldots, n+2$ identify $W_1 = (W[1], \ldots, W[n])^T$ and approximate

$$W_2 \approx \left(W(0), \frac{W(1) - W(0)}{h}, W(n+1), \frac{W(n+2) - W(n+1)}{h} \right)^T,$$

calculate covariance matrices and compute Z_r.

B Computation of $d^{\mathrm{nb}}(t)$

Simulation of the quarter vehicle is performed in time domain solving ordinary differential equations (ODEs) using a constant time step. In addition, the simulation method also allows for vehicle jumps. This non-linear effect makes the response non-Gaussian. Thus, if jumps occur frequently, this requires another approach, see for example [15]. Here, jumps occur very seldom and are neglected in the statistical analysis below. In the analysis we write the vehicle response using impulse response functions. (However, note that vehicle simulation using impulse response functions would imply very long computational time.) The response $Y(t)$ is given by (18) and the derivative of the response is

$$\dot{Y}(t) = \int_{-\infty}^{t} \tilde{h}(t-s) Z(vs) ds. \quad (32)$$

The impulse response functions $h(t)$ and $\tilde{h}(t)$ can be computed in several ways. Here, these are computed from simulation (using the ODE-solver) of a vehicle travelling over a small step: $Z(t) = 0$ if $t < 0$ and $Z(t) = \delta$ otherwise. The derivative of the step response, divided by δ, is $h(t)$ and the double derivative of the step response, divided by δ, is $\tilde{h}(t)$.

We need the joint density of $Y(t)$ and $\dot{Y}(t)$ to compute $\mu_t(u)$. However, since $Y(t)$ and $\dot{Y}(t)$ are multivariate Gaussian it is sufficient to compute their

mean, variance and covariance as a function of time. Their mean values are zero: $\mathrm{E}[Y(t)] = \int_{-\infty}^{t} h(t-s)\mathrm{E}[Z(vs)]ds = 0$ and $\mathrm{E}[\dot{Y}(t)] = 0$. The variances and covariance are written as

$$\begin{aligned}
\mathrm{Var}(Y(t)) &= \mathrm{Var}(Y_s(t)) + \mathrm{Var}(Y_r(t)) \\
&\equiv \sigma_{Ys}^2 + \sigma_{Yr}^2(t) \equiv \sigma_Y^2(t), \qquad (33) \\
\mathrm{Var}(\dot{Y}(t)) &= \mathrm{Var}(\dot{Y}_s(t)) + \mathrm{Var}(\dot{Y}_r(t)) \\
&\equiv \sigma_{\dot{Y}s}^2 + \sigma_{\dot{Y}r}^2(t) \equiv \sigma_{\dot{Y}}^2(t), \qquad (34) \\
\mathrm{Cov}(\dot{Y}(t), Y(t)) &= \mathrm{Cov}(\dot{Y}_s(t) + \dot{Y}_r(t), Y_s(t) + Y_r(t)) \\
&= \mathrm{E}[\dot{Y}_r(t)Y_r(t)] = c(t). \qquad (35)
\end{aligned}$$

The time varying parameters $\sigma_{Yr}^2(t), \sigma_{\dot{Y}r}^2(t)$ and $c(t)$ parameters are computed by

$$\begin{aligned}
\sigma_{Yr}^2(t) &= \mathrm{E}[Y_r^2(t)] \\
&= \int_{-\infty}^{t}\int_{-\infty}^{t} h(t-u)h(t-s)\mathrm{E}[Z_r(vs)Z_r(vu)]dsdu \qquad (36) \\
\sigma_{\dot{Y}r}^2(t) &= \mathrm{E}[\dot{Y}_r^2(t)] \\
&= \int_{-\infty}^{t}\int_{-\infty}^{t} \tilde{h}(t-u)\tilde{h}(t-s)\mathrm{E}[Z_r(vs)Z_r(vu)]dsdu \qquad (37) \\
c(t) &= \mathrm{E}[\dot{Y}_r(t)Y_r(t)] \\
&= \int_{-\infty}^{t}\int_{-\infty}^{t} \tilde{h}(t-u)h(t-s)\mathrm{E}[Z_r(vs)Z_r(vu)]dsdu \qquad (38)
\end{aligned}$$

The constant parameters σ_{Ys}^2 and $\sigma_{\dot{Y}s}^2$ are given by the frequency response function,

$$\begin{aligned}
\sigma_{Ys}^2 &= \int_0^\infty |H(\omega)|^2 \tilde{R}_v(\omega)d\omega \qquad (39) \\
\sigma_{\dot{Y}s}^2 &= \int_0^\infty \omega^2 |H(\omega)|^2 \tilde{R}_v(\omega)d\omega \qquad (40)
\end{aligned}$$

where $H(\omega) = \int_{-\infty}^{\infty} h(t)\mathrm{e}^{i\omega t}dt$, $\tilde{R}_v(\omega) = R(\frac{\omega}{2\pi v})\frac{1}{2\pi v}$ and R is given by (19). Now, the two dimensional density is

$$\begin{aligned}
& f_{\dot{Y}(t),Y(t)}(z,u) = f_{\dot{Y}(t)|Y(t)=u}(z) f_{Y(t)}(u) \\
= \; & \frac{1}{\sigma(t)\sqrt{2\pi}} e^{\left(\frac{-(z-m(t)u)^2}{2\sigma^2(t)}\right)} \frac{1}{\sigma_Y(t)\sqrt{2\pi}} e^{\left(\frac{-u^2}{2\sigma_Y^2(t)}\right)} \qquad (41)
\end{aligned}$$

where

$$\rho(t) = c(t)/(\sigma_Y(t)\sigma_{\dot{Y}}(t)), \quad m(t) = \rho(t)\sigma_{\dot{Y}}(t)/\sigma_Y(t)$$

and

$$\sigma(t) = \sigma_{\dot{Y}}(t)\sqrt{1-\rho^2(t)}.$$

The upcrossing intensity is

$$\begin{aligned}\mu_t(u) &= \int_0^\infty z f_{\dot{Y}(t)|Y(t)=u}(z) f_{Y(t)}(u) dz \\ &= \frac{e^{\frac{-u^2}{2\sigma_Y^2(t)}}}{\sigma_Y(t)\sqrt{2\pi}} \left(m(t)u(1-\Psi(-\frac{m(t)u}{\sigma(t)})) + \frac{\sigma(t)}{\sqrt{2\pi}} e^{-u^2 m^2(t)/2\sigma^2(t)} \right) \quad (42)\end{aligned}$$

where $\Psi(z) = \int_{-\infty}^{z} \frac{e^{-u^2/2}}{\sqrt{2\pi}} du$. Now, if $\rho(t) = 0$ then $m(t) = 0$ and $\sigma(t) = \sigma_{\dot{Y}}(t)$, and hence

$$\mu_t(u) = \frac{1}{2\pi} \frac{\sigma_{\dot{Y}}(t)}{\sigma_Y(t)} \exp\left(-\frac{u^2}{2\sigma_{\dot{Y}}^2(t)} \right), \quad (43)$$

which is unimodal and symmetrical around zero. Inserting (43) into (13) gives the local narrow-band approximation (15).

In Figure 11, $\rho(t)$ is plotted: The correlation between $Y(t)$ and $\dot{Y}(t)$ is varying between 0 and 0.15 in the interval $[0, t_0]$ and between -0.1 and 0 in the interval $[t_0, t_0+t_1]$. However, the correlation is too weak to have any significant effect on $\mu_t(u)$, as illustrated by Figure 12. In the figure $\int_0^{t_0+t_1} \mu_t(u)dt$ (i.e the expected number of upcrossings for $t \in [0, 4]$) is compared for the exact (42) and approximate (43) case. In addition, the average number of upcrossings of 1000 simulations of the quarter car is also plotted.

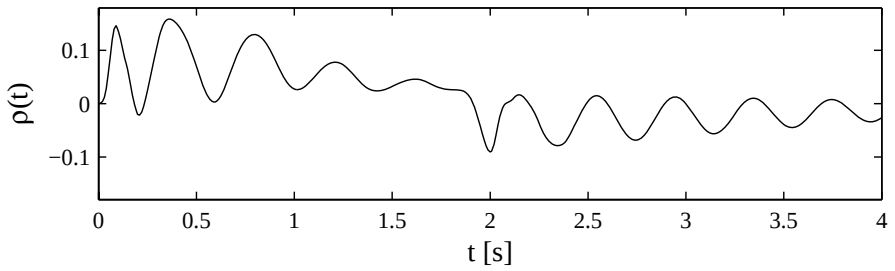

Figure 11: Correlation between $Y(t)$ and $\dot{Y}(t)$, $a_0 = -5$, $a_1 = -4$, $w_1 = 3$, $w_2 = 2$, $v = 72$ km/h, $t_0 = t_1 = 2$ s.

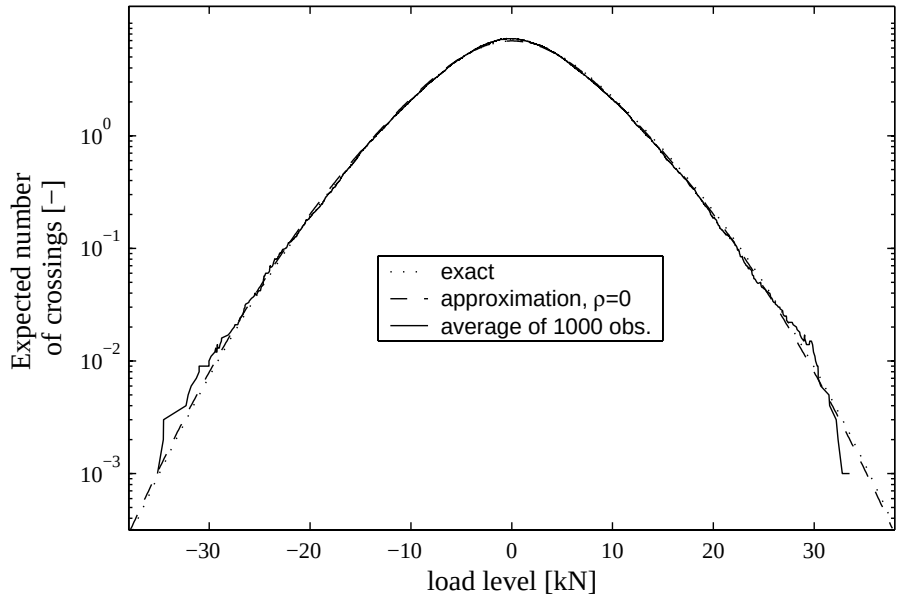

Figure 12: Exact, approximated and average (from 1000 simulations) number of upcrossings, $a_0 = -5$, $a_1 = -4$, $w_1 = 3$, $w_2 = 2$, $v = 72$ km/h, $t_0 = t_1 = 2$ s.